

Electronic Thesis and Dissertation Repository

---

10-26-2021 2:30 PM

## Active fluids: rheological properties and response to light of suspensions of *Synechocystis* sp. CPCC 534

Zahra Habibi, *The University of Western Ontario*

Supervisor: Hassan Peerhossaini, *The University of Western Ontario*

A thesis submitted in partial fulfillment of the requirements for the Master of Science degree in Civil and Environmental Engineering

© Zahra Habibi 2021

Follow this and additional works at: <https://ir.lib.uwo.ca/etd>



Part of the [Civil Engineering Commons](#), and the [Environmental Engineering Commons](#)

---

### Recommended Citation

Habibi, Zahra, "Active fluids: rheological properties and response to light of suspensions of *Synechocystis* sp. CPCC 534" (2021). *Electronic Thesis and Dissertation Repository*. 8321.  
<https://ir.lib.uwo.ca/etd/8321>

This Dissertation/Thesis is brought to you for free and open access by Scholarship@Western. It has been accepted for inclusion in Electronic Thesis and Dissertation Repository by an authorized administrator of Scholarship@Western. For more information, please contact [wlsadmin@uwo.ca](mailto:wlsadmin@uwo.ca).

## Abstract

Despite our current understanding of active fluid mechanics, more knowledge is required to fully understand their rheological properties, response to light, and details of the interactions between cells in diluted suspensions.

The focus of this thesis is on investigating the rheological properties of suspensions of cyanobacterium *Synechocystis* sp. CPCC 534 under shear, induced by stirring. Experiments were conducted at different stirring rates and results are compared with the stationary condition. A notable increase in growth and biomass of *Synechocystis* sp. under various shear conditions was observed and the yield was nearly doubled. Besides, the data showed Newtonian behavior for suspensions at different cell concentrations. Although cell concentration displayed a perceptible rise in the viscosity of suspensions, this rise is smaller than the one predicted for suspensions of hard spheres.

Moreover, experiments were carried out on diluted suspension of *Synechocystis* sp. CPCC 534 in a microfluidic chamber to investigate the response of cells to the light and cell-cell interactions. The cells were exposed to the light of the laser pointer and a white LED. Cell tracking was performed by image processing in Python programming language. It was observed that cells display an alternating intermittent motion that consists of high motility “run phases” and immobile “tumble phases”. Comparing the probability distributions of the ensemble-averaged mean square displacement (EMSD), and velocity variations with time, revealed that cells detect light and spend more time running with high-speed motility under white LED light, while spending more time tumbling when exposed to laser pointer light. Moreover, the frequency of cell-cell interactions shows that exposure to any light sources decreases the number of interactions significantly. The preliminary design and experimental setup of a multichannel microfluidic device are provided as well.

## Keywords

active fluid, cyanobacteria, *synechocystis* sp., rheological properties, microfluidics, cell tracking, motility, cell-cell interaction, light response, image processing, Python programming language

## Summary for Lay Audience

Active fluid is a fluid whose constituent elements can self-propel for instance, suspensions of bacteria, algae, and sperm cells. Active fluids display properties that differ fundamentally from conventional (passive) fluids. Contrary to conventional fluid flows in which one needs gradients of pressure, velocity, and temperature to drive the flow, in active fluids, cells as the microstructural elements of the fluid convert the chemical energy of nutrients into mechanical energy for driving the flow. It is essential to investigate the hydrodynamics of microorganisms due to their direct and indirect effects on human lives, the environment, and also its vast applications in industrial, medical, food, and energy fields such as harmful algal blooming, photobioreactors (PBR), biofuel production, water treatment industry, food hygiene, etc.

Experiments were conducted on the suspensions of cyanobacterium *Synechocystis* sp. under shear stress to investigate their rheological properties. A notable increase in growth and biomass production of *Synechocystis* sp. under various shear conditions was observed. Moreover, the data showed Newtonian behavior for suspensions at different cell concentrations. Besides, experiments were performed on cells exposed to the laser pointer light and white LED to study their response to light and their interactions. Cell tracking revealed that the intermittent motility of cells consists of high motility “run phases” and immobile “tumble phase”. Statistical analysis on displacement and velocity indicates that cells detect light and spend more time running with high-speed motility under white LED light, while spending more time tumbling when exposed to the laser pointer light. Moreover, the frequency of cell-cell interactions shows that exposure to light decreases the number of interactions. The preliminary design and experimental setup of a multichannel microfluidic device are provided as well.

## Co-Authorship Statement

Chapter 2 is part of a paper published in the Journal of Fluids Engineering. It is co-authored by M. Mehdizadeh Allaf, Z. Habibi, J. R. de Bruyn, C. T. DeGroot and H. Peerhossaini.

Chapter 2 presents parts of the results of a bigger interdisciplinary project which required knowledge in Fluid Mechanics, Physics and Biology. Dr. Malihe Mehdizade Allaf, the post-doctoral fellow is an expert in biology.

In short, the “biology” part of this project including carrying out the experiments and measurements was done in collaboration with Dr. Malihe Mehdizade Allaf and the “fluid mechanic” part of the work including statistical analysis and data visualization in MATLAB and Python is my independent work.

Regarding the intellectual property (IP) of the work, an agreement has been prepared by the School of Graduate and Postdoctoral Studies (SGPS), Western University, and signed by me, Dr. Malihe Mehdizade Allaf, and Dr. Ruth Martin, Associate Vice-Provost of SGPS on August 4, 2021.

Based on this agreement, Figure 2-4, Figure 2-7, Figure 2-8, Figure 2-9, Figure 2-10, Figure 2-11, Figure 2-12, Figure 2-13, Figure 2-14, and Figure 2-15 are the result of joint work.

## Acknowledgments

First and foremost, I would like to express my sincere appreciation and gratitude to Dr. Ruth Martin, Associate Vice-Provost of School of Graduate and Postdoctoral Studies (SGPS), Western University for the effort and time she has contributed to support and assist me.

I would like to thank Dr. Kamran Siddiqui, Associate Dean of Graduate and Postdoctoral Studies, Western Engineering, for his strong support and assistance.

I would also like to thank the co-authors of my publications: Dr. Malihe Mehdizadeh Allaf, Zahra Samadi, Dr. Christofer T. DeGroot, Dr. Lars Rehman, Dr. John R. de Bruyn, and Dr. Hassan Peerhossaini.

I am grateful to Dr. John R. de Bruyn, Dr. Lars Rehman, Dr. Eric Savory, and Dr. June Yang for their cooperation in accommodating me with using their lab and/or equipment for doing the experiments. This work would not have been possible without their help.

I would like to extend my thanks to Dr. Qiuquan Guo, at Dr. June Yang's lab; Priscilla De Luca, and Elisa Yaquian at the WindEEE Research Institute; Stephen Mallinson, and Paul Sheller at the Engineering Store.

I would like to give special thanks to Farnaz Hamedi Michalski and her family who very kindly welcomed me when I arrived in Canada and also Dr. Malihe Mehdizade Allaf who is more than a friend and is like a sister to me.

Thanks to Arash Ashrafi, Zahra Samadi, Kamran Shirzade, Hadil Abdallah, Aya Kassab, Muna Younis, Daniel Davalos, Marilena Enus, Anant Gairola, Hiroaki Shoji, Hang You, Tsinuel Geleta, Abiy Melaku, and Tewodros Alemayehu, for all the help and friendship I received.

At last but not least, I would like to thank my family: my parents (Fariba, Bahman, and Khanbaz), my husband (Dr. Mohammad Karami), my siblings (Farzaneh, Bahman, and Mohammad), and my niece (Aylin) who did all they could to support me. They are all the light and joy of my life.

# Table of Contents

Abstract.....	ii
Summary for Lay Audience.....	iii
Co-Authorship Statement.....	iv
Acknowledgments.....	ii
Table of Contents.....	iii
List of Tables.....	v
List of Figures.....	vi
List of Appendices.....	x
Chapter 1.....	1
1 « Introduction ».....	1
1.1 Overview.....	1
1.2 Cyanobacterium.....	3
1.3 <i>Synechocystis</i> sp.....	4
1.4 Biofilm.....	5
1.5 Hydrodynamics of Microorganisms.....	6
1.6 Rheological Properties of Suspension of Microorganisms.....	8
1.7 Cell-Cell Communication and Response to Environmental Change.....	9
1.8 Theoretical Grounds.....	12
1.9 Motivation and Contributions.....	12
1.10 Organization of the Thesis.....	13
Chapter 2.....	15
2 « Physical and Rheological Properties of <i>Synechocystis</i> sp. Suspension ».....	15
2.1 Methods and Material.....	15
2.1.1 Experiment Condition.....	15
2.1.2 Experimental Apparatus.....	16
2.1.3 Measurement of Bacterial Growth Rate (Ke).....	19
2.1.4 Viscosity Measurement of <i>Synechocystis</i> Suspensions.....	20
2.2 Results and Discussion.....	23
2.2.1 Effects of Shear on Biomass Production.....	23

2.2.2	Effects of Shear on the Cell Size .....	25
2.2.3	Rheology of <i>Synechocystis</i> Suspensions.....	27
2.3	Concluding remarks .....	33
Chapter 3	.....	35
3	« Cell Tracking of Active Fluids: Effects of Light on Diluted Suspensions of <i>Synechocystis</i> sp. CCCC 534» .....	35
3.1	Materials and Methods .....	36
3.1.1	Microorganism and Culture Conditions.....	36
3.1.2	Experimental Apparatus.....	36
3.1.3	External Light Source .....	45
3.1.4	Video Recording and Imaging Techniques.....	46
3.1.5	Image Processing .....	47
3.2	Results and Discussion.....	48
3.2.1	Bacteria Trajectories .....	48
3.2.2	Effect of Light on Cell Motility .....	53
3.3	Concluding remarks .....	61
Chapter 4	.....	63
4	« Conclusions and Recommendations ».....	63
4.1	Summary .....	63
4.2	Conclusions .....	64
4.3	Recommendations and future works .....	65
References	.....	66
Appendices	.....	76
Curriculum Vitae	.....	90

## List of Tables

Table 2-1. Composition of the BG11 medium [82].....	15
Table 2-2. Composition of trace metal solution [82].....	16
Table 2-3. Cannon-Ubbelohde viscometer information .....	22
Table 3-1. The first five rows of DataFrame including cells' coordinate, mass, and frame number .....	48
Table C-1. Small sample adapter information .....	80



## List of Figures

Figure 1-1. a) Harmful algal bloom, Lake Erie b) Lake Erie algae bloom, the southeast shore of Pelee Island, Ontario [12]. .....	2
Figure 1-2. a) A commercial plant of tubular manifold photobioreactors with vertical reactors located in Portugal [22] b) The BIQ clever treefrog house, Hamburg, Germany [23]. .....	2
Figure 1-3. The formation of <i>Bacillus cereus</i> on a stainless-steel surface. $\times 6330$ magnification; scale bar = $5 \mu m$ [25]. .....	3
Figure 1-4. Example of the different morphologies of cyanobacteria .....	4
Figure 1-5. <i>Synechocystis</i> sp. [31]. .....	5
Figure 1-6. A pictorial representation of microbial biofilm life cycle; Individual microbes: 1) Planktonic, Biofilm development: 2) Attachment 3) Growth 4) Maturity 5) Dispersion [33].	6
Figure 1-7. (a) Swimming in a bulk fluid using single polar flagellum; (b) Swarming on a solid surface of bacteria in the hyperflagellated state; (c) twitching through type IV pili; (d) gliding utilizing focal adhesion complexes [34]. .....	6
Figure 1-8. A transmission electron micrograph (TEM) of <i>Synechocystis</i> surrounded by its type IV pilis; scale bar = $1 \mu m$ . [35] .....	7
Figure 2-1. Left: Bacterial suspensions in flasks placed on magnetic stirrers (first day of the experiment); Right: Bacterial suspensions (final day of the experiment).....	16
Figure 2-2. Reynolds number as a function of rotation speed. ....	18
Figure 2-3. Power number as a function of rotation speed. ....	18
Figure 2-4. Average shear stress (Pa) as a function of rotation speed induced in the agitated reactors. ....	19
Figure 2-5. Cannon-Ubbelohde viscometer .....	21
Figure 2-6. AntonPaar Rheometer and the atachment used .....	22
Figure 2-7. Profiles of a) growth rate ( $Ke$ ) and b) doubling per day ( $k$ ) for <i>Synechocystis</i> sp. CPCC 534 under different stirring rates. Similar lower-case letters indicate no significant effect at the level of $p = 0.05$ among different stirring rates. Values are expressed as means $\pm$ standard deviation.....	24

Figure 2-8. Profiles of a) biomass production and b) yield for *Synechocystis* sp. CPCC 534 under various shear rates. The same lowercase letters indicate no significant effect at the level of 0.05 among different shear rates. Values are expressed as means  $\pm$  standard deviation.... 25

Figure 2-9. Effect of stirring rate on the cell size of *Synechocystis* sp. CPCC 534. Similar uppercase letters indicate no significant effect for similar sample treatment under different timelines. Similar lower-case letters indicate no significant effect among different treatments in the same timeline. Significance tested at  $p < 0.05$  level. Values are expressed as means  $\pm$  standard deviation. .... 26

Figure 2-10. a) *Synechocystis* sp. CPCC 534 viscosity as a function of biomass concentration (cell density), and under various stirring rates. b) Same plot without error bars..... 28

Figure 2-11. Normalized viscosity of suspensions of *Synechocystis* sp. CPCC 534 as a function of shear rate for different cell volume fractions..... 29

Figure 2-12. Micrographs of suspensions of live and dead *Synechocystis* sp. CPCC 534. .... 30

Figure 2-13. Variation of averaged normalized viscosity as a function of shear rate for the suspensions of live and dead *Synechocystis* sp. CPCC 534..... 31

Figure 2-14. Comparison of the variation of viscosity as a function of cell density for unsheared live and dead-cell suspensions as well as pre-sheared live-cell suspensions. Data for the first set of experiments extends to higher cell densities due to stirring. .... 32

Figure 2-15. Variation of the averaged viscosity of *Synechocystis* sp. CPCC 534 suspensions with cell density. .... 33

Figure 3-1. Schematic design of the experimental setup. The green dots represent cells. .... 37

Figure 3-2. a) Microscope slide and b) coverslip. After putting the droplet of the suspension on the microscope slide, c) coverslip is placed on top of the microscope slide for cover, and finally, d) sealed with the vacuum grease to avoid evaporation and drift. .... 37

Figure 3-3. Experimental setup..... 38

Figure 3-4. Microscope imaging (20X magnification) of a) cavity and b) plane microscope slide used as the microfluidic chamber. .... 38

Figure 3-5. Schematic view of the experimental setup of the preliminary design of the a) front view of the plane and b) top view of multiple branch microfluidic channel. The green dots represent cells..... 39

Figure 3-6. Dimensions of the master (mask). Each part of the master is labeled with specific words or letters. Highlights on the curve for point A provide the guide for reading dimensions. .....	42
Figure 3-7. Multichannel microfluidic device (left-hand side) and plane microfluidic channel (right-hand side) fabricated by lithography. ....	42
Figure 3-8. The plane microfluidic channel with its attachments. ....	43
Figure 3-9. Applying microalgal suspension into the microchannel by the syringe micropump. .....	43
Figure 3-10. A single frame of the recorded video of the flow of suspension of <i>Synechocystis</i> in the microchannel. ....	44
Figure 3-11. Schematic 3D design of the microfluidic device composed of the main channel and 11 microchambers with 100 micropillars each. ....	44
Figure 3-12. Flashlight with LED and its experimental setup .....	45
Figure 3-13. Laser pointer and its experimental setup.....	46
Figure 3-14. The procedure of obtaining cells' features. ....	48
Figure 3-15. a) Traces the trajectories of bacterial cells and the magnified trajectories denoted inside the blue square. The duration of the trajectories is 180 s. The size of a pixel is equal to 1 $\mu m$ .....	49
Figure 3-16. Trajectory of a bacterial cell (of duration 180 s). The twitching motility that is a combination of run and tumble motions is observable. Inset: the diffusion step in which $l_{run}$ , $\tau_{run}$ , and $\tau_{tumble}$ represents the distance traveled during a run, the run duration, and the tumble duration, respectively. The size of a pixel is equal to 1 $\mu m$ .....	50
Figure 3-17. a) The traces of bacterial cells, b) The last frame of the video (Media Appendix) from the dynamic trace of a single bacterial cell encircled in part (a). The size of a pixel is equal to 1 $\mu m$ . ....	51
Figure 3-18. Tumble motions (scape area) in two trajectories part (a) and (b) are detected and denoted with red circles. ....	52
Figure 3-19. Probability distribution of the ensemble-averaged mean-squared displacement (EMSD) along the x-axis for cells exposed to the light of the laser pointer and normal lighting conditions.....	54

Figure 3-20. Probability distribution of the ensemble-averaged mean-squared displacement (EMSD) along the x-axis for cells exposed to the light of LED and normal lighting conditions. ....	55
Figure 3-21. The variation of ensembled-averaged velocity with time for cells exposed to the a) white LED light b) laser pointer red light c) normal lighting condition. The colored areas demonstrate $\pm$ standard deviation.....	56
Figure 3-22. Superposition of the variation of ensembled-averaged velocity with time for cells exposed to a) white LED light and normal lighting condition b) laser pointer red light and normal lighting condition c) white LED light and laser pointer red light. The colored areas demonstrate $\pm$ standard deviation.....	57
Figure 3-23. Frequency of interactions for cells exposed to the light of laser pointer .....	59
Figure 3-24. Frequency of interactions for cells exposed to the light of LED .....	60
Figure 3-25. Mean of the total frequency of interactions in different lighting conditions. ....	61
Figure B-1. Scale and micropipette used for calculating density .....	77
Figure B-2. Sylgard 184 Silicone Elastomer Kit including a) Base and b) Curing agent .....	77
Figure B-3. a) Thermo Scientific™ Sorvall™ Legend™ XT/XF Centrifuge, US b) Thermo Scientific™, SPECTRONIC™ 200 Spectrophotometer, US. ....	78

## List of Appendices

Appendix A.....	76
Appendix B.....	77
Appendix C.....	78
Appendix D.....	80
Appendix E.....	81

## List of Abbreviations, Symbols, Nomenclatures

<b><math>K_e</math></b>	growth rate ( $d^{-1}$ )
<b><math>k</math></b>	doubling per day ( $d^{-1}$ )
<b><math>N</math></b>	rotation speed (Hz)
<b><math>b</math></b>	width of magnetic bar (mm)
<b><math>d</math></b>	length of magnetic bar (mm)
<b><math>D</math></b>	reactor inner diameter (mm)
<b><math>H</math></b>	liquid height in a vessel (mm)
<b><math>N_p</math></b>	power number
<b><math>P</math></b>	power (W)
<b><math>Re_d</math></b>	impeller Reynolds number
<b><math>\eta</math></b>	viscosity (mPa.s)
<b><math>\eta'</math></b>	viscosity history (mPa.s)
<b><math>\tau</math></b>	shear stress (Pa)
<b><math>\dot{\gamma}</math></b>	shear rate ( $s^{-1}$ )
<b>rpm</b>	rotation per minutes
<b>n</b>	speed of rotation (rpm)
<b><math>\phi</math></b>	volume fraction
<b><math>\omega</math></b>	rates od rotation (rpm)
<b>PBR</b>	photobioreactor
<b>APBR</b>	agitated photobioreactor
<b>DPBR</b>	draft tube airlift photobioreactor
<b><math>l_{run}</math></b>	distance traveled during a run ( $\mu m$ )
<b><math>\tau_{run}</math></b>	run duration (s)
<b><math>\tau_{tumble}</math></b>	tumble duration (s)
<b><math>d_{min}</math></b>	diameter of scape area ( $\mu m^2$ )
<b>t</b>	time (s)
<b>EMSD</b>	ensemble mean square displacement ( $\mu m^2$ )

# Chapter 1

## 1 « Introduction »

### 1.1 Overview

Photosynthetic micro-algae and cyanobacteria can be used as feedstock to produce 3<sup>rd</sup> generation biofuels. They do not need the food crops or arable land for their production and can use solar energy to convert inorganic carbon (e.g., CO<sub>2</sub>) to biomass and support their metabolism [1]. Moreover, they can propagate and survive in various climates and have a comparatively constant production rate [2]. Biofuels obtained from such sources are considered a sustainable alternative to fossil fuels, and on an area basis, are 15- 300 times more efficient than traditional crops [3]. High-value products, including pigments (chlorophyll (Chl<sub>a</sub>), carotenoids, and phycobilins such as phycocyanin (PC) and allophycocyanin) produced by different cyanobacteria, are important raw materials for food, cosmetics, and pharmaceutical products. They are utilized in chewing gum, beverages, confectionery, jelly, soft drinks, dairy products as food colorants as well as in lipstick, eyeliners, and sunscreen because of their strong coloring, fluorescent, and antioxidant properties [4, 5, 6, 7, 8, 9, 10].

In the environment and industrial applications, the microorganisms are in the form of suspension which is called “living” or “active fluid”. Active fluid is a fluid whose constituent elements can self-propel. Suspensions of microorganisms like bacteria, algae, and sperm cells are examples of active fluid. Active fluids display properties that differ fundamentally from passive fluids. Contrary to conventional fluid flows in which one needs gradients of pressure, velocity, and temperature to break equilibrium and drive the flow, in active fluids, cells as the microstructural elements of the fluid convert the chemical energy of nutrients into mechanical energy for driving the flow. Therefore, microorganisms in active fluids can develop complex spontaneous fluid motions in the absence of external gradients. Active fluids exhibit remarkable physical phenomena over a wide range of scales, from microscopic diffusion and motility of microbial suspensions to the large-scale colonization of aqueous spaces.

From the environmental point of view preventing and/or controlling harmful algal blooms are of great importance. In recent years, technical reports [11, 12, 13] have reported tremendous

economic losses caused by harmful algal blooms affecting the fishing, recreation, and tourism industries.

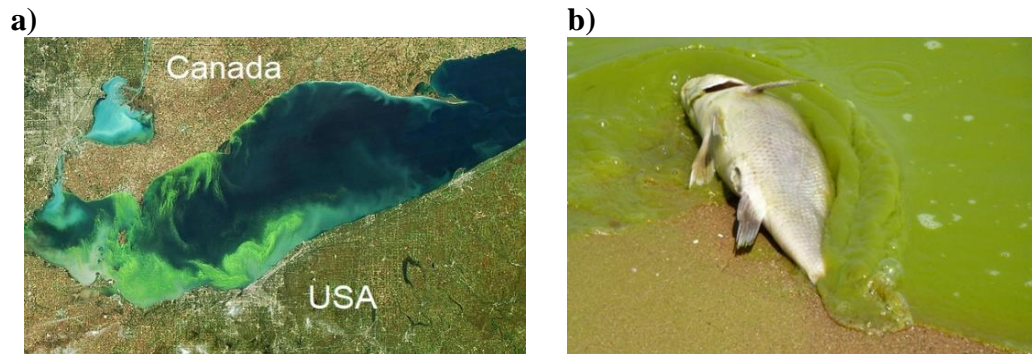


**Figure 1-1. a) Harmful algal bloom, Lake Erie b) Lake Erie algae bloom, the southeast shore of Pelee Island, Ontario [12].**

In biofuel production systems [14, 15, 16, 17, 18], it is crucial to understand the physical aspects of microorganisms' behavior, from cellular motility to stress effects on the mechanisms of division, growth, and size elongations. Moreover, designing and optimization of photobioreactors (PBRs) involve the interplay between fluid flow, microbe biokinetics [19], and radiative transport phenomena [20], in which the physical and rheological properties [21] of the active fluid play a fundamental role.

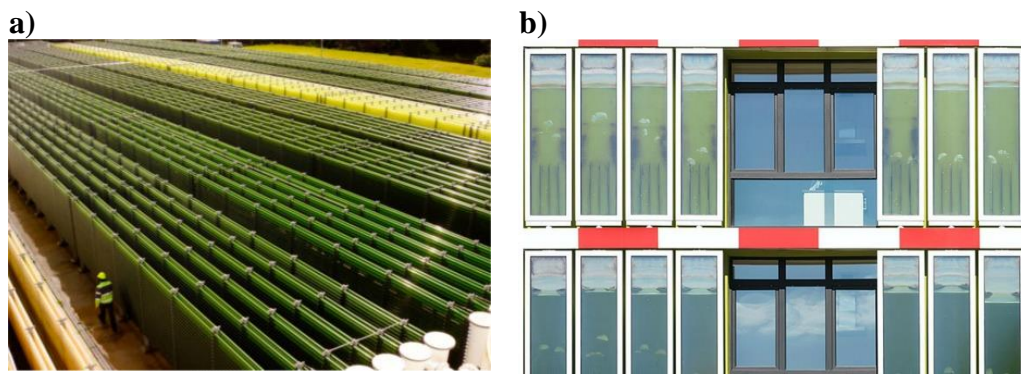


**Figure 1-2. a) A commercial plant of tubular manifold photobioreactors with vertical reactors located in Portugal [22] b) The BIQ clever treefrog house, Hamburg, Germany [23].**



Microorganisms can attach and grow on surfaces. As a result, in the food hygiene field [24], knowledge is essential for understanding the biofilm attachment and control on food contact surfaces.

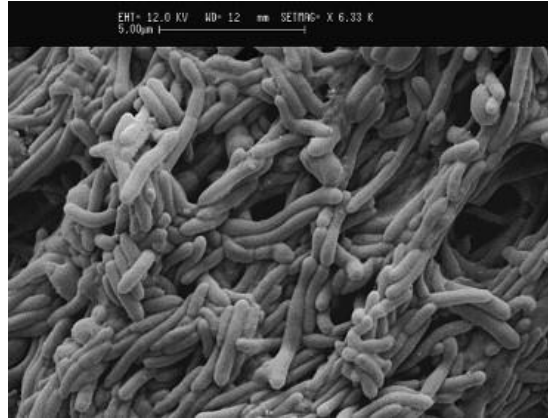


**Figure 1-3. The formation of *Bacillus cereus* on a stainless-steel surface. × 6330 magnification; scale bar = 5  $\mu\text{m}$  [25].**

In the biomedical industry [26], knowledge on the motility of cells sheds light on shutting down the motility of tumor cells that would largely prevent metastasis and thus can limit the spreading of cancers inside human bodies.

## 1.2 Cyanobacterium

In the current research work cyanobacterium *Synechocystis* sp. CPCC 534 was used as the model microorganism. Cyanobacteria is a phylum of bacteria that obtains its energy through photosynthesis. It is the only photosynthetic prokaryote<sup>1</sup> able to produce oxygen. Unlike

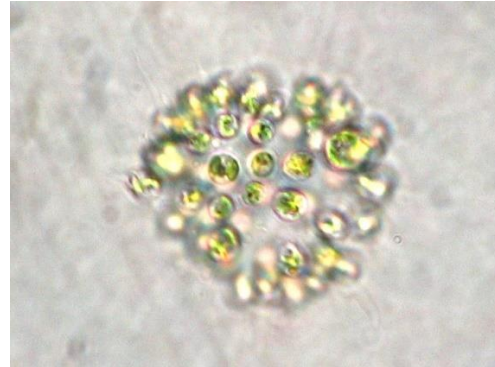
---

<sup>1</sup> Prokaryotes are unicellular organisms that consist of a single prokaryotic cell. Prokaryotic cells are simple cells that do not have a true nucleus or other cell organelles. Bacteria and Archaea are the two domains of life that are prokaryotes. Prokaryotes can be contrasted with eukaryotes, which have more complex eukaryotic cells with a nucleus and organelles. Eukaryotes include all complex multicellular organisms such as plants, animals, fungi, and protozoa. [113]

heterotrophic<sup>2</sup> prokaryotes, cyanobacteria have internal membranes which are flattened sacs called thylakoids where photosynthesis is performed (Figure 1-4).



*Aphanothece* [27]



*Microcystis aeriginosa* [28]



*Oscillatoria* [28]



*Nodularia spumigena* [28]

**Figure 1-4. Example of the different morphologies of cyanobacteria**

### 1.3 *Synechocystis* sp.

*Synechocystis* sp. PCC 6803 shown in Figure 1-5 is a unicellular, freshwater cyanobacterium with approximately 2-3  $\mu\text{m}$  cellular diameter [29]. Each cell typically has a thick, gelatinous cell wall [30]. It is capable of both phototrophic growth by oxygenic photosynthesis during light periods and heterotrophic growth by glycolysis and oxidative phosphorylation during dark periods. Reynolds number for such microorganisms with a density of  $1.1 \times 10^3 \text{ kg m}^{-3}$  and

---

<sup>2</sup> A heterotroph (/ˈhɛtərəˌtroʊf, -ˌtroʊf/) is an organism that cannot manufacture its own food by carbon fixation and therefore derives its intake of nutrition from other sources of organic carbon, mainly plant or animal matter. [113]

a diameter of 3  $\mu\text{m}$  are typically very low, of the order of magnitude of  $10^{-6}$ . When *Synechocystis* cells are not dividing, display a spherical shape and as a result, the diffusion coefficient remains a scalar.



**Figure 1-5. *Synechocystis* sp. [31]**

#### 1.4 Biofilm

In natural and even artificial environments bacteria live in self-organized, joined communities called biofilms [32]. Biofilm is masses of adherent cells embedded in slimy extracellular matrices which is essential to bacterial growth and survival to environmental stresses. In addition, the peripheral cells exposed to the noxious agents protect the internal cells. Biofilm also contributes to capturing nutrients in the vicinity of the cells (Figure 1-6). In the incipient stages of biofilm formation [32], bacteria move and attach to a wide range of surfaces. It is essential to understand the motility strategy of the microorganisms to identify the adhesion rate and clarify the subsequent colonization process. Biofilm formation is a major concern in health care or the food industry, but its control could also be profitable to photobioreactors design used in biofuel production and the bio-façade.

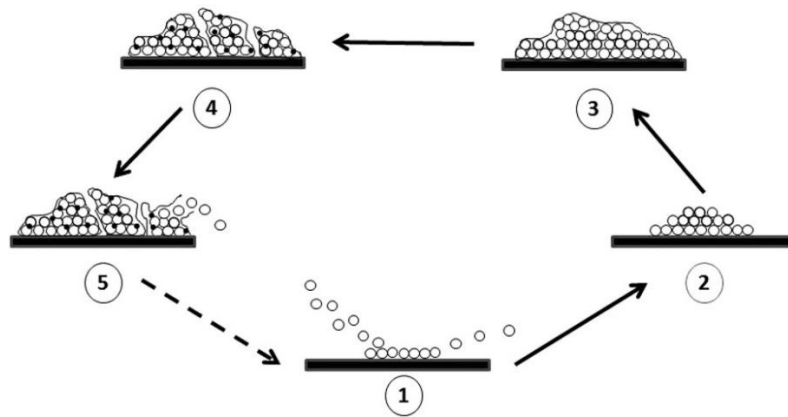


**Figure 1-6. A pictorial representation of microbial biofilm life cycle; Individual microbes: 1) Planktonic, Biofilm development: 2) Attachment 3) Growth 4) Maturity 5) Dispersion [33].**

### 1.5 Hydrodynamics of Microorganisms

Microorganisms have different modes of motility [34]. Among the most important of these are the four sketched in Figure 1-7. Except for swimming, all other modes are associated with the presence of a surface. Swimming at or near a surface involves one or more flagella.

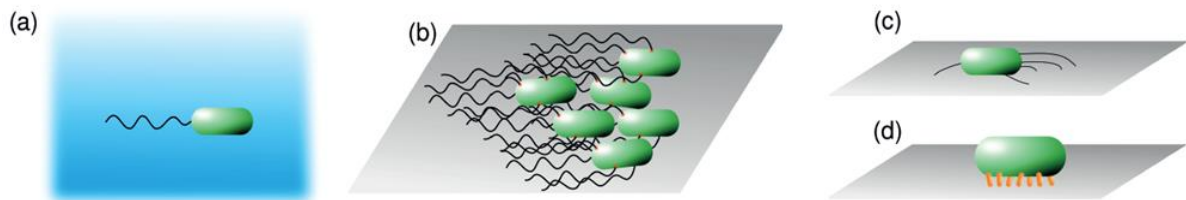


**Figure 1-7. (a) Swimming in a bulk fluid using single polar flagellum; (b) Swarming on a solid surface of bacteria in the hyperflagellated state; (c) twitching through type IV pili<sup>3</sup>; (d) gliding utilizing focal adhesion complexes [34].**

---

<sup>3</sup> A pilus (Latin for 'hair'; plural: pili) is a hair-like appendage found on the surface of many bacteria and archaea. Some pili, called type IV pili (T4P), generate motile forces. The external ends of the pili adhere to a solid substrate, either the surface to which the bacterium is attached or to other bacteria. Then, when the pili contract, they pull the bacterium forward like a grappling hook. Movement produced by type IV pili is typically jerky, so it is called twitching motility, as opposed to other forms of bacterial motility such as that produced by flagella. [114]

Figure 1-8 demonstrates a transmission electron microscopy (TEM) view of a *Synechocystis* surrounded by its type IV pili. It clearly shows the type IV pili, which look like long threads oriented in the radial direction. These cyanobacteria move thanks to their pili according to the twitching mode.

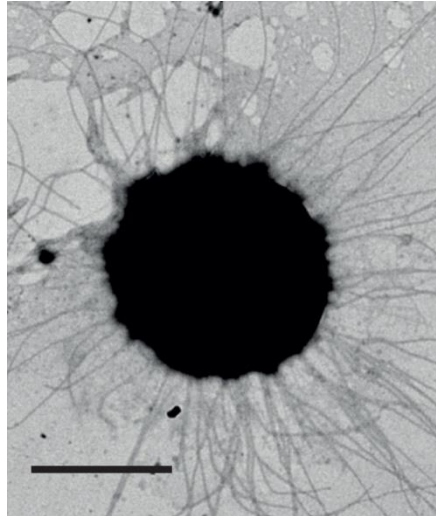


**Figure 1-8. A transmission electron micrograph (TEM) of *Synechocystis* surrounded by its type IV pili; scale bar = 1  $\mu\text{m}$  [35].**

Low-Reynolds number hydrodynamics is the most important part of the ability of flagella to produce propulsion at a microscale [36]. In a uniform chemical environment, bacteria move in a random-walk pattern, which is a type of motility with alternating immobile “tumble” and mobile “run” periods [29, 37]. Vourc’h et al. [29] have recently observed that the diffusion coefficient of *Synechocystis* sp. PCC 6803 on a solid-liquid interface in the dilute regime, tends to slow down with time.

Some high motility microorganisms show peculiar interactions with the motion of the continuous phase in which they travel. Of particular interest is the effect of this interaction in cell separation and cell sorting technology. Nguyen et al. [38] investigated the effect of pulsatile flow on the distribution of passive (non-motile) and active (motile) particles at the outlet of the double-Y microchannel, numerically and experimentally. Of special interest was to determine the effects of phase shift between two entering flows (only one includes the particles) into the Y channel on particle separation at the exit of the double-Y microchannel. The results showed that the separation of passive particles (dead cells of *Chlamydomonas*

*reinhardtii*) increases with the phase shift ( $\varphi$ ) when the velocity amplitude ratio ( $\beta$ ) was less than 2 and the highest efficiency was reached at  $\varphi = 180^\circ$ . If the pulsation period was short enough, a similar trend occurred for higher values of  $\beta$ . However, for motile particles (live *Chlamydomonas reinhardtii* cells) this effect was completely disappeared; motile cells randomly distributed at the exit of the double-Y microchannel.

## 1.6 Rheological Properties of Suspension of Microorganisms

Developing a 3<sup>rd</sup> generation of biofuels produced from microalga and cyanobacteria, which are generally more efficient in converting solar energy to biomass, have recently attracted much attention [14, 15, 16, 17, 18]. Biofuel production from photosynthetic microorganisms operates in aqueous suspensions of microorganisms which are cultivated in dedicated reactors referred to as photobioreactors (PBR). One of the crucial factors in PBR's operation and efficiency is proper mixing inside the vessel which is related directly to the hydrodynamic stress applied to microorganisms. The intensity of hydrodynamic stress dramatically affects the growth of microorganisms [39, 40, 41, 42, 43, 44, 45].

Although algal and bacterial suspensions have shown great potential as a source of high-value chemical products and biofuels, their physical and rheological properties have not been thoroughly studied. Hu et al. [18] used basic rheological analysis (i.e. variation in viscosity of microorganism suspensions at different stirring speeds) in order to provide a possible technical basis for assessing the effect of agitation on the growth rate and formation of high-value products. The red microalga *Porphyridium cruentum* was used as a model microorganism. The optimal agitation speed for increasing biomass concentration by about 19-57% was 150 rpm. Furthermore, the content of linoleic acid, arachidonic acid, and total fatty acids increased by a maximum of 103%, 58%, and 48%, respectively, compared with the micro-algae cultured at other agitation speeds.

In a thorough study on the suspensions of non-motile *Chlorella vulgaris* CCAP 211-19, Souliés et al. [46] observed several rheological regimes by a gradual increase in cell volume fractions. In this work, a Newtonian rheological behavior was noticed at low volume fractions of the suspensions while a shear thinning behavior was observed at intermediate values. Dependence on the volume fraction of the viscosity in these experiments was described by the Quemada

model [47] and the Simha model [48], respectively. For the largest values of the volume fraction, the suspensions exhibited an apparent yield stress behavior. Moreover, a thixotropic behavior was observed for the increment and decrement of stress ramps within this range of volume fractions.

Furthermore, to study the effects of cell motility, cell concentration and morphology on the rheological properties of microorganism suspensions, Cagney et al. [49] applied shear to the suspensions of *Tetraselmis chuii*, *Chlorella* sp., and *Phaeodactylum tricornutum* in a rotational rheometer. The range of shear was from 20 to 200  $s^{-1}$ , and the rheological measurements were fitted to the Herschel-Bulkley model. Moreover, both Einstein's equation and the Krieger-Dougherty model were employed to estimate the intrinsic viscosity; they agreed well for low concentrations. The intrinsic viscosity of *T. chuii* suspension showed less sensitivity to the cell concentration at high strain rates. Comparison of the rheology of motile and passive suspensions of *T. chuii* cells showed that for passive cell suspensions, the shear-thinning behavior was absent, and the effective viscosity was much lower. This confirms that the motility of *T. chuii* cells causes them to resist the flow. However, the *Chlorella* sp. suspensions demonstrated shear-thickening behavior, which was unexpected, especially in light of Souliés et al.'s [46] results. Investigations on the influence of the effective cell aspect ratio on the viscosity of cell suspensions indicated that there is a direct relationship between the cell aspect ratio and the intrinsic viscosity magnitude [49].

## 1.7 Cell-Cell Communication and Response to Environmental Change

Bacteria are social organisms [50, 51, 52] and can communicate with one another through a variety of chemical signals. Cell-cell communications make the bacteria able to organize their movement, growth, and biochemical activities. One of the best-studied cell-cell communication systems in bacteria is quorum sensing (QS) [53, 54, 55, 56] which is mediated by secretion and detection of small diffusible signaling molecules. When the concentration of these molecules reaches a threshold level, the cells respond to it and alter their gene expression and, consequently, their physiological activities.

On the surface, some bacteria can detect secreted trails of extracellular polysaccharides (EPS) and PsI exopolysaccharides and modify their motility. Vourc'h et al. [29] showed that



*Synechocystis* sp. PCC 6803 cells sense the EPS deposited on the surface, which triggers cellular changes that affect the temporal characteristics of the run and tumble motion.

In another study, Zhao et al. [57] reported that Psl trails guide exploration and microcolony formation in *Pseudomonas aeruginosa* biofilms. Both experiments and simulations indicated that the web of secreted Psl controls the distribution of surface visit frequencies. They worked with the wild-type and mutant strain cells which cannot produce Psl EPS. Interestingly, after a specific period, the surface coverage that showed bacterial trajectories for the wild type was about  $55 \pm 5 \%$  and for the mutant strain was about  $79 \pm 10 \%$ . It revealed that wild-type cells detected Psl trails deposited on the surface by other cells and followed the same trajectories instead of visiting fresh surfaces. In other words, Psl trails guide exploration and microcolony formation or distribution of surface visit frequencies.

Regarding microcolony formation, Vourc'h et al. [61] studied the clustering of *Synechocystis* sp. PCC 6803 into microcolonies by allowing bacteria to diffuse onto surfaces of different hardness and communicating with the others. Observations revealed that soft surfaces promote more microcolonies than hard ones. The model developed in this study suggested that the nature of the substrate only affects the motility and not cell-cell interactions.

Chemotaxis is the process by which bacterial cells migrate toward favorable chemicals and away from unfavorable ones. Mechanisms of chemotaxis [58] include “avoiding reaction” (or “shock reaction”), “phototaxis”, and “topotaxis”. The sensory mechanism and the signaling pathway that mediate bacterial chemotaxis have been the subject of many studies [59, 60, 61, 62, 63]. Long et al. [37] showed that *E. coli* cells respond to the gradient of chemoattractant in two ways, first by biasing their random-walk swimming pattern through the intracellular chemotaxis signaling and also by secretion of a chemical signal into the extracellular medium which is a mysterious communication signal transduction passageway.

The definition of phototaxis (phototactic response) is the behavior of cells in which they move toward or away from the light source [64]. This phenomenon was first recognized over a century ago. However, the mechanism by which such tiny cells can sense the direction of the light source has remained baffling. More functional and physiological studies accentuate a very



complicated control of cyanobacterial phototaxis through sensory proteins, histidine kinases, and response regulators [65].

The cyanobacterium *Synechocystis* sp. cell shows phototaxis and moves toward the light by means of Type IV pili and a phytochrome-like photoreceptor connected to a complex signal transduction pathway [66]. Phototaxis is linked with bacterial interaction and can generate mesoscopic finger-like instabilities [67]. Burriesci et al. [66] tracked and analyzed a large number of cells to probe the different phases of interaction in which cells progress through, before the development of fingerlike projections moving toward the light.

Schuerger et al. [68] showed that cyanobacterium *Synechocystis* sp. cell can measure light intensity and color with several photoreceptors. They observed that *Synechocystis* cells can sense the position of light source directly and accurately. The cells have the ability of directional light sensing because they function as spherical microlenses, so can recognize the light source and proceed towards it. These capabilities make spherical cyanobacteria probably the world's smallest and oldest example of a camera eye.

Many recent studies examined controlling the motility of bacteria knowing that light gradient can alter the collective movements of cells [69, 65, 70]. Vourc'h et al. [71] focused on the effect of the light perturbation on the diffusion coefficient of bacterial suspensions by tracking bacterial response to light stimuli under isotropic and non-isotropic conditions. They investigated the influence of illumination on the intermittent motility and found that the probability to be in the run state increases just after a rise in light intensity; this feature disappears after about 1 *hour*, and the initial probability of motility was recovered. When the light perturbation was anisotropic (directional), the characteristic time of runs was longer whatever the direction, similar to what was observed with isotropic conditions. Yet a collective motion toward the light source (phototaxis) was observed and showed that the bias emerges because of more frequent runs towards the light. This phototaxis phenomenon enables the controlling of microorganisms by light intensity and light direction.

## 1.8 Theoretical Grounds

Apart from experimental studies, many theoretical studies have been carried out on microorganisms' motility. For example, Bell [72] proposed a theoretical framework for the analysis of cells clinging to each other or of cells to surfaces when the attachment is mediated by reversible bonds between specific molecules. Two models which were developed for predicting the rate of bond formation and between cells showed that the required force for separating two cells should be greater than the expected electrical forces between cells and of the same order of magnitude as forces required to pull special molecules and proteins out of the cell membrane.

In 1992, Pedley et al. [73] summarized the progress made in understanding the nonlinear dynamical system of the concentrated population of suspended cells, tracing the thread from individual to collective dynamics. Dunkel et al. [74] argued that the phenomenology of active states (self-sustained dynamical phases of living matter) could be efficiently described in terms of fourth- and higher-order partial differential equations. They illustrated the idea through numerical simulations for two classes of continuum models for incompressible active fluids. In another study, Dunkel et al. [75] did experiments on active turbulence in highly concentrated 3-dimensional suspensions of *Bacillus subtilis* and compared the results with a minimal fourth-order vector-field theory for incompressible bacterial dynamics. Fluid dynamic forces affect a wide variety of aspects of bacteriology, ranging from cells' ability to reorient and search their surroundings to their communication within mechanically and chemically complex environments. Lauga [36] reviewed the biomechanics of bacterial motility by using hydrodynamics as an organizing framework.

## 1.9 Motivation and Contributions

A wide range of model organisms has been studied to investigate fundamental phenomena in biological fluid dynamics [76] and also physical and rheological behavior [46, 49, 77, 78, 79]. Among those species, *Synechocystis* sp. was used for the current research work because its genome is completely identified [80]. In addition, *Synechocystis* sp. CPCC 534 strain (rather than *Synechocystis* sp. PCC 6803) was used because it is available in Canada knowing that

previous research has shown that the global behavior of different strains of *Synechocystis* sp. is very similar [81].

As it is discussed under the heading “Rheological Properties of Suspension of Microorganisms”, rheological behavior of algal slurries such as *Chlorella* sp. [46, 77, 78], *Tetraselmis chuii* [46], *Phaedactylum tricornutum* [49, 78], and *Nannochloris* sp. [78], *Chlamydomonas reinhardtii* [79] have been studied. However, to the authors’ knowledge, there is no rheological data on the behavior of *Synechocystis* suspensions in the open literature. *Synechocystis* cell is almost spherical, non-flagellate, low motility, and suitable for studying near-surface motility. These characteristics make it comparatively different from the aforementioned species studied in the literature. This was the motivation for the research work presented in chapter 2.

As discussed under the heading “Cell-Cell Communication and Response to Environmental Change”, the phototaxis behavior of *Synechocystis* sp. has been studied [66, 67, 68, 69, 70, 71]. Because individual bacterial motility has a large random component, bacterial behavior is usually assessed using population-level assays that average over the behavior of thousands or millions of individuals. While these approaches are highly sensitive and precise in detecting small phototactic effects, they are blind to the underlying behavioral mechanisms. Almost all previous studies performed experiments on cells on agar surfaces and not on suspensions of cells. While highly diluted suspensions can provide a greater level of insight into the understanding of the link between individual motility and the overall dynamics of cells in quiescent conditions. Moreover, in previous studies, they did not examine the adaptation of motility of cells and cell-cell interaction to local lighting conditions (like a single dot). The research work presented in chapter 3 was an effort to fill these gaps.

## 1.10 Organization of the Thesis

This thesis follows the “monograph” format as per the thesis submission requirement of Western University.

Chapter 1 introduces photosynthetic microalgae, cyanobacteria, and active fluids, the importance and necessity of the knowledge, and its direct and indirect applications. The

introduction to cyanobacteria and *synechocystis* sp. sets the stage to explain the principal phenomenon of biofilm formation. Chapter 1 also includes the literature review of the hydrodynamics of microorganisms, the rheological properties of suspensions of microorganisms, and the models used for describing the behavior of the suspensions. Moreover, the experimental and theoretical studies on cell-cell communication and responses of microorganisms to environmental perturbations are reviewed. Finally, the motivation and contributions are presented.

Chapter 2 includes part of a paper published in the Journal of Fluid Engineering that investigates the physical and rheological properties of *synechocystis* sp. CPCC 534 suspension. The suspensions underwent shear stress, which was applied during cell growth. Experiments are conducted at three different stirring rates and the viscosity, cell size, biomass production, growth rate, and doubling per day of dilute suspensions of *Synechocystis* sp. CPCC 534 was measured and compared with the stationary condition. Moreover, the effects of cell concentration and cell motility on the rheological behavior of suspensions of *Synechocystis* sp. were examined.

The focus of Chapter 3 is on experiments carried out on highly diluted suspension of *Synechocystis* sp. CPCC 534 in a microfluidic chamber to investigate the response of cells to the light and cell-cell interactions. The cells were exposed to the light of a laser pointer (red light) and a white LED compared to ambient lighting (hereafter normal lighting condition). Cell tracking was performed by image processing in the Python programming language. In addition, the preliminary design and experimental setup of a multichannel microfluidic device are provided.

## Chapter 2

### 2 « Physical and Rheological Properties of *Synechocystis* sp. Suspension »

This chapter focuses on the effects of shear stress, which was applied during cell growth on the viscosity, biomass production, cell size, growth rate, and doubling per day of suspensions of *Synechocystis* sp. CPCC 534. Experiments were carried out at three different stirring rates in well-controlled conditions and the results were compared with stationary conditions where only molecular diffusion and cell motility govern the transport phenomena and biomass production. This work also endeavored to understand the effects of cell concentration and cell motility on the rheological behavior of suspensions of *Synechocystis*.

#### 2.1 Methods and Material

##### 2.1.1 Experiment Condition

*Synechocystis* sp. CPCC 534 was obtained from the Canadian Phycology Culture Centre (CPCC) and maintained in the BG-11 medium [82]. The composition of the BG11 is available in Table 2-1.

**Table 2-1. Composition of the BG11medium [82]**

Components	Concentration (mg/L)
NaNO <sub>3</sub>	1500
K <sub>2</sub> HPO <sub>4</sub>	30
MgSO <sub>4</sub> ·7H <sub>2</sub> O	75
CaCl <sub>2</sub> ·2H <sub>2</sub> O	36
Citric acid	6
Ferric citrate (C <sub>6</sub> H <sub>8</sub> FeNO <sub>7</sub> )	6
Na <sub>2</sub> EDTA·2H <sub>2</sub> O	1
Na <sub>2</sub> CO <sub>3</sub>	20
Trace Metal	See Table 2-2

**Table 2-2. Composition of trace metal solution [82]**

Components	Concentration (g/L)
H <sub>3</sub> BO <sub>3</sub>	2.86
MnCl <sub>2</sub> .4H <sub>2</sub> O	1.81
ZnSO <sub>4</sub> .7 H <sub>2</sub> O	0.222
Na <sub>2</sub> MoO <sub>4</sub> .2 H <sub>2</sub> O	0.390
CuSO <sub>4</sub> .5H <sub>2</sub> O	0.079
Co(NO <sub>3</sub> ) <sub>2</sub> .6H <sub>2</sub> O	0.0494

Experiments were performed in 500 ml Erlenmeyer flasks containing 250 ml culture and incubated at  $20 \pm 1$  °C under a light-dark cycle of 12:12 hours and light flux of  $70 \pm 10$   $\mu\text{mol photons m}^{-2} \text{s}^{-1}$ . Before the experiments, the cells were grown for 5-6 days (mid-exponential growth phase) and a constant inoculum of 500,000 cells.ml<sup>-1</sup> was transferred to each experimental flask.

### 2.1.2 Experimental Apparatus

Shear stress was applied to the working fluid (aqueous suspensions, as described in Experiment Condition) by generating a vortical flow in experimental flasks of 80 mm inner diameter. Magnetic stir bars with a diameter of 7.9 mm and a length of 19.8 mm were used to stir the bacterial suspension in the experimental flasks using a digitally controlled magnetic stirrer (VWR, Canada). The agitation speeds were set at 0, 450, 900, and 1500 rpm corresponding to 0, 7.5, 15, and 25 Hz, respectively (Figure 2-1).



**Figure 2-1. Left: Bacterial suspensions in flasks placed on magnetic stirrers (first day of the experiment); Right: Bacterial suspensions (final day of the experiment).**

To determine the average shear stress-induced on the working fluid by rotation of the stirring bars the theoretical procedure developed by Pérez *et al.* and Rushton *et al.* [83, 84] has been used (see Appendix A). This procedure gives the average shear rate as a function of rotation speed, fluid properties, and the geometrical parameters for turbulent flows using the following equations:

$$\gamma = N^{\frac{3}{2}} \cdot \left( \frac{4N_p \rho d^2}{27\pi d} \right)^{\frac{1}{2}} = \beta \cdot N^{\frac{3}{2}} \quad \text{Equation 2-1}$$

Where  $N_p = \frac{P}{\rho N^3 d^5}$  Equation 2-2

$$Re_d = \frac{\rho N d^2}{\eta} \quad \text{Equation 2-3}$$

Here  $\gamma$  is the average shear rate,  $N$  is the rotation speed (Hz),  $N_p$  is the power number,  $P$  is the input power,  $d$  is the diameter of the magnetic stirring bars,  $\eta$  and  $\rho$  are respectively the viscosity and density of the fluid, and  $Re_d$  is the corresponding impeller Reynolds number. The Erlenmeyer flask is assumed as the reactor of inner diameter  $D = 80$  mm, and a magnetic stirring bar of a diameter of  $b=7.9$  mm and length of  $d=19.8$  mm was used; the liquid height  $H$  was equal to 35 mm.

The impeller Reynolds number  $Re_d$ , has been calculated by using Equation 2-3 and exhibited in Figure 2-2 varies between 10,000 and 30,000. The flow is therefore turbulent, consistent with the assumptions of Equation 2-1.

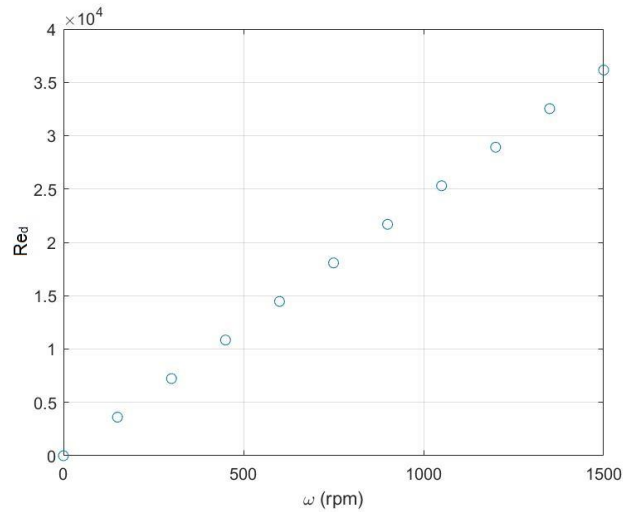


**Figure 2-2. Reynolds number as a function of rotation speed.**

To determine the magnitude of the average shear rate  $\dot{\gamma}$  in Equation 2-1, the power number  $N_p$  was needed, so the power consumption  $P$  is required for calculating  $N_p$  using Equation 2-2. Since determining the power input inside the reactor was impossible, empirical correlations developed for propeller and Pfaudler-type impellers in agitated reactors were used [85, 86] and solved by MATLAB. The equations are available in Appendix A.

The variation of  $N_p$  as a function of rotation speed  $N$ (Hz) is presented in Figure 2-3.

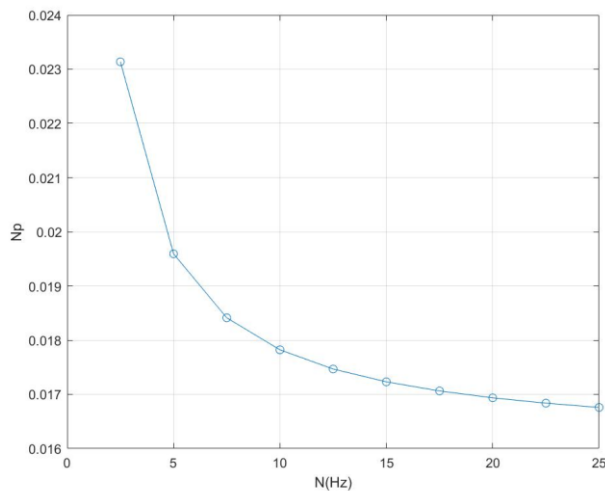


**Figure 2-3. Power number as a function of rotation speed.**



After calculating  $\beta$  for different values of  $N_p$  corresponding to each agitation rotation speed  $N$ , the average shear rate  $\dot{\gamma}$  was determined using Equation 2-1. Then the average shear stress  $\tau$  is obtained from Equation 2-4.

$$\eta = \tau / \dot{\gamma} \quad \text{Equation 2-4}$$

The relationship between the average shear stress and rotation speed  $N$  is plotted in Figure 2-4.

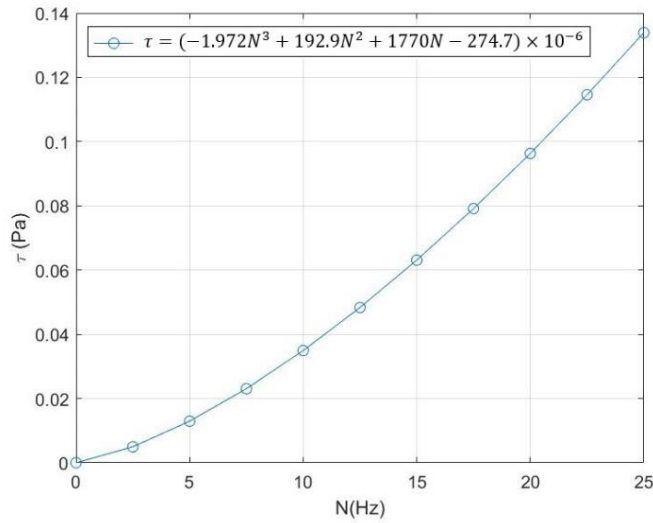


**Figure 2-4. Average shear stress (Pa) as a function of rotation speed induced in the agitated reactors.**

It is worth mentioning, the stirring generated waves which energy may increase the temperature that was ignored. Moreover, the possible effect of air on bacteria is not taken into account.

### 2.1.3 Measurement of Bacterial Growth Rate ( $K_e$ )

To measure the culture growth, the cell density was measured at an absorbance wavelength of 750 nm which corresponds to particle density [87], using a spectrophotometer (see Appendix B Figure B-3 (b)). The calibration curve in Equation 2-5 has been established between the measured optical density and cell numbers ( $\text{cells} \cdot \text{ml}^{-1}$ ) using a hemocytometer count.

$$\text{Absorbance @ 750 nm} = 0.0163 (\text{Cell/ml} * 10^6) + 0.0123, \quad (R^2 = 0.9996) \quad \text{Equation 2-5}$$

The increase of cell density (cells per unit time) in the exponential growth phase is proportional to the number of cells present in the culture at the beginning of any unit of time. To put it another way, the population growth follows Equation 2-6 ( $r$  represents the exponential growth rate of the population, equal to “ $K_e$ ” by Guillard [88]):

$$\frac{dn}{dt} = rN \quad \text{Equation 2-6}$$

The solution of Equation 2-6 is:

$$N_t = N_0 e^{rt} \quad \text{Equation 2-7}$$

where  $N_0$  is the population size at the beginning of a time span,  $N_t$  is the population size at the end of the time span, and  $r$  ( $t^{-1}$ ) is the populational rate of change. The solution of Equation 2-7 for  $r$  gives:

$$r = \frac{\ln(N_t/N_0)}{\Delta t} = \frac{\ln(N_t) - \ln(N_0)}{\Delta t} \quad \text{Equation 2-8}$$

where  $\Delta t$  is the length of the time span ( $t_t - t_0$ ), so the the specific growth rate ( $K_e$ ) is presented as [89]:

$$K_e = \frac{\ln(N_t) - \ln(N_0)}{(t_t - t_0)} \quad \text{Equation 2-9}$$

The growth rate  $K_e$  can be used to calculate the number of cell divisions per day, known as doubling per day ( $k$ ), using the following equation [88]:

$$k = K_e / \ln 2 = K_e / 0.6931 \quad \text{Equation 2-10}$$

Cell yield of *Synechocystis* sp. CPCC 534 was determined at the early stationary phase of the growth curve.

#### 2.1.4 Viscosity Measurement of *Synechocystis* Suspensions

In this chapter “viscosity” shall be used to refer to the “effective viscosity” which is the global rheological measure of a suspension sample’s properties; the local viscosity experienced by a bacterium is equal to the viscosity of the surrounding culture medium in the suspension.

A Cannon-Ubbelohde viscometer (Cannon Instrument Company) shown in Figure 2-5 was used to measure the viscosity of the bacterial samples. The glass tube was filled with a 12 ml sample at 20 °C and placed into the holder. Suction was applied until the sample reached the top of the red line of the top bulb and the time of the descent between two sets of fiduciary lines was measured.

During the experiments, care was taken to ensure that no air bubbles were created. The suspension viscosity was calculated using the following equation:

$$\eta = K\rho t \quad \text{Equation 2-11}$$

where  $\eta$  is the viscosity (cp) of the cell suspension,  $\rho$  is the density of bacterial cell suspension and it is equal to 1.005875 (gm.ml<sup>-1</sup>),  $t$  is the time of descent (s), and  $K$  is viscometer constant (0.004447 (cST.s-1)).

The viscometer constant is the same at all temperatures. More detail on the precision of the viscometer and the kinematic viscosity range is available in Table 2-3.

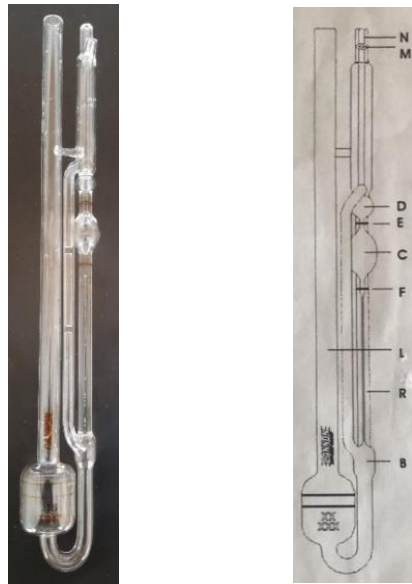


**Figure 2-5. Cannon-Ubbelohde viscometer**

**Table 2-3. Cannon-Ubbelohde viscometer information**

Size 50		Serial Number C158	
Constant	Expanded Uncertainty (k=2)	Kinematic Viscosity Range	
mm <sup>2</sup> /s <sup>2</sup> , (cSt/s)	%	mm <sup>2</sup> /s, (cSt)	
0.004447	0.16	0.8-4	

The sample density was calculated using the following equation using the scale (Sartorius, United States) and micropipette (VMR, United States) shown in Figure B-1 in Appendix B.

$$\rho = \frac{m}{V} \quad \text{Equation 2-12}$$

Finally, the samples' viscosity  $\eta$  (*mPa.s*) has been obtained using Equation 2-13.

$$\eta = \rho\nu \quad \text{Equation 2-13}$$

To evaluate the effects of cell concentration on the rheological behavior (Newtonian or non-Newtonian) of the suspensions of *Synechocystis* sp. CPCC 534, the viscosity for samples of different volume fractions was also measured by an Anton-Paar Modular Compact Rheometer (MCR302, Austria) with a concentric cylinder geometry displayed in Figure 2-6.

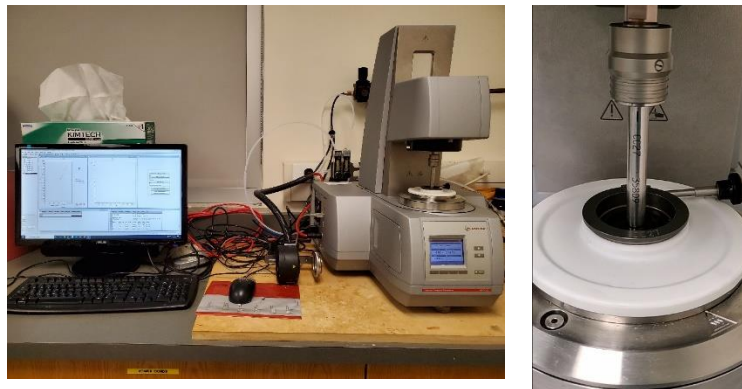


**Figure 2-6. AntonPaar Rheometer and the attachment used**

The diameters of the inner and outer cylinders were 22 *mm* and 26 *mm*, respectively. The temperature was maintained at 20 °C during all experiments. Samples of cell suspensions were centrifuged at 2700 *g* for 20 minutes (see Appendix B Figure B-3(a)) and supernatants were collected for diluting the pellets in the next step. The viscosity of suspensions was studied in

two series of experiments, called experiment series 1 and 2, which were carried out on two different cultures of *Synechocystis* sp. CPCC 534, prepared according to the same protocol. Suspension samples with known volume fractions (1.25, 2.5, 5, 7.5, 10, 12.5, 15, 17.5, and 20%) were prepared in each series by diluting the pellets with the collected supernatant. Approximately 20 ml of samples with different volume fractions were poured into the cylinder to perform the experiments. Measurements were carried out for shear rates in the range of 50 – 100  $s^{-1}$ . The rheometer was insensitive below 50  $s^{-1}$  since the suspension viscosity was very close to that of water.

It is worth mentioning, there were 6 failed trial experiments in which different viscometers and rheometers were used but the results were not satisfactory enough mainly because of the reason that the samples' viscosity was not in the accuracy range of the device. At first, some preliminary measurements were performed with a type of plate rheometer and a small sample adapter laboratory viscometer (AMETEK Brookfield). Then a falling-ball viscometer (Gilmont Instruments) with a glass ball and tube, Cannon-Fenske viscometer (Cannon Instrument Company), and Cannon-Ubbelohde viscometer size 75 (Cannon Instrument Company) were utilized. More details on all these trials are brought in Appendix C.

#### 2.1.4.1 Cell size measurement

To determine the size of *Synechocystis* cells following exposure to shear, cells were observed using an Imager Z1 Zeiss Microscope and the data were analyzed using Digimizer software.

#### 2.1.4.2 Statistical analysis

A one-way ANOVA was used to investigate the significant differences in growth, doubling per day, yield. Statistical analyses were performed using OriginPro 2017 (OriginLab Corporation, Northampton, MA, USA), and  $p < 0.05$  was considered significant.

## 2.2 Results and Discussion

### 2.2.1 Effects of Shear on Biomass Production

During the exponential growth phase and in the presence of sufficient light, cell density increases as a result of nutrient up-take [90]. The growth rate and doubling per day were calculated during this phase for samples subjected to different average shear stresses and

plotted in Figure 2-7 (a) and (b). The results revealed a significant difference between the cultures grown under stationary conditions and those grown under shear ( $p < 0.05$ ). Exerting turbulent shear stress on the cultural system and causing the suspension to be mixed, improved the growth rate as well as doubling per day in comparison with the stationary condition where only molecular diffusion and cell motility govern the transport phenomena and nutrient uptake.

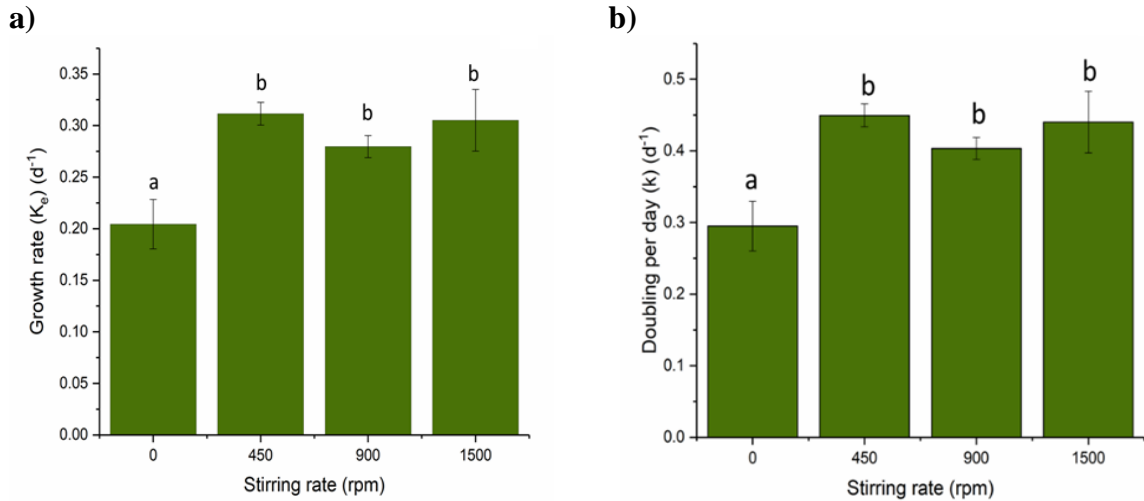


**Figure 2-7. Profiles of a) growth rate ( $K_e$ ) and b) doubling per day ( $k$ ) for *Synechocystis* sp. CPCC 534 under different stirring rates. Similar lower-case letters indicate no significant effect at the level of  $p = 0.05$  among different stirring rates. Values are expressed as means  $\pm$  standard deviation.**

The data suggest that adding stirring causes a change but increasing the stirring rate does not. Therefore, for the range of the mixing intensities considered in this study, the cells grow faster, but the amount of mixing does not make a significant change in the growth rate and doubling per day. However, it was reported that *Synechocystis* sp. cell growth is collapsed when cells were subjected to shear stress over  $0.35 Pa$  [90]. Increasing the stirring rate in this study did not show any significant variation in the growth and doubling per day, suggesting that *Synechocystis* cells are highly shear resistant microorganisms. This is likely due to their pseudo-spherical shape, small size ( $1-3 \mu m$ ), and low motility ( $1-3 \mu m \cdot s^{-1}$ ), which makes them less sensitive to friction forces and shear stress [91]. Similar results were reported for *Synechocystis* sp. PCC 6803 for shear rates up to  $900 rpm$  [91].

Biomass production is a proxy for autotrophic cultivation in the bacteria system while it is often limited by light deficiency due to the shading of the cells which leads to low biomass yield [92]. Light as an energy source is required for the cell's maintenance and growth [93]. Mixing intensification is one of the best strategies to enhance cell exposure to light and increase biomass yield from solar radiation [94]. Moreover, sufficient mixing of continuous phase fluid assists each cell to have more contact with nutrients, and CO<sub>2</sub> [95]. Our results presented greater biomass and therefore yield production due to the addition of shear stress to the cultures ( $p < 0.05$ ), as is shown in Figure 2-8-A and Figure 2-8-B. These results suggest that the better mixing that results in the cases with increased shear to improved nutrient uptake and light and CO<sub>2</sub> utilization by the cells. Due to experimental limitations, the impacts of other parameters such as light, temperature, nutrients, CO<sub>2</sub> concentration were not measured in this study. However, each of these parameters and their interaction with one another and combined with stirring rate can play a crucial role in biomass and other valuable products [96].

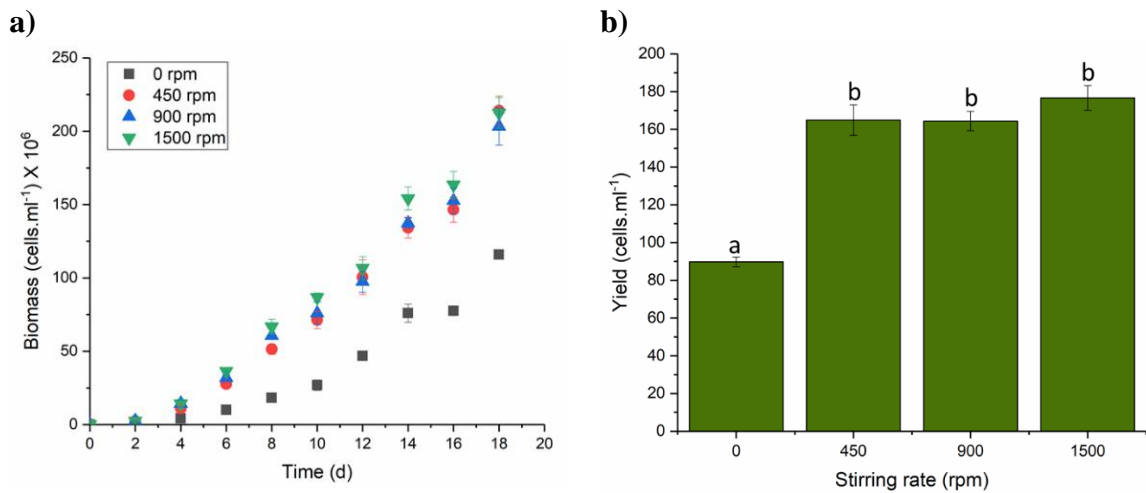


**Figure 2-8. Profiles of a) biomass production and b) yield for *Synechocystis* sp. CPCC 534 under various shear rates. The same lowercase letters indicate no significant effect at the level of 0.05 among different shear rates. Values are expressed as means  $\pm$  standard deviation.**

### 2.2.2 Effects of Shear on the Cell Size

The cellular size of microorganisms can impact the ecophysiological traits of the cell such as metabolic rate, growth, nutrient uptake, light absorption. [97, 98, 99]. To investigate the impact

of stirring rate on the size of *Synechocystis* sp. CPCC 534 the cells were imaged observed under a 20X objective lens, and then the images were analyzed. The results demonstrated two features. First, the addition of shear stress into the culture system reduced the cellular size of *Synechocystis* cells compared to those grown in the static culture (Figure 2-9). For the stirring rates considered in this study, the smallest cell size of the cells was observed at the highest stirring rate; however, there are no significant differences among various stirring speeds. Second, in 5-6 days (mid-exponential growth phase), cell size was reduced as the cells aged, although this shrinkage is not statistically significant. We speculate that this might be due to the *ecophysiological* behavior of the cell. Cell size enlargement increases self-shading effects in a system with no mixing and reduces cell access to light. The addition of stirring and improving mixing enhanced the exposure of the cells to light and resulted in a smaller cell size. Moreover, the culture with the highest growth rate presented the smallest size of cells, which is directly in line with the previous finding that reported a negative correlation between cell size and growth rate [100]. The nutrient uptake in smaller cells is more efficient due to their higher specific surface area; besides, the addition of mixing may increase the advective transport of nutrients to the cell surface, which improves the nutrient uptake rate [97].

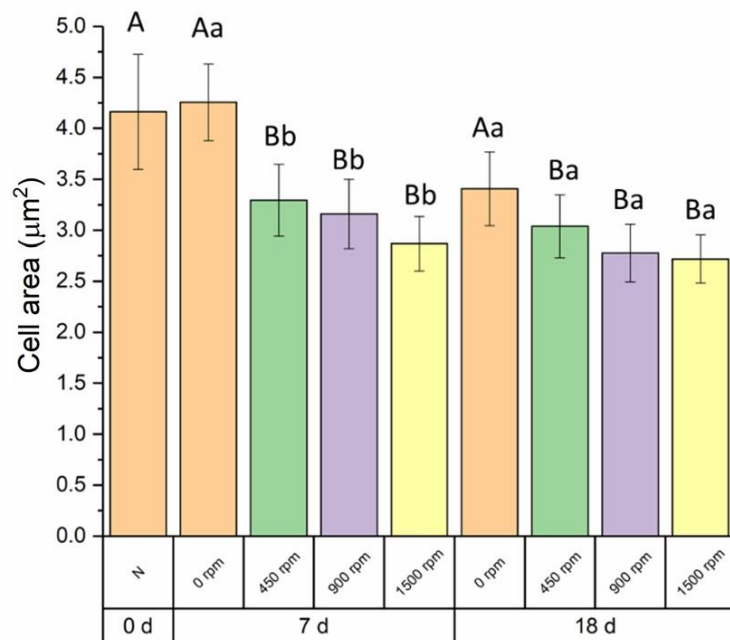


**Figure 2-9. Effect of stirring rate on the cell size of *Synechocystis* sp. CPCC 534. Similar uppercase letters indicate no significant effect for similar sample treatment**



**under different timelines. Similar lower-case letters indicate no significant effect among different treatments in the same timeline. Significance tested at  $p < 0.05$  level. Values are expressed as means  $\pm$  standard deviation.**

### 2.2.3 Rheology of *Synechocystis* Suspensions

This section focuses on the rheological behavior of dilute cell suspensions of *Synechocystis* with interest in the effects of cell shear history, cell concentration, and cell motility on this behavior. For this purpose, *Synechocystis* suspensions of different concentrations were pre-sheared by vortex stirring at 450, 900, and 1500 *rpm*, corresponding to average shear rates of 23, 63, and 134  $s^{-1}$ , until the cell growth reached the stationary state. Then suspension viscosity was measured. Measured viscosity,  $\eta$ , did not show an effect of shear history within the accuracy of measurements, implying that shearing had not changed the cell characteristics which could affect the rheological properties of the *Synechocystis* suspensions.

#### 2.2.3.1 Effects of cell volume fraction

We then investigated the dependence of viscosity on the bacterial volume fraction of suspensions. Volume fractions ranged between 0 % (culture medium) and 20 % corresponding to cell densities ranging from 0 to  $\sim 550 \times 10^6 \text{ cell.ml}^{-1}$  for unsheared suspensions. In the following, where it is justified, cell density is used instead of cell volume fraction for making it possible to compare the viscosities of suspensions with live and dead bacteria; this will be elaborated upon later. In Figure 2-10, the viscosity,  $\eta$  normalized by the viscosity  $\eta_0$  of the culture medium, is plotted as a function of the cell density. This figure shows that suspension viscosity is an increasing function of volume fraction, as it is for a suspension of rigid passive particles. The linear dependence of normalized viscosity on cell density in Figure 2-10 is fitted to a linear function expressed below:

$$\eta = \eta_0 (1 + \beta\varphi) \quad \text{Equation 2-14}$$

where  $\eta$  and  $\eta_0$  are the suspension and culture-medium viscosities respectively  $\varphi$  is the cell density (expressed in  $\text{cell.ml}^{-1}$ ) and  $\beta$  is the linear proportionality factor.

It has been shown that suspensions of dilute ( $\phi < 1-2\%$ ) passive spherical rigid particles have a concentration-dependent viscosity. Einstein (1906, and corrected 1911) [101, 102] derived an analytical solution for the flow of solvent around the spherical particles, which yields:

$$\eta = \eta_0 (1 + \alpha\phi) \quad \text{Equation 2-15}$$

where  $\eta$  and  $\eta_0$  are the suspension and the solvent viscosity, respectively,  $\phi$  is the solid fraction (expressed in volume fraction, %), and  $\alpha$  is called ‘‘Einstein’s intrinsic viscosity’’ which takes on a value of 2.5 for rigid spherical particles. In the present experiments, we found  $\beta$  (the equivalent of  $\alpha$  in Einstein’s equation) between 0.3 and 0.4 for different volume fractions which are lower than Einstein’s intrinsic viscosity value. The smaller increases in viscosity with cell volume fraction, compared to the one predicted for a suspension of hard spheres, can be attributed to the fact that particles in this study are soft and deformable; thus, some of the energy of the flow is dissipated through deformation of the cells. This decreases energy dissipated by hydrodynamic interactions compared to hard spheres, so the viscosity is less than it would be for hard spheres.

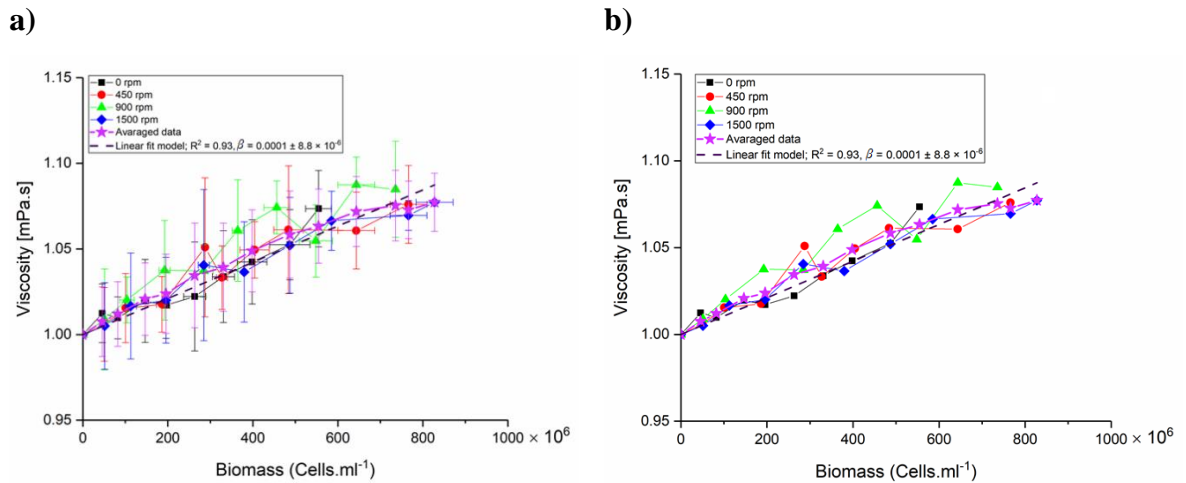


**Figure 2-10. a) *Synechocystis* sp. CPCC 534 viscosity as a function of biomass concentration (cell density), and under various stirring rates. b) Same plot without error bars**

### 2.2.3.2 Newtonian or non-Newtonian?

To assess the Newtonian or non-Newtonian behavior of *Synechocystis* suspensions the suspension viscosity was measured as a function of the imposed shear rate, for different cell volume fractions by the Anton-Paar rheometer, the results of which are shown in Figure 2-11.

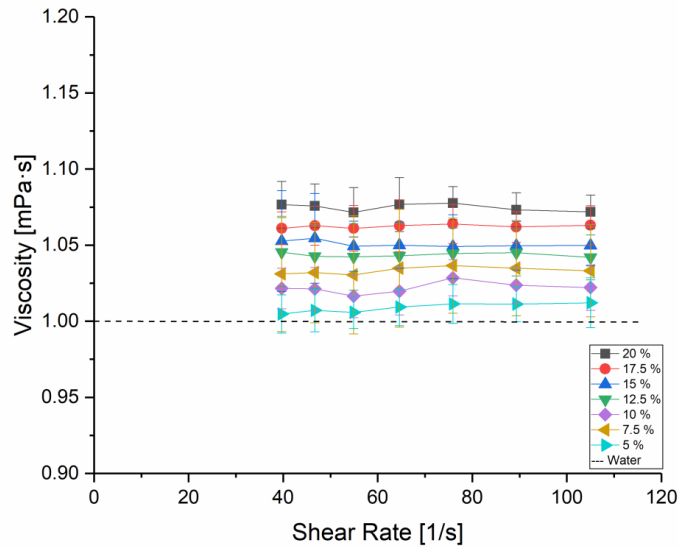


**Figure 2-11. Normalized viscosity of suspensions of *Synechocystis* sp. CPCC 534 as a function of shear rate for different cell volume fractions.**

The viscosity shows no variation under the imposed shear rate, which implies Newtonian behavior of the suspensions. To the authors' knowledge, there is no rheological data on the behavior of *Synechocystis* suspensions in the open literature for comparison. However, rheological behavior of several algal slurries such as *Chlorella* sp. [46, 77, 78], *Tetraselmis chuii* [46], *Phaedactylum tricornutum* [49, 78], and *Nannochloris* sp. [78] have been studied. Among those species, the alga *Chlorella* sp. has more similarities to *Synechocystis*; it is almost spherical, non-flagellate, and has low motility (though higher than *Synechocystis*) 3 to 4 times larger than *Synechocystis*. Souliès *et al.* [46] examined suspensions of *Chlorella vulgaris* at very low shear stress (10 – 100 *mPa*). They observed that the rheology was Newtonian, similar to the present study, for cell volume fractions  $\phi = 8.2\%$ , and shear thinning for  $\phi = 16.5\%$ . Cagney *et al.* [49] found a suspension of *Chlorella* sp. ( $\phi = 10\%$  and  $20\%$ ) was shear-thinning at low shear rates and shear thickening at higher shear rates. The underlying physical

mechanism for the rheological behavior of microorganism suspensions is not clear yet and needs more local viscosity measurements under shear and also microscopic observation of the microorganism orientation with implied shear field direction.

#### 2.2.3.3 Effects of Cell Motility

Samples of different volume fractions (0 to 20%) were prepared, and the viscosity was measured for both live and dead-cell suspensions using Anton-Paar and Cannon- Ubbelohde rheometers. Dead suspensions were obtained by adding 10% of H<sub>2</sub>O<sub>2</sub> to live suspensions of the same volume fraction. Experiments were run twice with the Anton-Paar rheometer and four times with Cannon-Ubbelohde for each concentration. Before experiments, the dead-cell and live-cell suspensions were observed under a 20X objective lens microscope to verify the difference between the morphology of samples; Figure 2-12 shows microscopic images of a live-cell and a dead-cell sample.

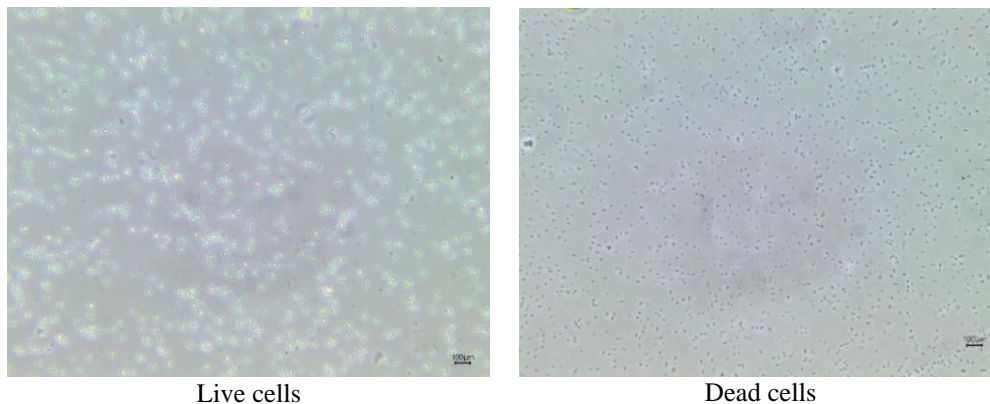


**Figure 2-12. Micrographs of suspensions of live and dead *Synechocystis* sp. CPCC 534.**

Figure 2-12 shows that cells shrink after bleaching and therefore, for the same cell population per unit volume of suspension (cell density) the cell volume fraction is smaller for the dead samples. Thus, for comparing the variation of the viscosity of live cell and dead cell samples, “cell density” was used rather than “cell volume fraction”. Figure 2-13 shows the variation of the normalized viscosity with shear rates for live-cell and dead-cell suspensions. Each data point is the average of two assays.

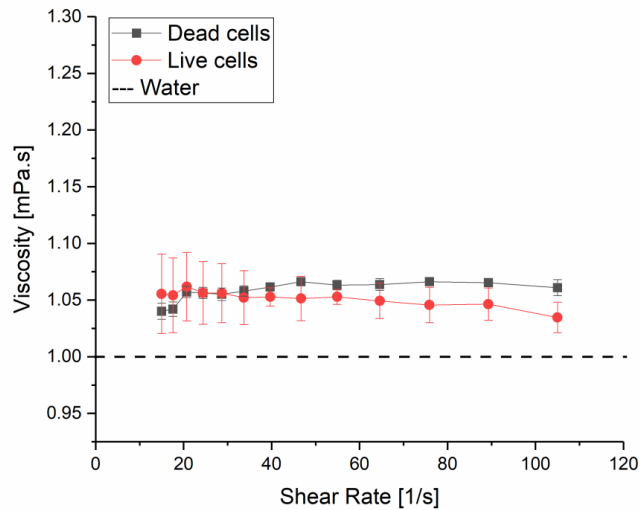


**Figure 2-13. Variation of averaged normalized viscosity as a function of shear rate for the suspensions of live and dead *Synechocystis* sp. CPCC 534.**

Figure 2-13 shows that the suspension behaves as a Newtonian fluid in both cases (live and dead cells), and the normalized viscosity of live and dead suspensions are equal within the measurement accuracy. Rafäi *et al.* [79] measured the viscosity of suspensions of live and dead *Chlamydomonas reinhardtii* as a function of cell volume fraction. They showed that the relative viscosity ( $(\eta - \eta_0) / \eta_0$ ) of live suspensions was quantitatively higher than that of dead suspensions; this observation is different from ours for suspensions of *Synechocysts*. While the viscosity of dead suspensions, in Rafäi *et al.*'s [79] experiments, followed Kreiger and Dougherty's semi-empirical law [103] for suspensions of passive rigid particles, the viscosity of the live suspensions did not. These authors attributed the difference to the effects of *Chlamydomonas reinhardtii* motility. By imaging the cells, while they were subjected to a shear flow, they showed dead cells follow a regular rotation, as would passive spherical particles. However, live cells resisted the flow rotation most of the time and eventually flipped very rapidly. In the present study, *Synechocysts* is a low motility twitching (moving by sticking to solid surfaces and pulling by contraction) cell that has no means (flagella) to resist the flow rotation. Therefore, it behaves as soft deformable passive particles, and thus shows no difference between the viscosity of live and dead suspensions.

In Figure 2-14 the normalized viscosity is plotted as a function of cell density for unsheared live and dead-cell suspensions (from experiment series 2) as well as the averaged values of the normalized viscosity for pre-sheared live-cell suspensions from experiment series 1; the latter series was already plotted in Figure 2-10. The data shows that within the accuracy of measurements; live, dead, sheared and unsheared suspensions all have the same normalized viscosity value for a given cell density. Also, they show the same Newtonian trend of viscosity increase with cell density.

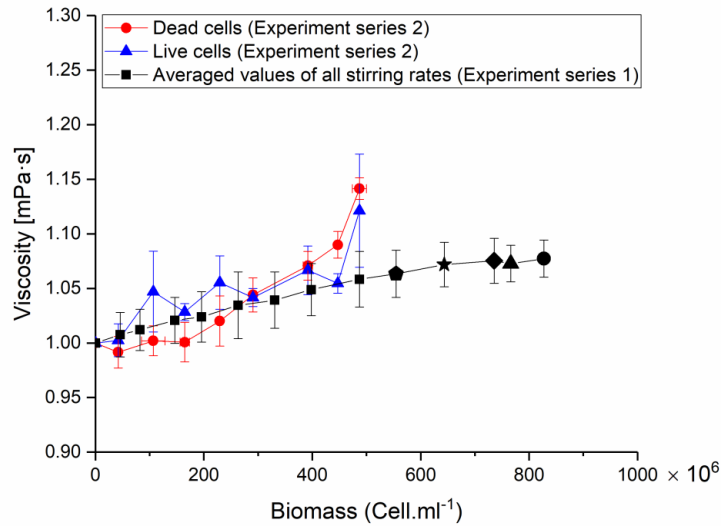


**Figure 2-14. Comparison of the variation of viscosity as a function of cell density for unsheared live and dead-cell suspensions as well as pre-sheared live-cell suspensions. Data for the first set of experiments extends to higher cell densities due to stirring.**

To obtain the general trend of the viscosity variation with cell density, the data in Figure 2-14 is averaged and plotted against the cell density in Figure 2-15. It is fitted to a linear correlation, which yields:

$$\eta = \eta_0 (1 + 0.0001 \varphi) \quad \text{Equation 2-16}$$

where,  $\eta$  and  $\eta_0$  are the suspension and the culture-medium viscosities, respectively, expressed in (mPa.s), and  $\varphi$  is the cell density (cell.ml<sup>-1</sup>), and  $\beta$  is the linear proportionality factor.

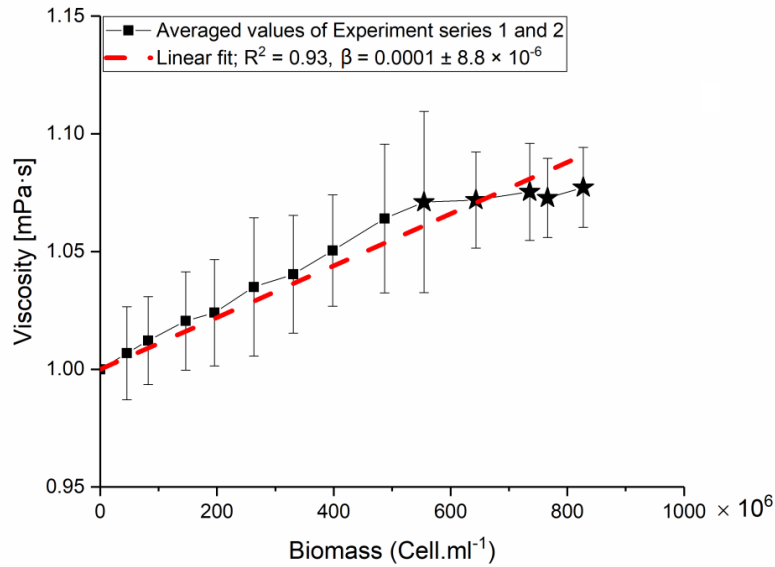


**Figure 2-15. Variation of the averaged viscosity of *Synechocystis* sp. CPCC 534 suspensions with cell density.**

### 2.3 Concluding remarks

This chapter focused on investigating the effects of shear on the growth, doubling per day, biomass production, and rheological properties of *Synechocystis* sp. CPCC 534 suspensions in agitated vessel reactors. The data revealed a significant increase in biomass, doubling per day and yield production as a result of flow in comparison with the non-agitated suspension. Meanwhile, mixing had a negative impact on cell size.

On the other hand, the rheological behavior in terms of the viscosity of cell suspensions, which experienced various shear rates during growth, was studied. The viscosity, normalized at a constant biovolume fraction, showed Newtonian behavior at all cell concentrations. This behavior was observed for both pre-sheared and un-sheared samples, implying the shear history does not influence the rheological behavior of suspensions. Concerning the effect of cell motility, experiments showed no difference between the viscosity of live-cell and dead-cell suspensions. This behavior is attributed to the low and twitching nature of the motility of *Synechocystis* sp. CPCC 534., in contrast to the high motility of swimmers such as *Chlamydomonas reinhardtii*. Cell concentration showed a noticeable influence on the viscosity of cell suspensions. It was observed that viscosity is a linearly increasing function of the cell

volume fraction, as it is for passive rigid particles; a correlation was given for this variation. However, this increase was smaller than the one observed in suspensions of rigid particles. The smaller observed increase in viscosity with cell volume fraction is attributed to the fact that in the present study soft particles (*Synechocystis* sp. CPCC 534 bacteria) can deform; thus, some of the energy of the flow is dissipated in deforming the cells. This decreases the amount of energy dissipated by hydrodynamic interactions compared to rigid particles, so the viscosity is less than it would be for rigid particles.



## Chapter 3

### 3 « Cell Tracking of Active Fluids: Effects of Light on Diluted Suspensions of *Synechocystis* sp. CPCC 534»

In active fluids, the particles often show an intermittent motion consisting of alternating high-motility “run” and immobile “tumble” periods. The average motion can be altered by external attractant or repellent stimuli. Two examples of attractants are nutrients or light gradients that result in a directed movement called chemotaxis and phototaxis, respectively. This result of such investigations paves the way for the distinct pathways for the recognition of light response in prokaryote microorganisms, which can be used in the active control of bacterial flows.

This chapter focuses on cell tracking by image processing technique to investigate the effects of light on highly diluted bacterial suspensions. *Synechocystis* sp. CPCC 534 has been used as the model microorganism. The experiments were carried out on suspension of *Synechocystis* sp. in a closed microfluidic chamber and under three different lighting conditions.

Cell tracking helps to investigate cell motility, get access to interaction frequency between cells as a function of time (cell-cell interaction) and phototaxis. The knowledge of the motility of cells paves the way for many applications including shutting down the motility of the tumor cells that would largely prevent metastasis and as a result, can limit the spreading of cancers [26]; preventing damages and defects in the cellular motility during fetal development that are the origin of many common birth problems (cleft palate, spina bifida); development of actuators harnessing molecular motors and sensors that can alert the presence of pathogens or guide drugs delivery [104]; and wound healing, and the immune response [105]. For cell tracking, image processing was done by Python programming language. Moreover, this chapter presents the preliminary microfluidic channels designs for future use, and the experimental setup that can be used for further investigation in the presence of laminar flow.

## 3.1 Materials and Methods

### 3.1.1 Microorganism and Culture Conditions

*Synechocystis* sp. CPCC 534 strain was obtained from the Canadian Phycological Culture Center (Waterloo ON, Canada) and used as the model microorganism. *Synechocystis* sp. CPCC 534 was sub-cultivated by diluting 3 ml of mother culture in 47 ml of fresh BG-11 medium in a 100 ml Erlenmeyer flask. The composition of the BG-11 is available in Table 2-1.

Two sets of data were collected at different times and under the same conditions to ensure the statistical relevance of the study. The first dataset is attributed to “Sample 1” and the second one to “Sample 2”, hereafter. Before the experiments, the cells were grown for 6 days (mid-exponential growth phase). Bacterial suspensions had been stirred by a magnetic stirring bar with a diameter of 7.9 mm and a length of 19.8 mm using a digitally controlled magnetic stirrer (VWR, Canada). The agitation speed was set at 360 rpm. It was placed under a white light intensity of  $70 \pm 10 \mu\text{mol photons m}^{-2} \text{s}^{-1}$  in a room at  $20 \pm 1 \text{ }^\circ\text{C}$  for 7 days followed by 24 hours dark and subsequent 2 hours light before running the experiments [71].

At this stage the cell density was measured at an absorbance wavelength of 750 nm which corresponds to particle density [87], using a spectrophotometer. The calibration curve in Equation 2-5 was used to obtain the concentration of cyanobacteria that was approximately  $140 \times 10^6 \text{ cells.ml}^{-1}$ .

### 3.1.2 Experimental Apparatus

#### 3.1.2.1 Microfluidic Device

##### 3.1.2.1.1 Microfluidic Chamber

The schematic design of the microfluidic chamber is presented in Figure 3-1. It consists of a microscope slide and glass coverslip that is sealed after the introduction of *Synechocystis* sp. suspension. The light sources are from the microscope lighting house and external light. The full capacity of the microfluidic chamber is approximately 20 ml. However, for every experiment 10 ml of *Synechocystis* sp. suspension was placed on a microscope slide (VMR™, GoldLine 26×76 mm).

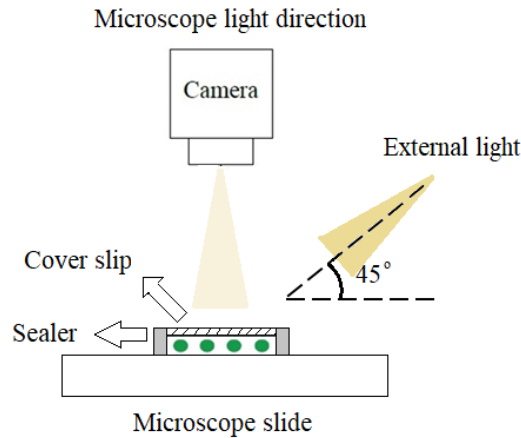


**Figure 3-1. Schematic design of the experimental setup. The green dots represent cells.**

The droplet was then covered with a glass coverslip (Fisherbrand™, 22×22 mm) and sealed with high vacuum grease (Dow Corning®, United States) to avoid evaporation and drift. Figure 3-2 shows the parts and the steps of the procedure.

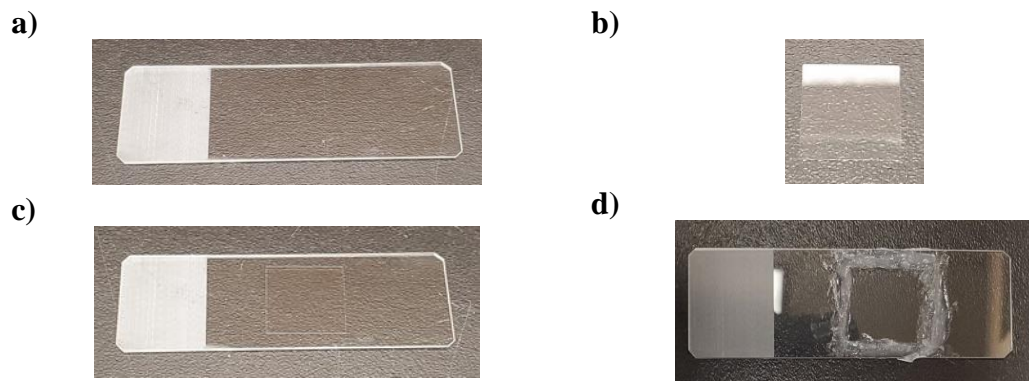


**Figure 3-2. a) Microscope slide and b) coverslip. After putting the droplet of the suspension on the microscope slide, c) the coverslip is placed on top of the microscope slide for cover, and finally, d) sealed with the vacuum grease to avoid evaporation and drift.**

Before putting the microscope slide under the microscope (Fisherbrand™ Inverted Microscope), cells were allowed to reach their motility plateau for 20 min. Then the motility of the cells was recorded by the camera (Fisherbrand™ C-Mount Digital) mounted on top of the microscope and saved on the computer connected to the camera. The experimental setup is displayed in Figure 3-3.

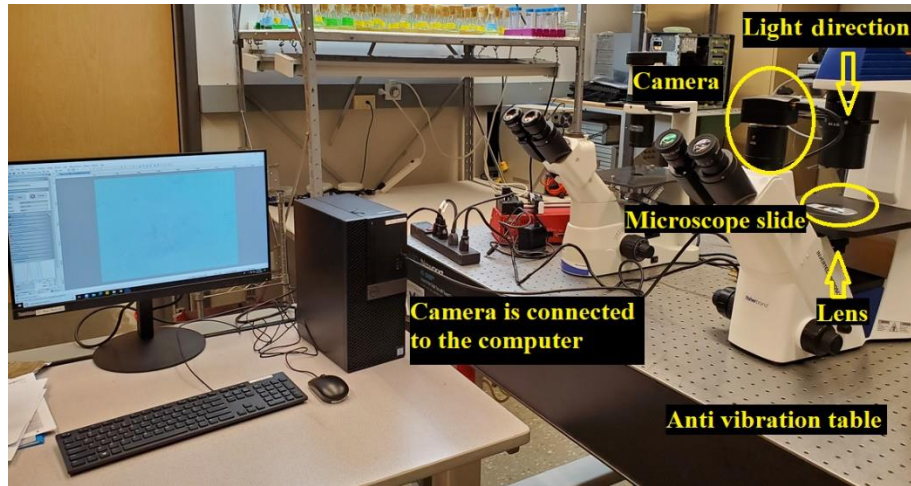


**Figure 3-3. Experimental setup**

It is worth mentioning that, before using a plane microscope slide, a cavity microscope slide (Fisherbrand™, 26×76 mm) was used as the microfluidic chamber. Comparing microscope imaging in **Error! Reference source not found.** revealed that the image taken from the droplet of bacterial suspension in the cavity microscope slide is not suitable for particle tracking.

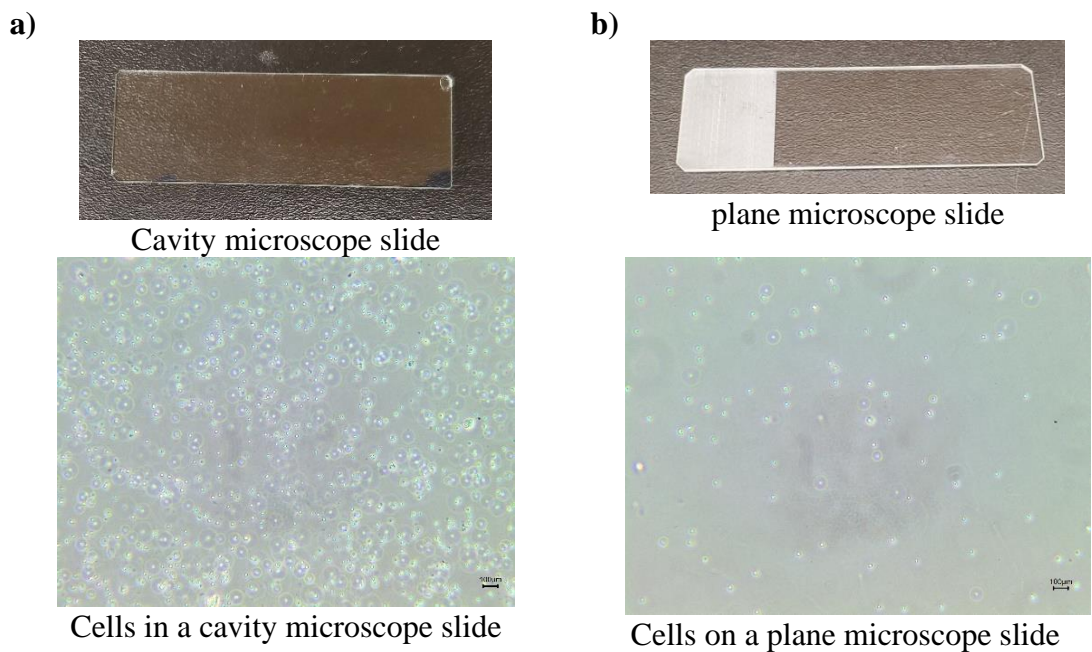


**Figure 3-4. Microscope imaging (20X magnification) of a) cavity and b) plane microscope slide used as the microfluidic chamber.**

In fact, the depth in the cavity created a blurry view of the cells that made it difficult to track them in 2D dimensions. For this reason, the plane microscope slide was used for microscope imaging and recording videos in the experiments.

### 3.1.2.1.2 Microfluidic Channel

The schematic design of the plane microfluidic channel and the multichannel microfluidic device is presented in Figure 3-5. The plane microfluidic channel is suitable for the preliminary study of cell motility, cell-cell interactions, chemotaxis and phototaxis phenomenon in the presence of laminar flow. The multichannel microfluidic device is suitable for studying the above-mentioned behaviors by introducing live and dead cells to the device from separate inlets and observing the distribution of cells at the outlet. To fabricate a microfluidic device by lithography, a master (mask) is required.

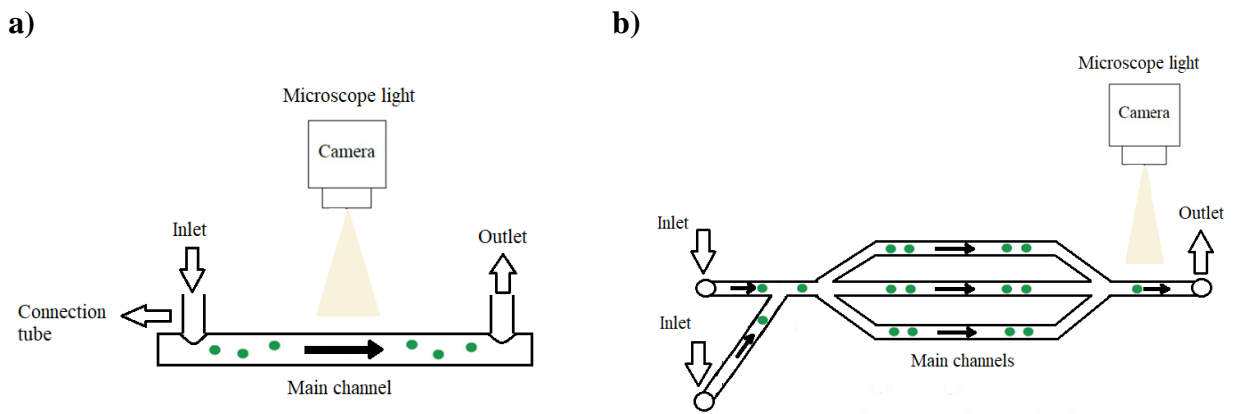
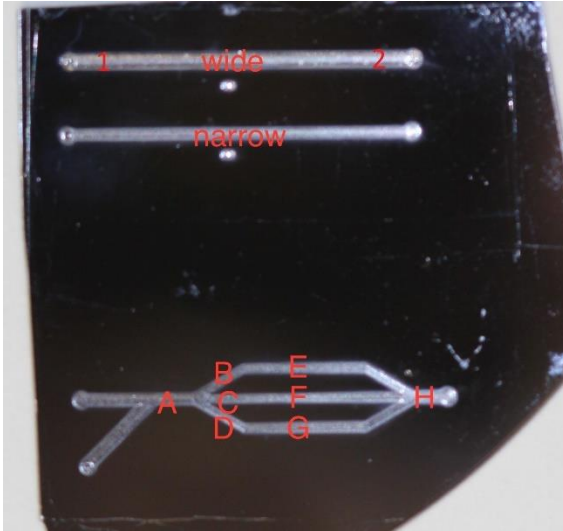
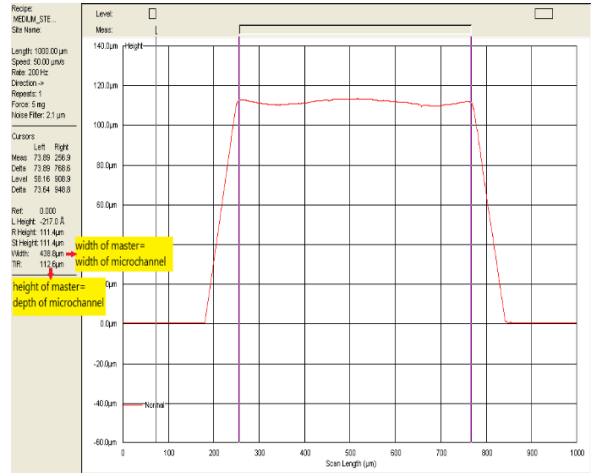


**Figure 3-5. Schematic view of the experimental setup of the preliminary design of the a) front view of the plane and b) top view of multiple branch microfluidic channel. The green dots represent cells.**

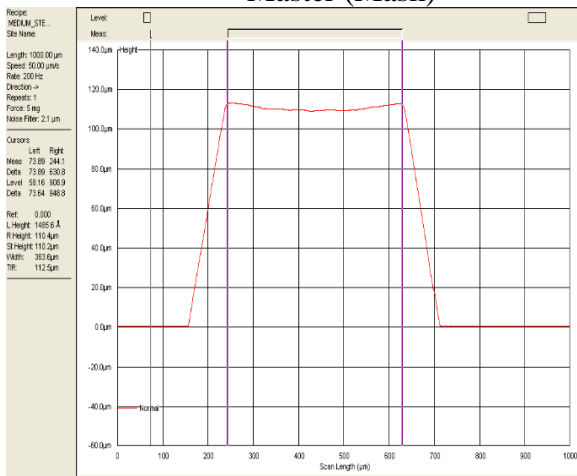
The master (mask) in Figure 3-6 was used for fabricating the microfluidic channel. The dimensions of the master (mask) measured at NanoFab, University of Western Ontario, are also presented in Figure 3-6. The master accommodates three geometries that are labelled with wide, narrow, and single letters to simplify tracking the dimensions.



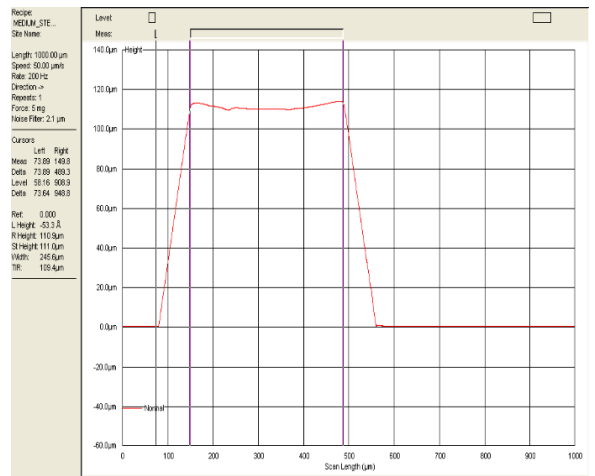
Master (Mask)



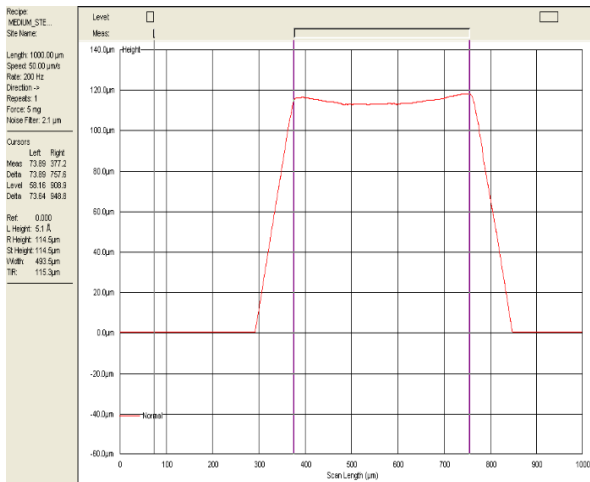
Point A on the mask



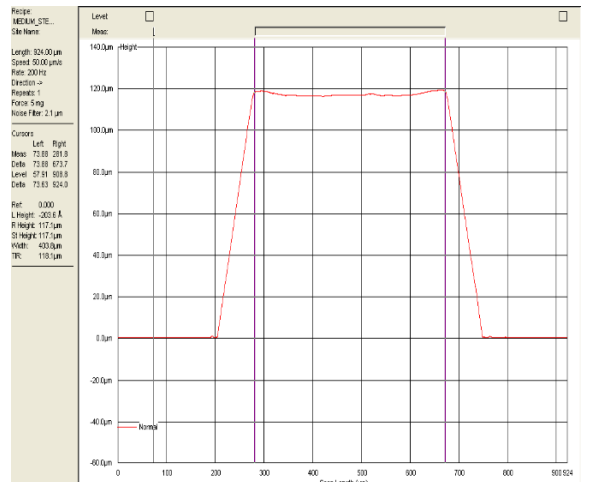
Point B on the mask



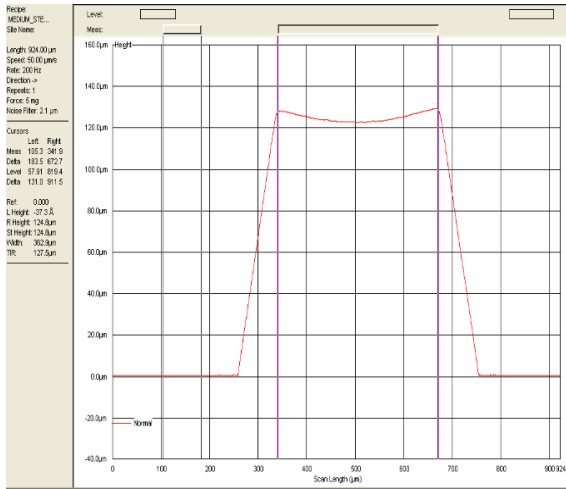
Point C on the mask



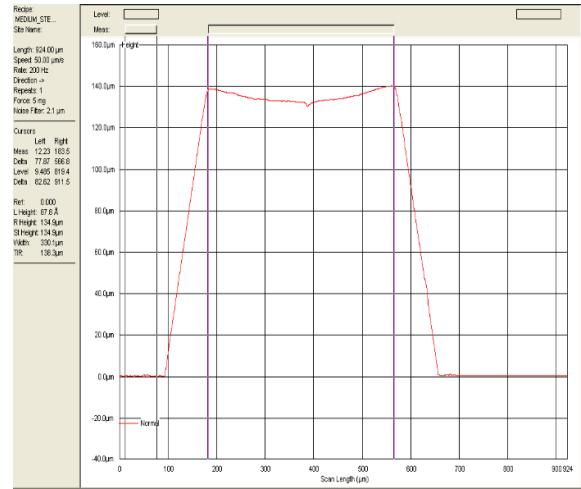
Point D on the mask



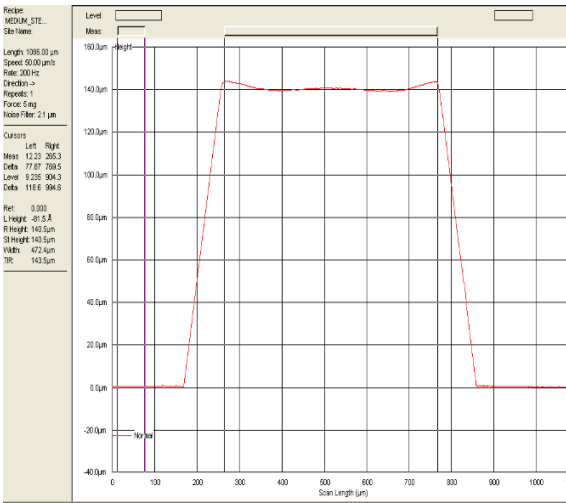
Point E on the mask



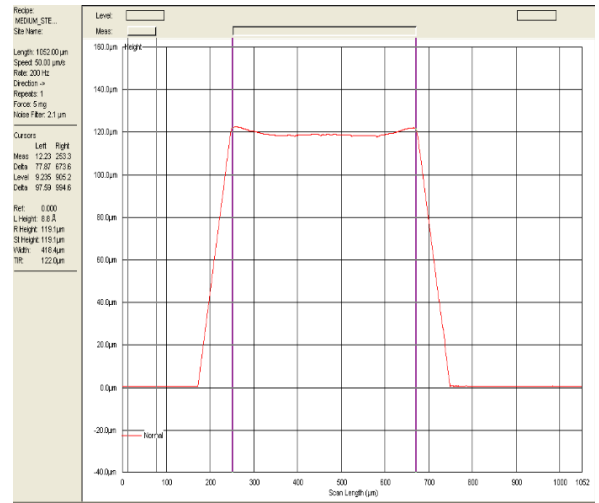
Point F on the mask



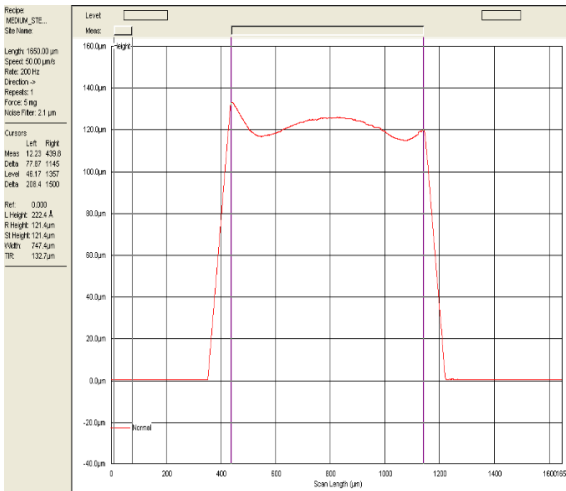
Point G on the mask



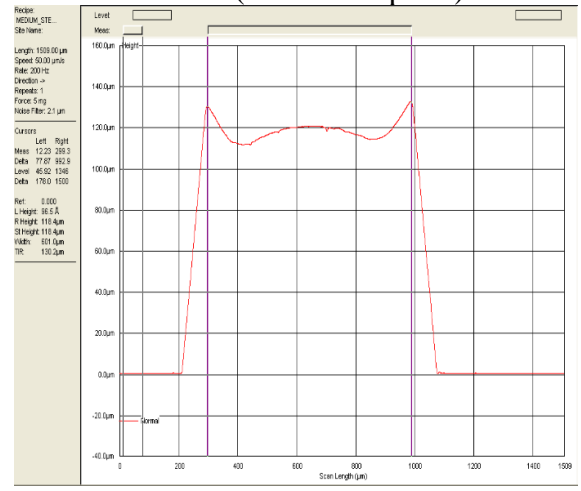
Point H on the mask



Narrow (the middle point)



Wide (point 1)



Wide (point 2)



**Figure 3-6. Dimensions of the master (mask). Each part of the master is labeled with specific words or letters. Highlights on the curve for point A provide the guide for reading dimensions.**

The microfluidic channels fabricated by lithography are shown in Figure 3-7. In the fabrication process, PDMS was made with Sylgard 184 Silicone Elastomer Kit (see Figure B-2 in Appendix B) and then bonded with glass slides by Oxygen Plasma treatment at the NanoFab, University of Western Ontario.



**Figure 3-7. Multichannel microfluidic device (left-hand side) and plane microfluidic channel (right-hand side) fabricated by lithography.**

The holes in the PDMS were drilled using the tip of the syringe size 21 G 1 (BD PrecisionGlide Needle, United States). The metal connecting tubes were made from cutting the tip of the same syringe in a proper size. In the next step, the sharp edges were polished with sandpaper and then placed in the holes, and the plastic connecting tubes (McMaster Caar, United States) were attached. Figure 3-8 displays the microchannel and its attachments. The inlet and outlet were made from a metal connecting tube and a drain was designed to collect the outflow.



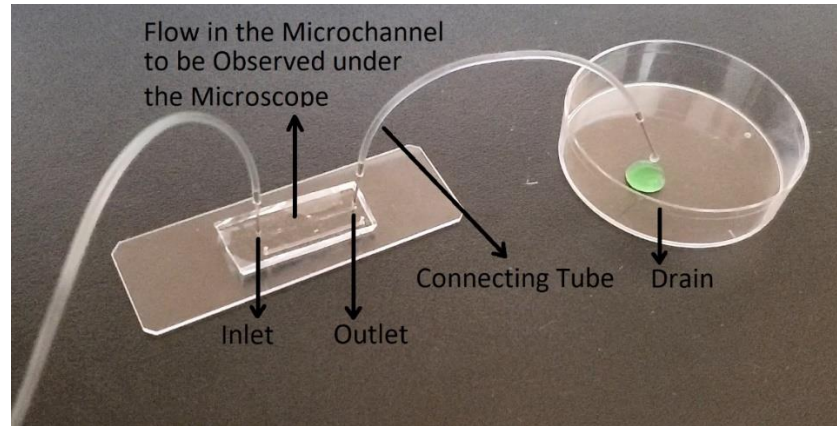


**Figure 3-8. The plane microfluidic channel with its attachments.**

The flow of microalgal suspension was introduced into the plane microfluidic channel through connecting tubes by a syringe micropump (Braintree Scientific, Inc. United States, BS-8000) shown in Figure 3-9 and then the migration of cells was observed and recorded by a camera mounted on a microscope connected to the computer.

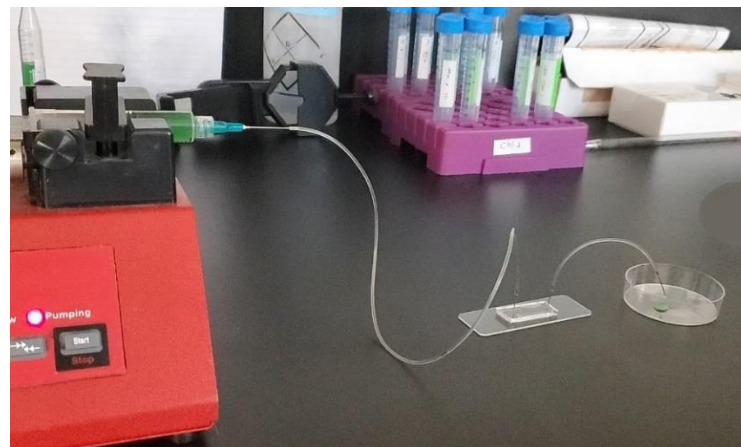


**Figure 3-9. Applying microalgal suspension into the microchannel by the syringe micropump.**

A single frame of the video recorded from the flow of suspension of *Synechocystis* sp. in the plane microfluidic channel is presented in Figure 3-10.

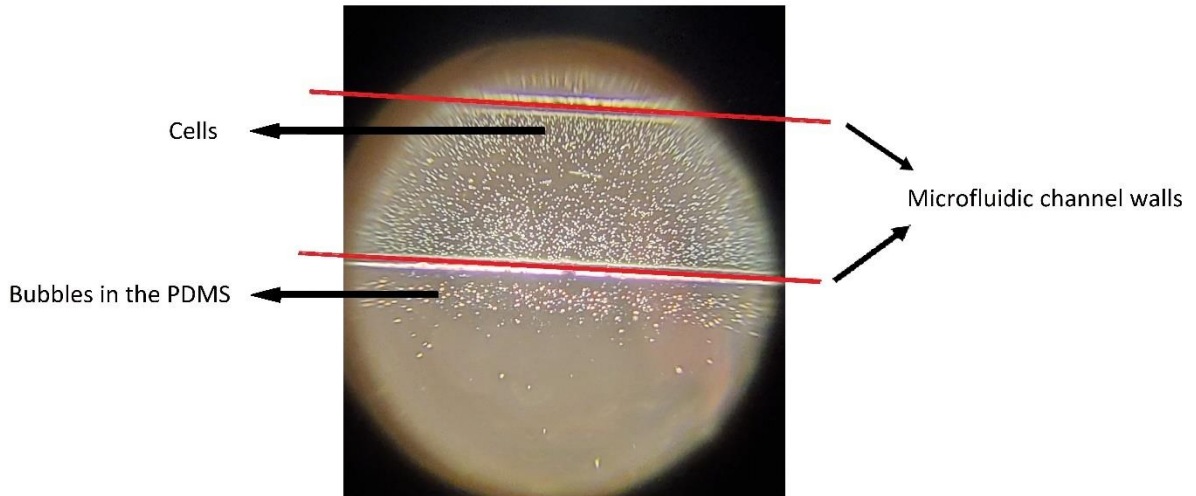


**Figure 3-10. A single frame of the recorded video of the flow of suspension of *Synechocystis* in the microchannel.**

For further experiments on chemotaxis and/or phototaxis of cells in suspensions of the *Synechocystis* sp. in the presence of a flow, a second microfluidic device in Figure 3-11 was designed inspired by the study performed by Jahromi [106]. It has a main channel that is connected to 11 microchambers and each microchamber contains 100 micropillars. The stimuli can be an attractant or repellent chemical or even light introduced into the microchannel that allows examining the interaction of the cells.

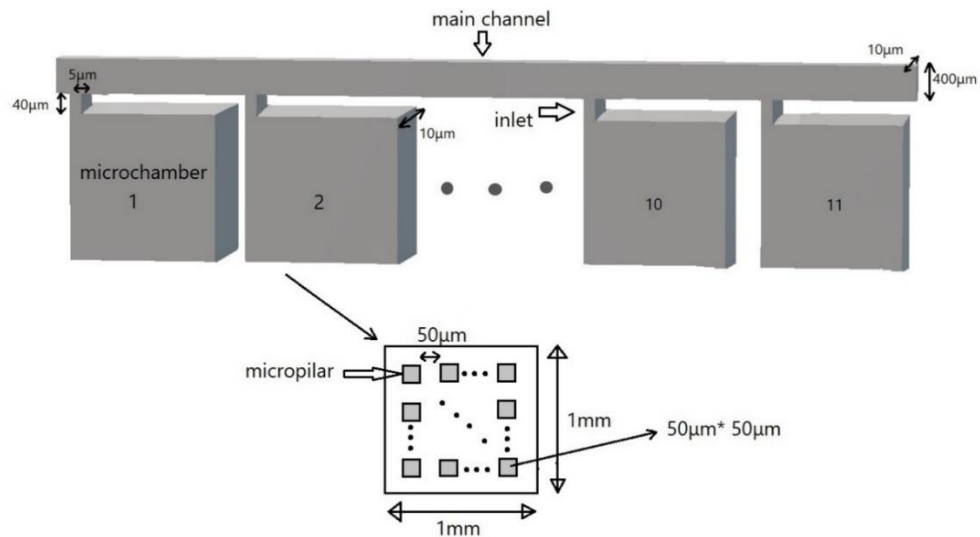


**Figure 3-11. Schematic 3D design of the microfluidic device composed of the main channel and 11 microchambers with 100 micropillars each.**

### 3.1.3 External Light Source

For investigation on phototaxis, assay bacteria were exposed to an external light source. Two devices were used in experiments separately. The first was an LED with a white light intensity of  $100 \pm 5 \mu\text{mol photons m}^{-2}\text{s}^{-1}$ . The second was a laser pointer with one red light beam (single dot), an output wavelength of  $650 \text{ nm}$  (maximum), and an intensity of  $39.15 \times 10^{10} \mu\text{mol photons m}^{-2}\text{s}^{-1}$  (in a single dot). More details about the laser pointer and its light intensity calculation are provided in Appendix D. For performing the experiments, the device was fixed at a  $45^\circ$  angle. The experimental setups are shown in Figure 3-12 and Figure 3-13, respectively. The white incident light from the microscope lighting house was tuned to the minimum ( $85 \pm 5 \mu\text{mol photons m}^{-2}\text{s}^{-1}$ ) so that imaging and/ or video recording was possible. The intensity of the ambient lighting which hereafter is called normal lighting condition was  $60 \pm 5 \mu\text{mol photons m}^{-2}\text{s}^{-1}$ .

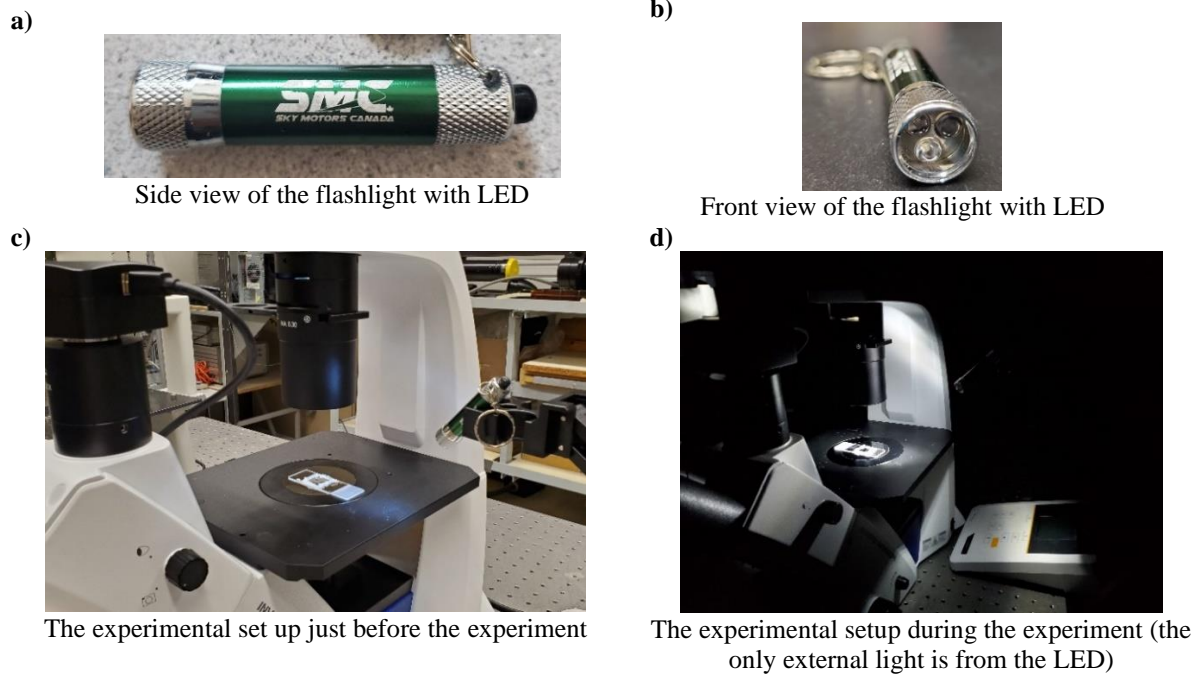


**Figure 3-12. Flashlight with LED and its experimental setup**

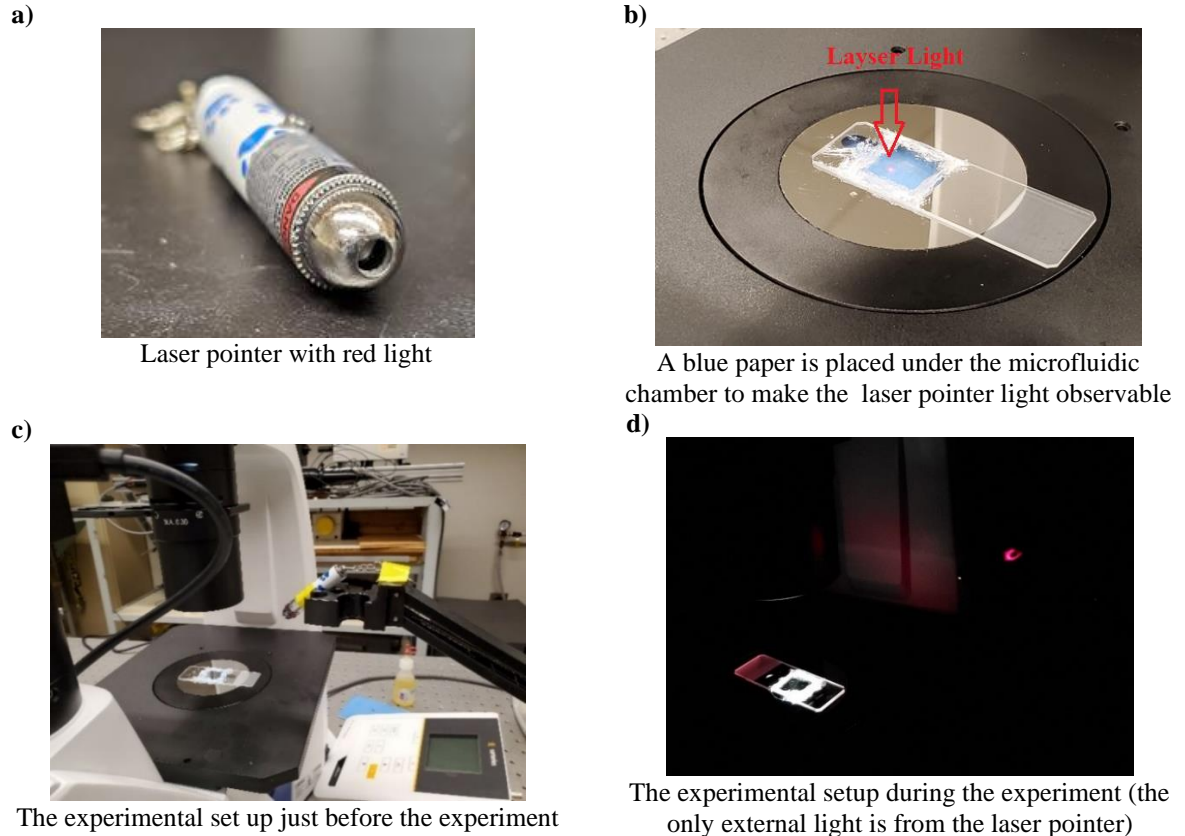


**Figure 3-13. Laser pointer and its experimental setup**

### 3.1.4 Video Recording and Imaging Techniques

Images and videos were taken and recorded by the camera (Fisherbrand™ C-Mount Digital) mounted on top of the microscope and saved on the computer connected to the camera. The resolution for 20X magnification, used for imaging and video recording is 1 pixel per micron. For video recording, in the digital imaging software (SeBaView), videos' frame rate and length have been set to 1 frame per second and 1800 seconds, respectively. The calculation result accuracy in the software was 2 decimals.

The “Auto Contrast” command automatically adjusts the overall contrast and mixture of colors in an RGB image. Since it does not adjust channels individually, “Auto Contrast” does not introduce or remove color casts. It maps the lightest and darkest pixels in the image to white and black, making highlights appear lighter, and shadows appear darker. When identifying the lightest and darkest pixels on an image, “Auto Contrast” clips the white and black pixels by 0.5% - that is, it ignores the first 0.5% of either extreme. Moreover, in the “Histogram” that

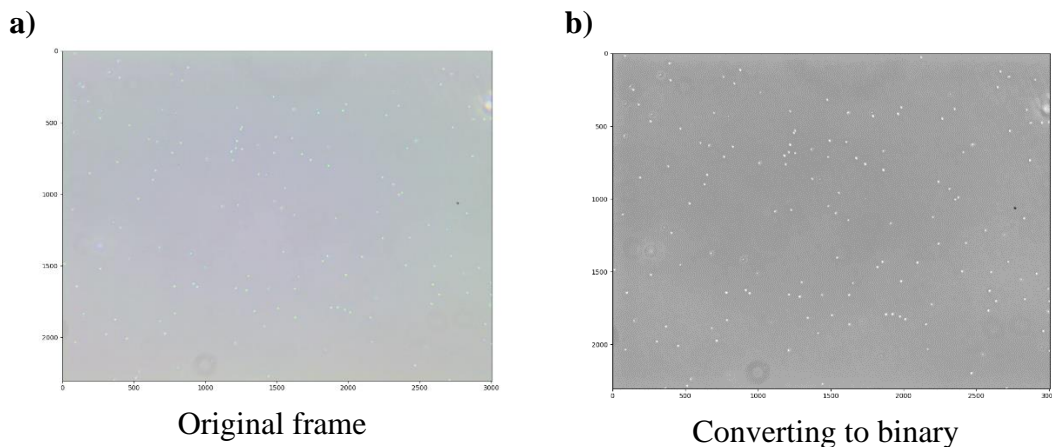
illustrates how pixels in an image are distributed by graphing the number of pixels at each color intensity level the R, G, and B tolerance values were 10.

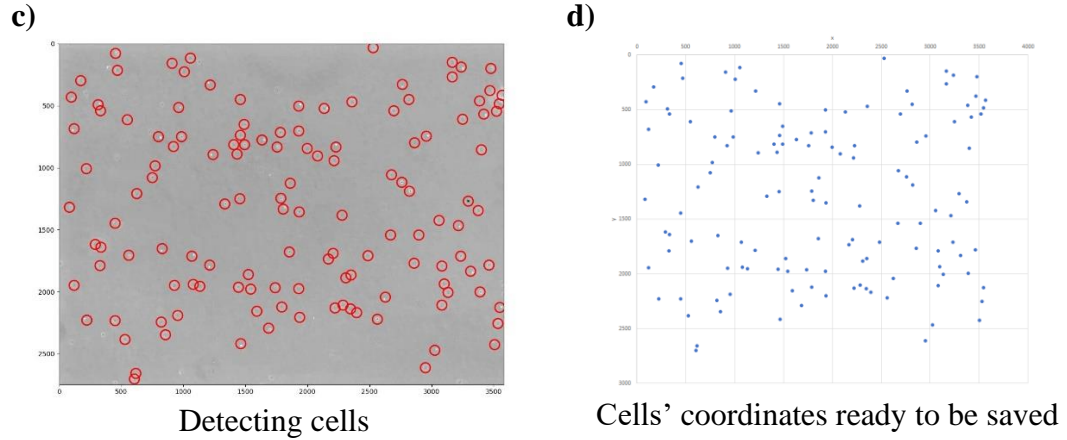
### 3.1.5 Image Processing

Image processing has been done by Tarckpy (v 0.4.2) that is a Python package for particle tracking [107]. It has been customized to serve the purpose of particle tracking analysis and investigation of the correlation between the motilities of neighboring bacteria. It follows the widely-used particle tracking algorithm [108] which is separated into three steps.

In the first step, the videos will be used as the input and then split up into single frames. In other words, it will be converted to an image sequence, and then by feature finding initial feature coordinates will be obtained from the images. In the second step, the sub-pixel precision will be obtained in coordinate refinement. Finally, the coordinates will be linked in time yielding the feature trajectories. Figure 3-14 exhibits the procedure of finding initial feature coordinates at a glance.

Each video is composed of many single frames that indeed is an image sequence. Since the cells are features with light color in every frame of the video, the algorithm looks for bright features. Then it returns the features' information such as coordinates and mass on every frame as a spreadsheet-like object called a DataFrame that can be exported to CSV format. Table 3-1 presents the first five rows of the DataFrame. It is worth mentioning that the Python programming language uses 0-based indexing. Indeed, the first frame is frame number 0.





**Figure 3-14. The procedure of obtaining cells' features.**

**Table 3-1. The first five rows of DataFrame including cells' coordinate, mass, and frame number**

particle	x	y	mass	frame
0	2528.91	31.52099	2545.568	0
1	451.5172	77.94206	3495.859	0
2	1055.271	115.9639	4563.114	0
3	906.3253	156.983	3070.601	0
4	3164.995	148.6178	4363.19	0

## 3.2 Results and Discussion

### 3.2.1 Bacteria Trajectories

The traces of trajectories of bacterial cells (of duration 180 s) in a diluted suspension of *Synechocystis* sp. are demonstrated in Figure 3-15. Also, this figure presents the magnified trajectories of four particles denoted inside the blue square. It should be noted that the algorithm detects cells' displacements in 2D dimensions. Therefore, only the movements in x and y-directions are considered but not in the z-direction.



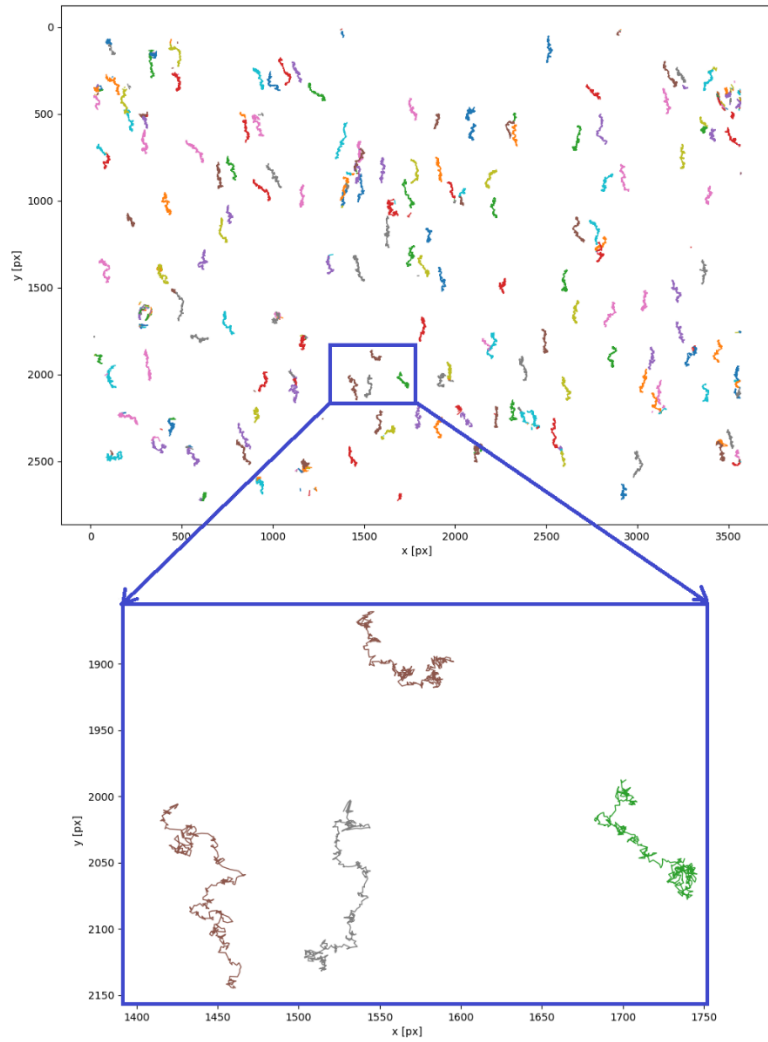


**Figure 3-15. a) Traces the trajectories of bacterial cells and the magnified trajectories denoted inside the blue square. The duration of the trajectories is 180 s. The size of a pixel is equal to 1  $\mu m$ .**

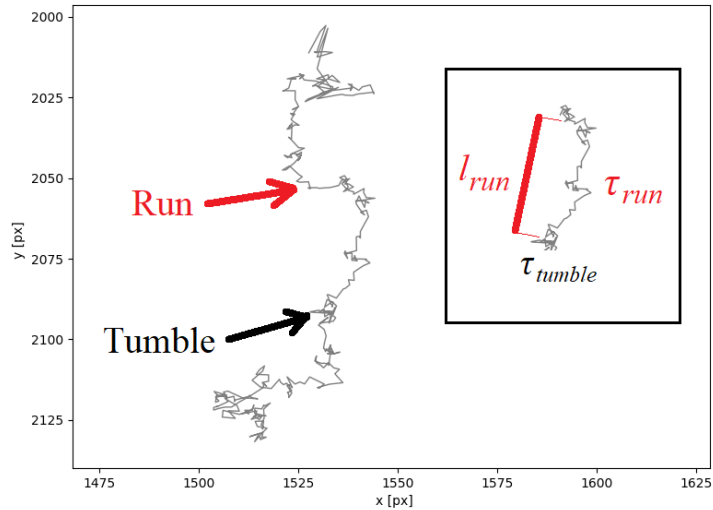


**Figure 3-16. Trajectory of a bacterial cell (of duration 180 s). The twitching motility that is a combination of run and tumble motions is observable. Inset: the diffusion step in which  $l_{run}$ ,  $\tau_{run}$ , and  $\tau_{tumble}$  represents the distance traveled during a run, the run duration, and the tumble duration, respectively. The size of a pixel is equal to 1  $\mu\text{m}$ .**

Figure 3-16 displays a trajectory of 180 s duration in detail. It can be observed that the motility of *Synechocystis* is intermittent. In fact, it consists of two alternating phases that can be highlighted as:

- “high-speed” motility, also called “run phases” or “runs”, during which bacteria move swiftly from one position to another. These phases are noticeable in Figure 3-16.
- “low-speed” motility, also called “tumble phases” or “tumbles”, during which the bacterial motility is limited to a restricted area. Similar positions build up over time and create spot-like shapes.

Vourc’h et al. [25] observed similar motility for *Synechocystis* sp. PCC 6803.

These intermittent motions are related to the optimal search strategies [90], in which the frequency of run periods is controlled by the gradient of a chemical or non-chemical attractant and/or repellent. This type of motion is also widely observed in nature [109]. For instance, intermittency has been noticed in low-temperature glasses or athermal systems [110, 111]. The cause of the emergence of these types of dynamics and is still vague but may have a relation



with collective motion in which in a high-density medium the diffusion of the particle is restricted by the neighbors that form a “cage” and long-range motions are inhibited in it. This phenomenon is equivalent to what happens in a tumble phase motion. The limited lifetime of the cage results in the appearance of long-range motion which is equivalent to run phase motion.

### 3.2.1.1 *Dynamic Trace of Trajectories*

For a better interpretation of the motility and behavior of bacterial cells, it is essential to have access not only to typical images but also to the dynamic traces of trajectories. It paves the way for inspecting the motion of a single cell, a small number, or a large population of cells. To serve this purpose, in this thesis, a droplet of a highly diluted suspension of *Synechocystis* sp. was used. The highly diluted suspension is the suspension that has been diluted tenfold in BG-11 before introduction in the closed microfluid chamber. To reduce the size of the original video (1800 s length), before image processing, the speed of the original videos was accelerated 20 times (20 frames per second) by the FFmpeg package. FFmpeg is a command-line tool for converting video or audio formats. The trace of trajectories and also the last frame of the video (Media Appendix) from the dynamic trace of a single bacterial cell is presented in Figure 3-17. The python script is provided in Appendix E, part 1.

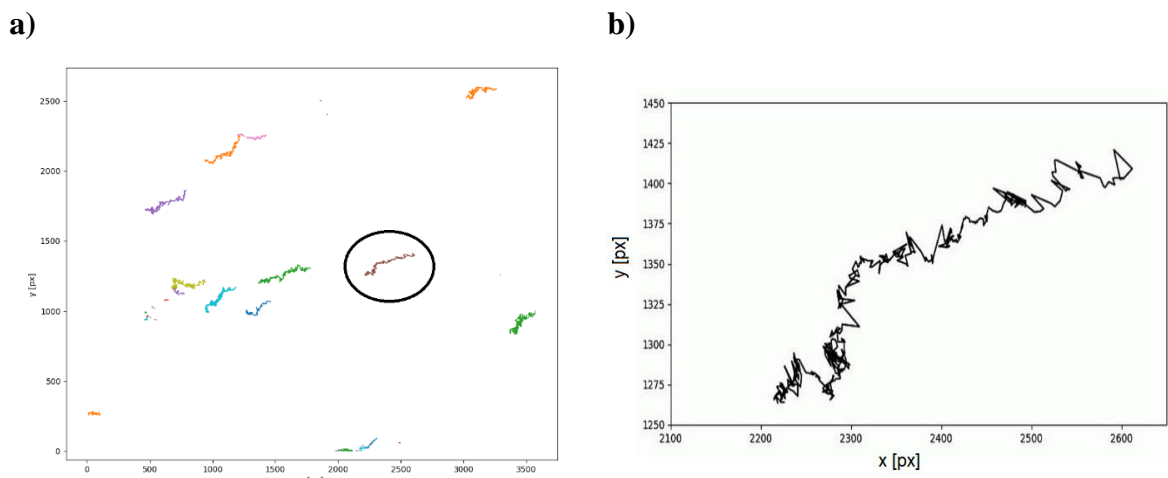


**Figure 3-17. a) The traces of bacterial cells, b) The last frame of the video (Media Appendix) from the dynamic trace of a single bacterial cell encircled in part (a). The size of a pixel is equal to 1  $\mu\text{m}$ .**

### 3.2.1.2 Detecting Run and Tumble Motions

It is of interest to detect the run and tumble motions of bacterial cells. This ability can set the stage for any further analysis of their trajectories. Moreover, it gives access to the frequency and duration of tumbles. Longer tumble durations,  $\tau_{\text{tumble}}$  indicate that the bacterial cell is spending more time idling and/or trying to reorient the next run with high speed. By image processing using Python programming language, the tumble motions of any bacterial cells in the field of view can be detected. For this purpose, two parameters were defined, the first was an area around the bacterium corresponding to a disk of radius  $d_{\text{min}} = 3 \mu\text{m}$  which is about the value of a typical bacterium diameter and the second was the time  $t$  needed for a particle to escape this area. If  $t < t_{\text{min}}$  the bacteria is tumbling, and running otherwise. After some investigations, it became apparent that a  $t_{\text{min}} = 25 \text{ s}$  gives a good description of the phases. Two processed trajectories in which tumble motions were detected and denoted with red circles are displayed in Figure 3-18. Most of the displacement occurs during run phases. The Python script is provided in Appendix E part 2.

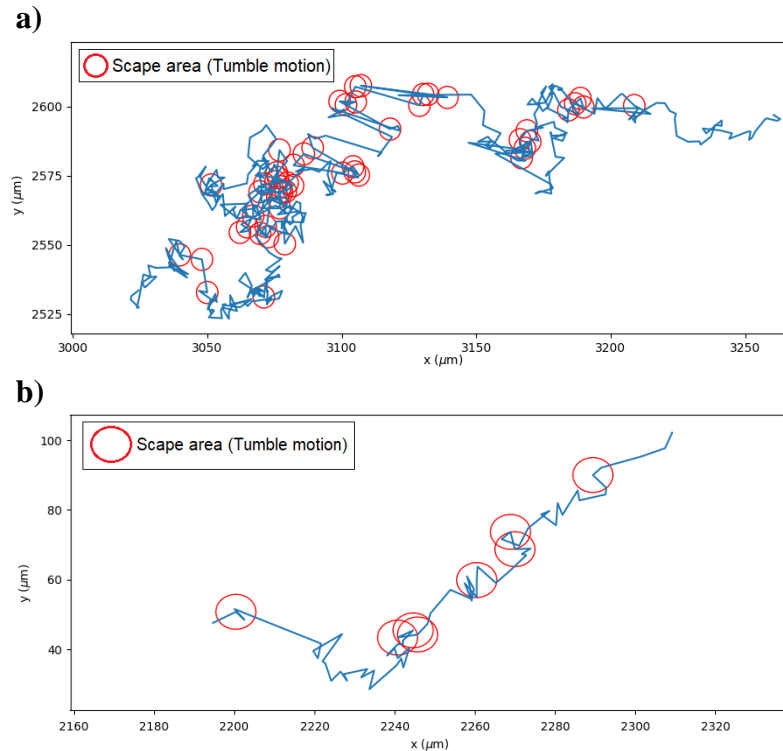


**Figure 3-18. Tumble motions (scape area) in two trajectories parts (a) and (b) are detected and denoted with red circles.**

### 3.2.2 Effect of Light on Cell Motility

#### 3.2.2.1 Mean Squared Displacement

The ensemble-averaged mean-squared displacement (EMSD) is defined as:

$$MSD(t) = \langle [x_i(t) - x_i(0)]^2 \rangle \quad \text{Equation 3-1}$$

where  $x_i(t)$  denotes the positions of particle  $i$  at time  $t$  and  $\langle \rangle$  denotes ensemble average.

The probability distributions of the ensemble-averaged mean-squared displacement (EMSD) along the x-axis of cells exposed to the light of laser pointer and LED are presented in Figure 3-19 and Figure 3-20, respectively. The error of measurements in this plot is linked to the accuracy of the software mentioned under the heading “Video Recording and Imaging Techniques”. In both figures, ensemble-averaged mean-squared displacement (EMSD) of the normal lighting condition is included for comparison. The probability distribution for the normal lighting condition is almost symmetric and zero-centered. The distributions for Sample 1- test 1 & 2 and Sample 2- test 1 are bimodal, with a sharp central part and broad tails.

In the studies performed on *Synechocystis* sp. 3068 [25, 87], distributions of ensemble-averaged mean-squared displacement (EMSD) showed that during run phases, the distributions broadened, without the sharp center. Besides, during tumble phases, the distributions are sharp at the center. Indeed, in the central part, non-diffusive behavior describes the tumbles for which bacteria are “trapped” or immobile. Moreover, the tails broaden sharply, which indicates the diffusive behavior that tends to be Gaussian. This interpretation of ensemble-averaged mean-squared displacement (EMSD) distribution is a criterion for deconvolving the total displacement into run and tumble phases.

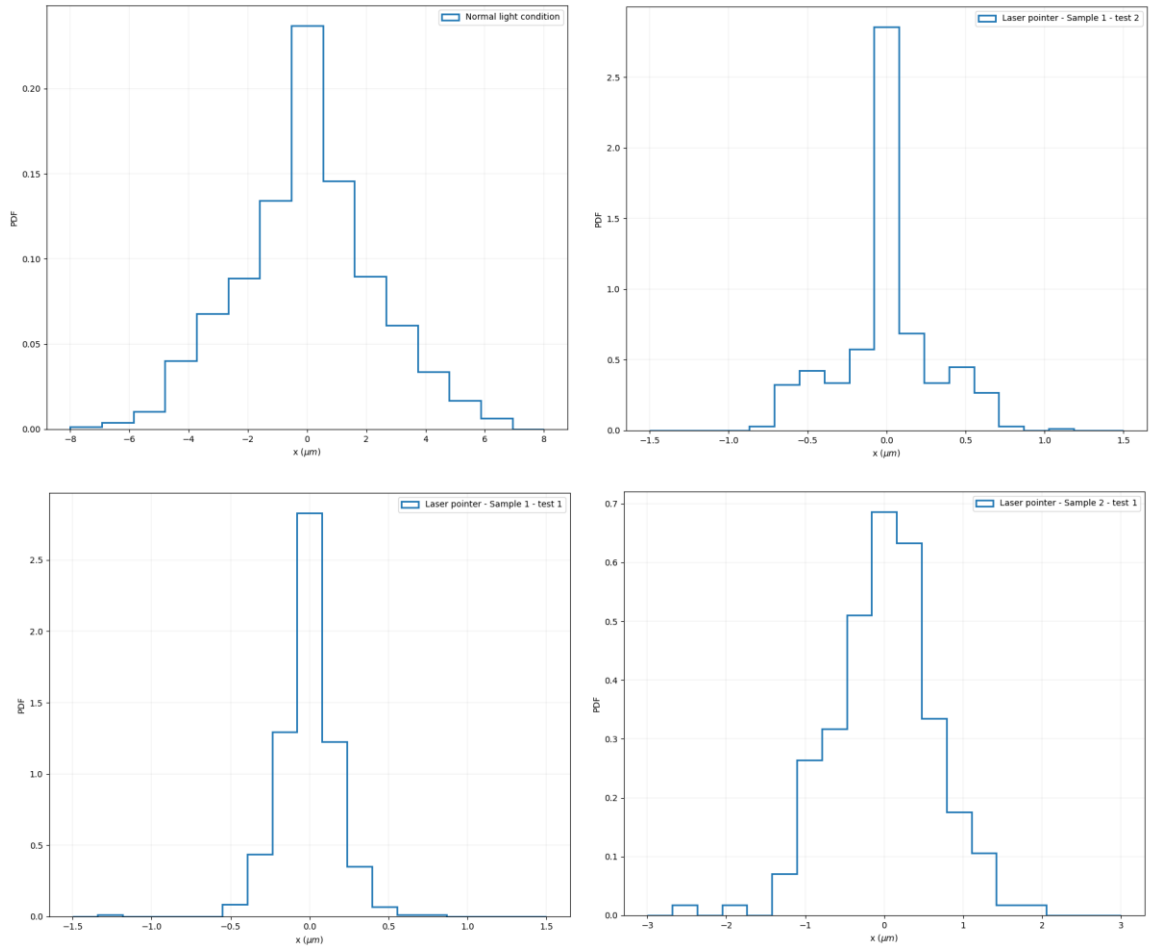


**Figure 3-19. Probability distribution of the ensemble-averaged mean-squared displacement (EMSD) along the x-axis for cells exposed to the light of the laser pointer and normal lighting conditions.**

Therefore, the distribution of ensemble-averaged mean-squared displacement (EMSD) suggests that the motility of the cells had a balanced combination of run and tumble phases, thereby the distribution is closest to the Gaussian (Normal) distribution compared to the distribution of cells exposed to an external light source. However, in the distributions for cells that were exposed to laser pointer light, the tumbling phase is the dominant phase in total displacement. In other words, when the cells were exposed to the light of the laser pointer, have spent more time tumbling and were more immobile.

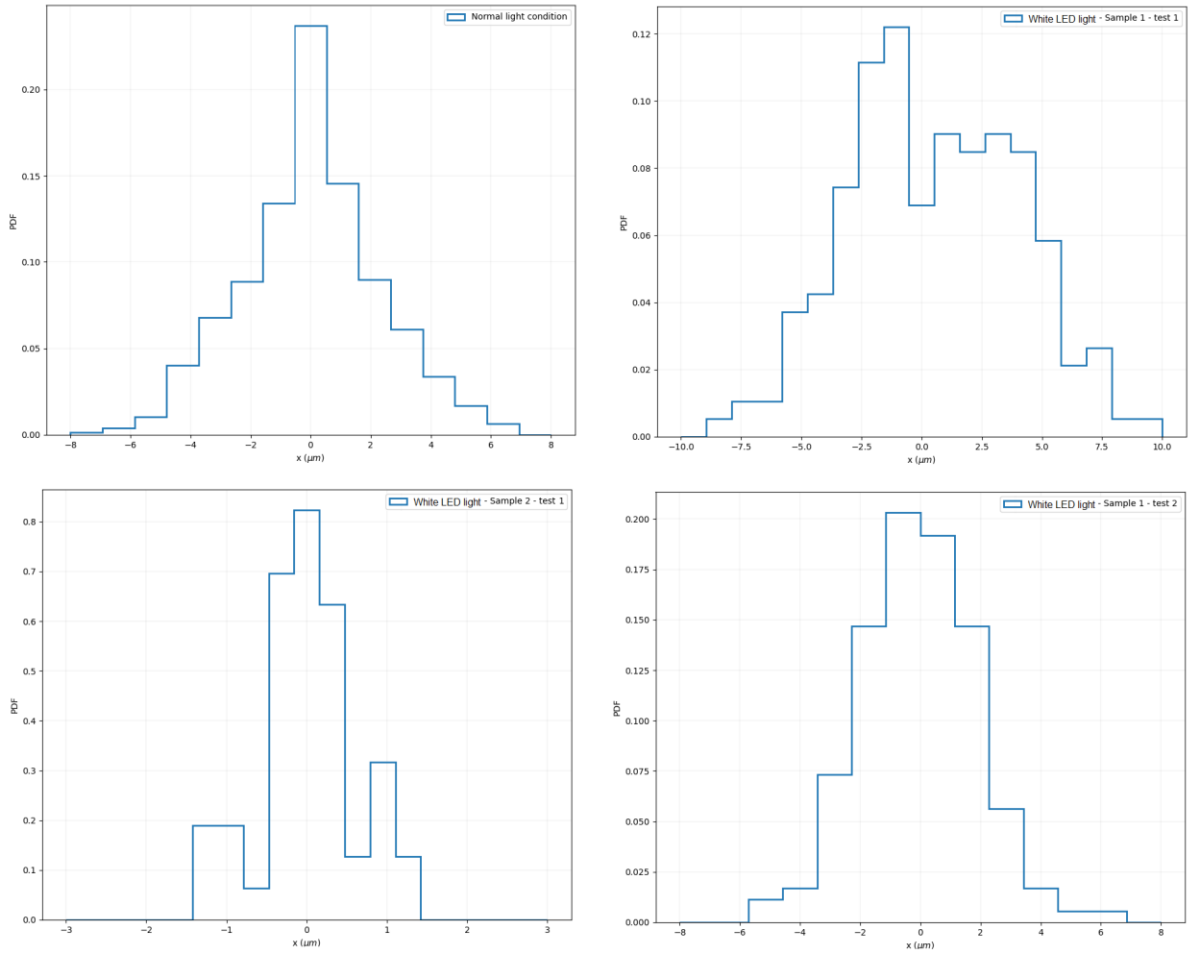


**Figure 3-20. Probability distribution of the ensemble-averaged mean-squared displacement (EMSD) along the x-axis for cells exposed to the light of LED and normal lighting conditions.**

In Figure 3-20 the distributions of Sample 1- test 1, Sample 1 – test 2, and Sample 2 – test 1 have a smoother central part compared to their counterpart distributions in Figure 3-19. Under light flux, *Synechocystis* sp. cells do phototactic motility and head toward the light source. The distributions suggest that the tumble motions decreased and run phase motion is the dominant phase in total displacement. In other words, when cells were exposed to the light of the LED, have spent more time moving quickly from one point to another point than idling in the same spot.

This result is consistent with the finding of another study [71] that observed the biased motility of cells as a result of averaged displacements during run periods, which was no longer random. They showed that it stems from the number of runs and not the longer run durations.

### 3.2.2.2 Velocity

The variations of ensembled-averaged velocity with time for cells exposed to the laser pointer red light, white LED light and normal lighting condition are depicted in Figure 3-21.

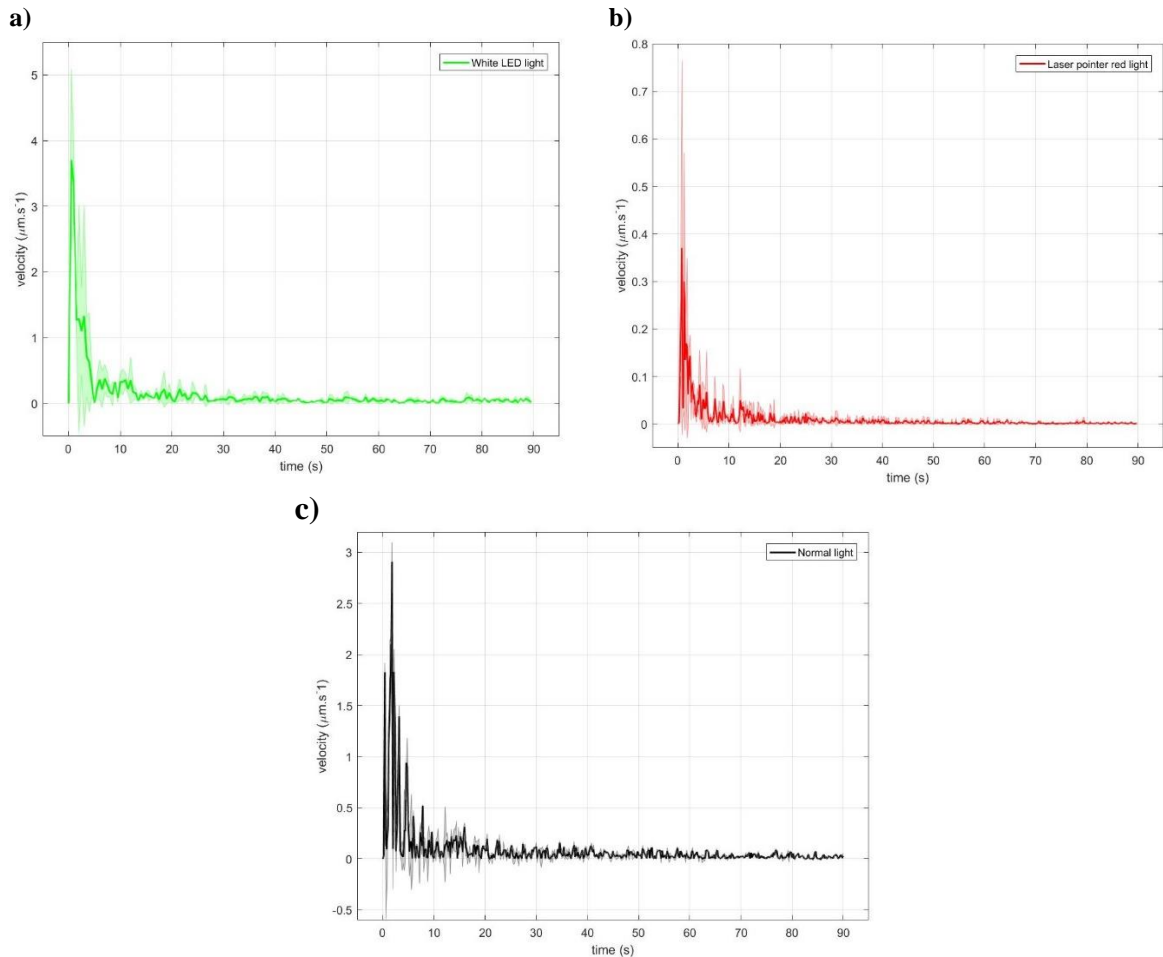


**Figure 3-21. The variation of ensembled-averaged velocity with time for cells exposed to the a) white LED light b) laser pointer red light c) normal lighting condition. The colored areas demonstrate  $\pm$  standard deviation.**

It can be observed that the ensembled-averaged velocity of all cases has fluctuations with high peaks that denote the high-speed motility in run phases. These peaks are higher for the cells

exposed to the white LED light compared to the laser pointer red light. This suggests that the white LED light was a stronger stimulus or attractant for the cells. Moreover, the ensembled-averaged velocity variations for all cases with any lighting conditions have a reducing trend that indicates the slowdown of motion of bacterial cells in the suspensions over time. The same behavior is also observed in another study [29] on *Synechocystis* sp. 3068.

In Figure 3-22 the ensembled-averaged velocity variation with time for the normal lighting condition, the laser pointer red light, and white LED light are superposed.

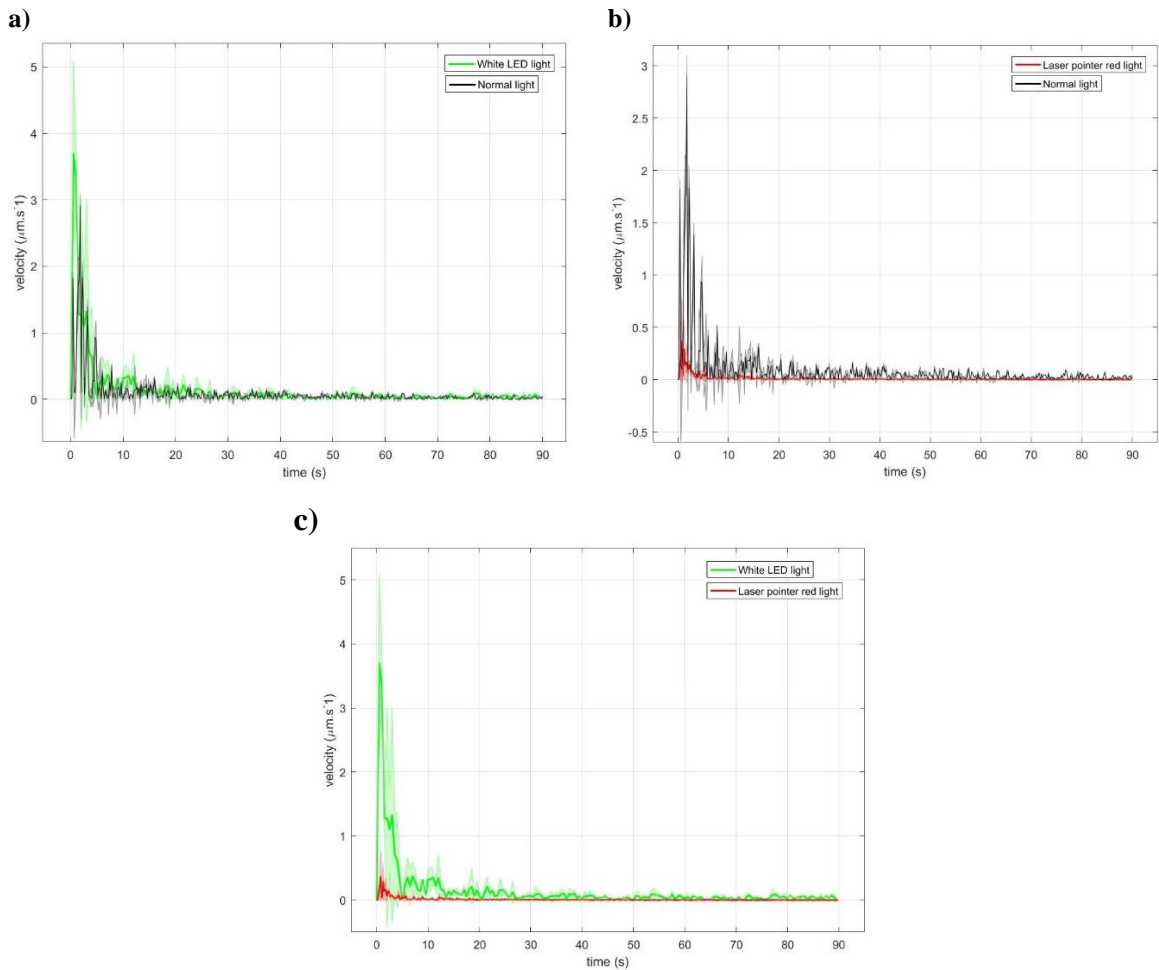


**Figure 3-22. Superposition of the variation of ensembled-averaged velocity with time for cells exposed to a) white LED light and normal lighting condition b) laser pointer red light and normal lighting condition c) white LED light and laser pointer red light.**

**The colored areas demonstrate  $\pm$  standard deviation.**

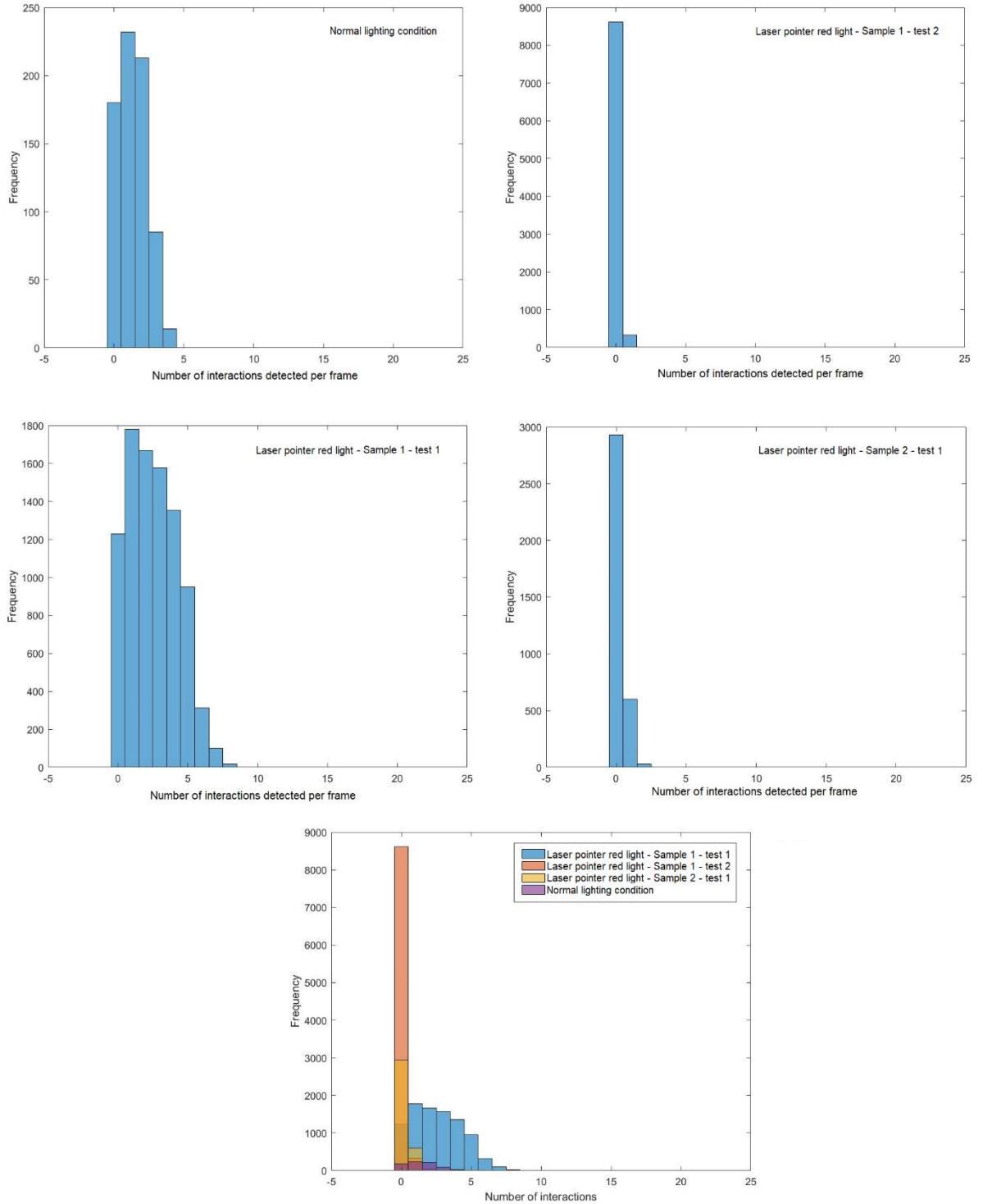
Figure 3-22 shows that the ensembled-averaged velocity variation of the cells exposed to the white LED light has a higher value compared to the normal lighting condition. However, the ensembled-averaged velocity variation of cells exposed to the laser pointer red light has a lower value compared to the normal lighting condition. This confirms that white LED light was a stronger stimulus for the cells.

### 3.2.2.3 Interactions Frequency

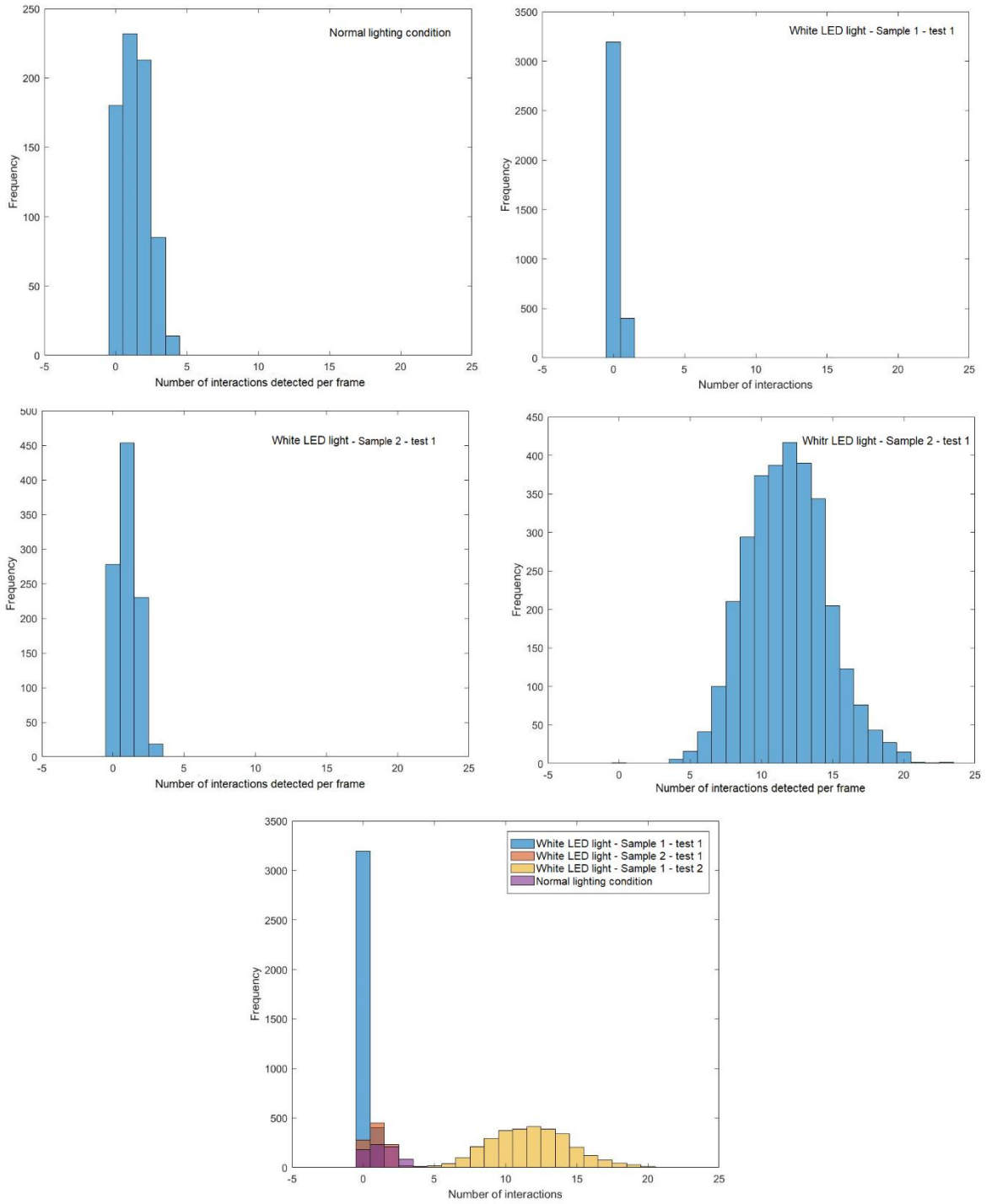
The studies performed on the behavior of the bacteria revealed that they are social organisms [50, 51, 52] and can communicate with one another through chemical signals such as secretion and detection of small diffusible signaling molecules. Image processing is a tool that gives access to cell interaction frequency. The frequency of cell interactions is presented in Figure 3-23 and Figure 3-24 for cells exposed to the light of laser pointer and LED, respectively. The error of measurements in this plot is connected to the accuracy of the aforementioned software under the heading “Video Recording and Imaging Techniques”. The minimum distance for detecting cell interactions was considered  $35\ \mu\text{m}$  and the Python script is provided in Appendix E.

Figure 3-25 demonstrates the mean of the total frequency of the cell interactions. The frequency of cell interactions is highest for the normal lighting condition and then reduced for cells exposed to the light of LED and lowest for the ones exposed to laser pointer light. Figure 3-25 implies that any external lighting condition will reduce the interactions between cells in the highly diluted suspensions of the *Synechocystis* sp. CPCC 534.





**Figure 3-23. Frequency of interactions for cells exposed to the light of laser pointer**



**Figure 3-24. Frequency of interactions for cells exposed to the light of LED**

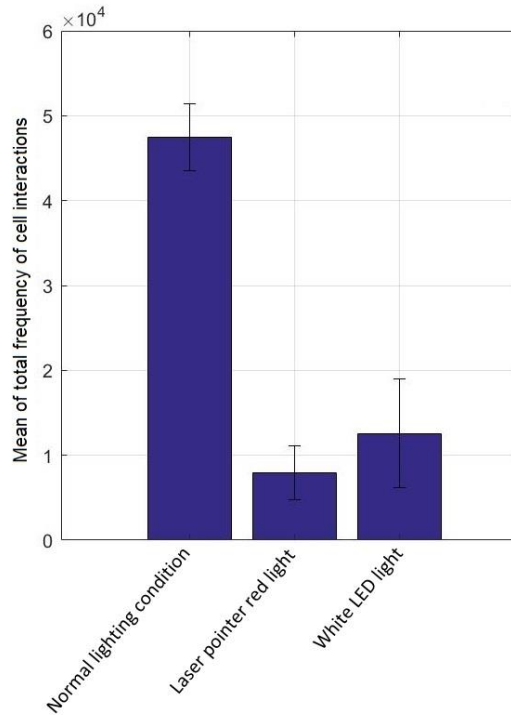


**Figure 3-25. Mean of the total frequency of interactions in different lighting conditions.**

### 3.3 Concluding remarks

This chapter deals with the qualitative and quantitative (statistical) analysis of the motion of cells in diluted suspensions of *Synechocystis* sp. C-PCC 534 using cell tracking by image processing technique in a microfluidic device. Moreover, it investigates the response of *Synechocystis* sp. cells to light.

The trajectories of bacterial cells display an alternating intermittent motion that consists of “run phases” during which bacteria have high-speed motility and “tumble phases” during which bacteria are restricted to a limited area. This intermittence becomes explicit when analyzing the ensembled-averaged mean square displacement (EMSD) distributions. In fact, the distributions have two parts, the sharp central part that corresponds to the non-diffusive tumble phase and the tails that broaden and tend to Gaussian (Normal) distribution and corresponds to the diffusive run phases.

The photosynthetic microorganisms are sensitive to light and can adapt their motility. In stronger illumination, the bacteria have a higher propensity to be in a run phase and thereby a greater number of higher peaks in velocity variations with time.

Comparing the distributions of the probability of displacements of cells exposed to the light of the LED, laser pointer, and normal lighting condition revealed that cells spend more time tumbling and idling under laser pointer light while spending more time running when exposed to white LED light. Moreover, the frequency of cell-cell interactions shows that exposure to an external light decreases the number of interactions.

## Chapter 4

### 4 « Conclusions and Recommendations »

#### 4.1 Summary

Active fluid is defined as the suspension of self-propelled particles, for instance, bacteria, alga, and sperm cells. The science and engineering of active fluids is an emerging area with many applications that incorporates both prevention or promotion of the growth of microorganisms; examples are algal blooms (AB) and photobioreactors (PBR) used for biofuel production. Despite our current understanding of active fluid mechanics, more knowledge is required to fully understand the physical and rheological properties of bacterial suspensions as well as phototaxis and interactions between cells. These basic building blocks of knowledge are essential for the vast applications in industrial, medical, food, and energy fields; and their direct and indirect effects on the environment and human lives.

This research (in chapter 2) aimed to study the effects of shear stress applied during cell growth on the viscosity, biomass production, cell size, growth rate, and doubling per day of suspensions of *Synechocystis* sp. CPCC 534. Experiments were conducted at three different stirring rates in well-controlled conditions and the results were compared with stationary conditions where only molecular diffusion and cell motility governed the transport phenomena and biomass production. Moreover, the effects of cell concentration and cell motility on the rheological behavior of suspensions of *Synechocystis* sp. were investigated.

This research (in chapter 3) also focused on cell tracking by image processing technique to investigate the effects of light on highly diluted bacterial suspensions. The experiments were performed in a closed microfluidic chamber under three different lighting conditions to investigate cell motility, get access to interaction frequency between cells as a function of time (cell-cell interaction), and phototaxis. To serve this purpose, image processing was done by Python Programming Language. In addition, a preliminary microfluidic channel and its experimental setup were presented that can be used for further investigation on highly diluted suspensions of *Synechocystis* sp. in the presence of laminar flow.

## 4.2 Conclusions

The outputs of the first part of the research are: (I) A significant increase was observed in biomass, doubling per day, and yield production as a result of flow in comparison with the non-agitated suspension. (II) Mixing had a negative impact on cell size. (III) The viscosity of cell suspensions which experienced various shear rates during growth showed Newtonian behavior at all cell concentrations. (IV) Shear history does not influence the rheological behavior of suspensions. (V) Cell motility plays no role in the viscosity of suspensions that corresponds to the low and twitching nature of the motility of *Synechocystis* sp. CPCC 534. (VI) Cell concentration showed a noticeable influence on the viscosity of cell suspensions. (VII) Viscosity is a linearly increasing function of the cell volume fraction, as it is for passive rigid particles. However, this increase is smaller than the one observed in suspensions of rigid particles. This can be attributed to the fact that the *Synechocystis* sp. cells are soft particles and can deform. The rheological output of this research is new to the literature of active fluid to the best of the author's knowledge. The obtained results can be used to improve the bioreactor design for better productivity.

The outputs of the second part of the research are: (I) The trajectories of bacterial cells display an alternating intermittent motion that consists of "run phases" during which bacteria have high-speed motility and "tumble phases" during which bacteria are restricted to a limited area. (II) The analysis of the distribution of ensembled-averaged mean square displacement (EMSD) and velocity variations with time showed that in stronger illumination, the bacteria have a higher propensity to be in a run phase (III) Cells spend more time tumbling in weaker light while spending more time running when exposed to stronger light. (IV) Based on the frequency of cell-cell interactions, that exposure to an external light decreases the number of interactions between cells.

To sum up, the technique in the current research work can be used to develop numerical simulations and analytical models to describe the dynamics of the interaction of *Synechocystis* sp. with each other, to optimize the design of bioreactors for biofuel production and other applications in food, hygiene fields.

### 4.3 Recommendations and future works

For the first part of the research, a greater level of insight into the underlying physical mechanism of the rheological behavior of microorganism suspensions is achievable by measuring local viscosity under shear and also conduction microscopic observation of the microorganism orientation with implied shear field direction. For measuring the viscosity of suspensions of *Synechocystis* sp. by Anton-Paar Modular Compact Rheometer (MCR302, Austria), a double-gap Couette tool can be used. This tool is more sensitive and provides the opportunity to perform viscosity measurements in a wider range of shear rates,  $\dot{\gamma}$  ( $s^{-1}$ ) without facing the hydrodynamic instability - Taylor vortices - in the annular ring of fluid inside the concentric cylinder geometry tool.

For the second part of the research, a superior understanding of the link between individual cells' motility, the adaptation of motility of cells, and cell-cell interaction to local lighting conditions in quiescent conditions can be achieved by studying bacterial behavior in highly diluted suspensions. The future work recommendations are: (I) The work can focus on studying the phototaxis motion of cells in the suspension of *Synechocystis* with a combination of different angles, directions, light colors, and wavelengths. (II) Cell motility and cell-cell interaction can be investigated in presence of other external and/or internal stimuli for instance thermotaxis and chemotaxis. (III) Wild-type and mutant strains of taxD 1 (negative phototaxis) and taxD 3 (lack of motility) can be used. (IV) Different designs of microfluidic devices like multichannel microfluidic devices can be used to study phototaxis and chemotaxis in diluted suspensions of bacterial flows. (V) From the computer science and programming point of view, a Graphical User Interface (GUI)<sup>4</sup> can be established that takes a video as input and the output would be the trace of trajectories, dynamic trajectories, the probability density of displacements such a GUI can be super beneficial for use in research labs.

---

<sup>4</sup> The graphical user interface is a form of user interface that allows users to interact with electronic devices through graphical icons and audio indicator such as primary notation, instead of text-based user interfaces, typed command labels or text navigation.

## References

- [1] F. Sarsekeyeva, B. K. Zayadan, A. Usserbaeva, V. S. Bedbenov, M. A. Sinetova and D. A. Los, "Cyanofuels: Biofuels From Cyanobacteria. Reality," *Photosynthesis Research*, vol. 125, p. 329–340, 2015.
- [2] B. G. Subhadra, "Comment on “Environmental Life Cycle Comparison of Algae to Other Bioenergy Feedstocks”," *Environmental Science & Technology*, vol. 44, no. 9, pp. 3641-3642, 2010.
- [3] G. Dragone, B. Fernandes, A. A. Vice and J. A. Teixeira , "Third generation biofuels from microalgae," *Current Research, Technology and Education Topics in Applied Microbiology and Microbial Biotechnology*, , pp. 1355-1366, 2010.
- [4] G. M. LimaPedro , P. C. N. Teixeirab , C. M. L. L. Teixeira, D. Filócomo and C. . L. S. Lage, "Influence of spectral light quality on the pigment concentrations and biomass productivity of *Arthrospira platensis*," *Algal Research*, vol. 31, pp. 157-166, 2018.
- [5] N. T. Eriksen, "Production of phycocyanin—a pigment with applications in biology, biotechnology, foods and medicine," *Applied Microbiology and Biotechnology*, vol. 80, no. 1, pp. 1-14, 2018.
- [6] S. Sekar and M. Chandramohan , "Phycobiliproteins as a commodity: trends in applied research, patents and commercialization," *Journal of Applied Phycology*, vol. 20, no. 2, pp. 113-136, 2008.
- [7] I. de O Moreira, T. S. Passos, C. Chiapinni, G. K. Silveira, J. C. M. Souza, L. G. Coca-Vellarde, R. Deliza and K. G. de Lima Araújo, "Colour evaluation of a phycobiliprotein-rich extract obtained from *Nostoc PCC9205* in acidic solutions and yogurt," *The Journal of the Science of Food and Agriculture*, vol. 92, no. 3, pp. 598-605, 2011.
- [8] R. Prasad Rastogi, R. Raghav Sonani and D. Madamwar, "Cyanobacterial Sunscreen Scytonemin: Role in Photoprotection and Biomedical Research," *Applied Biochemistry and Biotechnology*, vol. 176, no. 6, p. 1551–1563, 2015.
- [9] P. Derikvand, C. A. Llewellyn and S. Purton, "Cyanobacterial metabolites as a source of sunscreens and moisturizers: a comparison with current synthetic compounds," *European Journal of Phycology*, vol. 52, no. 1, pp. 43-56, 2017.
- [10] A. Jaiswal, . D. Kumar Koli, . A. Kumar, S. Kumar and S. Sagar, "Pigments analysis of cyanobacterial strains," *International Journal of Chemical Studies*, vol. 6, no. 2, pp. 1248-1251 , 2018.



- [11] I. Sanseverino, D. Conduto, L. Pozzoli, S. Dobricic and T. Lettieri, "Algal bloom and its economic impact," European Union, Italy, 2016.
- [12] M. Bingham, S. K. Sinha and F. Lupi, "Economic Benefits of Reducing Harmful Algal Blooms in Lake Erie," Environmental Consulting & Technology, Inc., October 2015.
- [13] D. M. Anderson, P. Hoagland, Y. Kaoru and A. W. White, "Estimated Annual Economic Impacts from Harmful Algal Blooms (HABs) in the United States," Woods Hole Oceanographic Institution, 2000.
- [14] Y. Chisti, "Biodiesel from microalgae," *Biotechnology Advances*, vol. 25, no. 3, pp. 94-306, 2007.
- [15] P. M. Schenk, S. R. Thomas-hall, E. Stephens, U. C. Marx, J. H. Mussgnug, C. Posten, O. Kruse and B. Hankamer, "Second generation biofuels: high-efficiency microalgae for biodiesel production," *BioEnergy Research*, vol. 1, pp. 20-43, 2008.
- [16] A. Converti, A. A. Casazza, E. Y. Ortiz, P. Perego and M. Del Borghi, "Effect of temperature and nitrogen concentration on the growth and lipid content of *Nannochloropsis oculata* and *Chlorella vulgaris* for biodiesel production," *Chemical Engineering and Processing*, vol. 48, pp. 1146-1151, 2009.
- [17] E. Jacob-Lopes, C. H. G. Scoparo, L. M. C. F. Lacerda and T. T. Franco, "Effect of light cycles (night/day) on CO<sub>2</sub> fixation and biomass production by microalgae in photobioreactors," *Chemical Engineering and Processing*, vol. 48, no. 1, pp. 306-310, 2009.
- [18] H. Hu, H. F. Wang, J. Y. Li, L. L. Ma, X. F. Shen and R. J. Zeng, "Evaluation of the effect of agitation speed on the growth and high-value LC-PUFA formation of *Porphyridium cruentum* based on basic rheological analysis," *The Journal of Chemical Technology & Biotechnology*, vol. 94, p. 2158–2166, 2019.
- [19] A. Solimeno, F. G. Acien and J. García, "Mechanistic model for design, analysis, operation and control of microalgae cultures: Calibration and application to tubular photobioreactors," *Algal Research*, vol. 21, pp. 236-246, 2017.
- [20] S. K. Yatirajula, A. Shrivastava, V. K. Saxena and J. Kodavatyc, "Flow behavior analysis of *Chlorella Vulgaris* microalgal biomass," *Heliyon*, vol. 5, no. 6, p. e01845, 2019.
- [21] J. F. Cornet, C. G. Dussap and D. G., "A structured model for simulation of cultures of the cyanobacterium *Spirulina platensis* in photobioreactors: I. Coupling between light transfer and growth kinetics," *Biotechnology and Bioengineering*, vol. 40, pp. 817-825, 1992.

- [22] C. Gonzalez-Fernandez and R. Muñoz, "Photobioreactors for the production of microalgae," in *Microalgae-Based Biofuels and Bioproducts: From Feedstock Cultivation to End-products*, Woodhead Publishing, 2018, pp. 1-44.
- [23] Ongreening, "Ongreening," 2013. [Online]. Available: <https://ongreening.com/en/Projects/biq-the-clever-treefrog-1072#images>. [Accessed 22 April 2021].
- [24] C. Ganesh Kumar and S. K. Anand, "Significance of microbial biofilms in food industry: a review," *International Journal of Food Microbiology*, vol. 42, no. 1-2, pp. 9-27, 1998.
- [25] M. Simoes, L. C. Simoes and M. J. Vieira, "A review of current and emergent biofilm control strategies," *Lwt-Food Science and Technology*, vol. 43, no. 4, pp. 573-583, 10 April 2010.
- [26] D. Bray, *Cell Movements: From Molecules to Motility*, New York: Garland Science, Taylor & Francis Group, 2001.
- [27] T. A. Sarma, *Handbook of Cyanobacteria*, Taylor & Francis, 2013.
- [28] K. Peters, "Korseby Online - Cyanobacteria," [Online]. Available: <https://www.korseby.net/outer/flora/algae/cyanobacteria/index.html>. [Accessed 22 April 2021].
- [29] T. Vourc'h, H. Peerhossain, J. Leopoldes, A. Mejean, F. Chauvat and C. Cassier-Chauvat, "Slowdown of the surface diffusion during early stages of bacterial colonization," *Physical Review*, vol. 97, no. 3, 2018.
- [30] V. Singh, *Text Book Of Botany, Diversity Of Microbes And Cryptogams*, Fourth revised ed., Rastogi Pulications, 2008.
- [31] R.-L. Heng and L. Pilon, "Radiation characteristics and effective optical properties of dumbbell-shaped cyanobacterium *Synechocystis* sp.," *Journal of Quantitative Spectroscopy & Radiative Transfer*, vol. 174, pp. 65-78, 2016.
- [32] A. Karimi, D. Karig, A. Kumarc and A. M. Ardekani, "Interplay of physical mechanisms and biofilm processes: review of microfluidic methods," *Lab Chip*, vol. 15, p. 23-42, 2015.
- [33] M. Wilkins, L. Hall-Stoodley, R. N.Allan and S. N.Faust, "New approaches to the treatmentof biofilm-related infections," *Journal of Infection*, vol. 69, pp. S47-S52, 2014.

- [34] M. G. Mazza, "The physics of biofilms—an introduction," *Journal of Physics D: Applied Physics*, vol. 49, no. 20, 2016.
- [35] D. Nakanea and T. Nishizakaa, "Asymmetric distribution of type IV pili triggered by directional light in unicellular cyanobacteria," *Proceedings of the National Academy of Sciences*, vol. 114, no. 25, p. 6593–6598, 2017.
- [36] E. Lauga, "Bacterial Hydrodynamics," *The Annual Review of Fluid Mechanics*, vol. 48, p. 105–30, 2016.
- [37] Z. Long, B. Quaiife, H. Salman and Z. N. Oltvai, "Cell-cell communication enhances bacterial chemotaxis toward external attractants," *Scientific Reports*, vol. 7, no. 12855, 2017.
- [38] M. Ch. Nguyen, H. Peerhossaini , M. M. Salek and M. Jarrahi, "Control of particle distribution at the outlet of double Y-microchannel using pulsatile flow," in *ASME-JSME-KSME 2019 Joint Fluids Engineering Conference*, San Francisco, CA, USA, 2019.
- [39] R. Bronnenmeier and H. Märkl, "Hydrodynamic stress capacity of microorganisms," *Biotechnology and Bioengineering*, vol. 24, no. 3, pp. 553-578, 1982.
- [40] E. M. Grima, Y. Chisti and M. Moo-young, "Characterization of shear rates in airlift bioreactors for animal cell culture," *of Biotechnology*, vol. 54, pp. 195-210, 1997.
- [41] F. G. Camacho, A. C. Gómez, T. M. Sobczuk and E. M. Grima, "Effects of mechanical and hydrodynamic stress in agitated, sparged cultures of *Porphyridium cruentum*," *Process Biochemistry*, vol. 35, no. 1, pp. 1045-1050., 2000.
- [42] Y. Chisti and U. J. Jauregui-Haza, "Oxygen transfer and mixing in mechanically agitated airlift bioreactors," *Biochemical Engineering Journal*, vol. 10, pp. 143-153, 2002.
- [43] T. M. Sobczuk, E. M. Camacho, E. M. Grima and Y. Chisti, "Effects of agitation on the microalgae *Phaeodactylum tricorutum* and *Porphyridium cruentum*," *Bioprocess and Biosystems Engineering*, vol. 28, no. 4, pp. 243-250, 2006.
- [44] P. Kaiwan-Arporn, P. D. Hai, N. T. Thu and A. P. Annachhatre, "Cultivation of cyanobacteria for extraction of lipids," *Biomass & Bioenergy*, vol. 44, pp. 142-149, 2012.
- [45] M. Leupold, S. Hindersin, G. Gust, M. Kerner and D. Hanelt, "Influence of mixing and shear stress on *Chlorella vulgaris*, *Scenedesmus obliquus*, and *Chlamydomonas reinhardtii*," *Journal of Applied Phycology*, vol. 25, pp. 485-495, 2013.

- [46] A. Souliès, J. Pruvost, J. Legrand, C. Castelain and T. I. Burghilea, "Rheological properties of suspensions of the green microalga *Chlorella vulgaris* at various volume fractions," *Rheologica Acta*, vol. 52, p. 589–605, 2013.
- [47] D. Quemada, "Rheological modelling of complex fluids. I. The concept of effective volume fraction revisited," *The European Physical Journal Applied Physics*, vol. 1, pp. 119-127, 1997.
- [48] R. Simha, "A treatment of the viscosity of concentrated suspensions," *Journal of Applied Physics*, vol. 23, p. 1020–1024, 1952.
- [49] N. Cagney, T. Zhang, R. Bransgrove, M. J. Allen and S. Balabani, "Effects of cell motility and morphology on the rheology of algae suspensions," *Journal of Applied Phychology*, vol. 29, pp. 1145-1157, 2017.
- [50] A. B. Goryachev, "Understanding Bacterial Cell-Cell Communication with Computational Modeling," *Chemical Reviews*, vol. 111, p. 238–250, 2011.
- [51] R. P. Ryan and J. M. Dow, "Diffusible signals and interspecies communication in bacteria," *Microbiology*, vol. 154, p. 1845–1858, 2008.
- [52] R. P. Ryan and J. M. Dow, "Small molecule control of bacterial biofilms," *Organic and Biomolecular Chemistry*, vol. 10, p. 7457–7474, 2012.
- [53] Y. H. Li and X. L. Tian, "Quorum Sensing and Bacterial Social Interactions in Biofilms," *Sensors*, vol. 12, p. 2519–2538, 2012.
- [54] A. Jayaraman and T. K. Wood, "Bacterial quorum sensing: Signals, circuits, and implications for biofilms and disease," *Annual Review of Biomedical Engineering*, vol. 10, p. 145–167, 2008.
- [55] C. M. Waters and B. L. Bassler, "Quorum sensing: Cell-to-cell communication in bacteria," *Annual Review of Biomedical Engineering*, vol. 21, p. 319–346, 2005.
- [56] J. M. Henke and B. L. Bassler, "Bacterial social engagements," *Trends in Cell Biology*, vol. 14, p. 648–656, 2004.
- [57] K. Zhao, B. S. Tseng, B. Beckerman, F. Jin, M. L. Gibiansky, J. J. Harrison and E. Luijten, "Psl trails guide exploration and microcolony Psl trails guide exploration and microcolony," *NATURE*, vol. 497, pp. 388-392, 2013.
- [58] J. Adler, "Chemotaxis in Bacteria," *Science*, vol. 153, p. 708–716, 1966.
- [59] J. Adler, "My Life with Nature," *Annual Review of Biochemistry*, vol. 80, p. 42–70, 2011.

- [60] T. W. Grebe and J. Stock, " Bacterial chemotaxis: The five sensors of a bacterium," *Current Biology*, vol. 8, no. 5, pp. R154-7, 1998.
- [61] G. H. Wadhams and J. P. Armitage, " Making sense of it all: Bacterial chemotaxis," *Nature Reviews Molecular Cell Biology*, vol. 5, p. 1024–1037, 2004.
- [62] M. Eisenbach, *Bacterial Chemotaxis*, John Wiley & Sons , Ltd, 2011.
- [63] G. L. Hazelbauer, J. J. Falke and J. S. Parkinson, "Bacterial chemoreceptors: high-performance signaling in networked arrays," *Trends in Biochemical Sciences*, vol. 33, p. 9–19, 2008.
- [64] S. . M. King, *Dyneins: Structure, Biology and Disease (Second Edition)*, Academic Press, 2018, pp. 629-652.
- [65] N. Schuergers, C. W. Mullineaux and A. Wilde, "Cyanobacteria in motion," *Current Opinion in Plant Biology*, vol. 37, pp. 109-115, 2017.
- [66] M. Burriesci and D. Bhaya, "Tracking phototactic responses and modeling motility of *Synechocystis* sp. strain PCC6803," *Journal of Photochemistry and Photobiology B: Biology*, vol. 91, pp. 77-86, 2008.
- [67] T. Ursell, R. Man Wah Chau, S. Wise and D. Bhaya, "Motility Enhancement through Surface Modification Is Sufficient for Cyanobacterial Community Organization during Phototaxis," *PLoS Comput Biol*, vol. 9, no. 9, p. e1003205, 2013.
- [68] N. Schuergers, T. Lenn, R. Kampmann, M. V. Meissner, T. Esteves, M. Temerinac-Ott, J. G. Korvink, . A. R. Lowe, C. W. Mullineaux and A. Wilde, "Cyanobacteria use micro-optics to sense light direction," *eLife*, vol. 5, p. e12620, 2016.
- [69] A. Wilde and C. W. Mullineaux, "Light-controlled motility in prokaryotes and the problem of directional light perception," *FEMS Microbiology Reviews*, vol. 41, no. 6, p. 900–922, 2017.
- [70] R. Man Wah Chau, D. Bhaya and K. C. Huang, "Emergent Phototactic Responses of Cyanobacteria under Complex Light Regimes," *mBio*, vol. 8, no. 2, p. 1–15, 2017.
- [71] T. Vourc'h, J. Léopoldès and H. Peerhossaini, "Light Control of the Diffusion Coefficient of Active Fluids," *Journal of Fluids Engineering*, vol. 142, no. 3, p. 031109 (7 pages), 2020.
- [72] G. I. Bell, "Models for the Specific Adhesion of Cells to Cells," *American Association for the Advancement of Science*, vol. 200, no. 4342, pp. 618-627, 1978.

- [73] T. J. Pedley and J. O. Kessler, "Hydrodynamic phenomena in suspensions of swimming microorganisms," *Annual Review Fluid Mechanics*, vol. 24, pp. 313-358, 1992.
- [74] J. Dunkel, S. Heidenreich, M. Bar and R. E. Goldstein, "Minimal continuum theories of structure formation in dense active fluids," *New Journal of Physics*, vol. 15, no. 045016, 2013.
- [75] D. Dunkel, S. Heidenreich, K. Drescher, H. H. Wensink, M. Bar and R. E. Goldstein, "Fluid Dynamics of Bacterial Turbulence," *Physical Review Letters*, vol. 110, no. 228102, 2013.
- [76] R. E. Goldstein, "Green Algae as Model Organisms for Biological Fluid Dynamics," *Annual Review of Fluid Mechanics*, vol. 1, no. 47, p. 343–375, 2015.
- [77] H. Chen, Q. Fu, Q. Liao, H. Zhang, Y. Huang and X. Xi, "Rheological properties of microalgae slurry for application in hydrothermal pretreatment systems," *Bioresource Technology*, vol. 249, pp. 599-604, 2018.
- [78] A. Wileman, A. Ozkan and H. Berberoglu, "Rheological properties of algae slurries for minimizing harvesting energy requirements in biofuel production," *Bioresource Technology*, vol. 104, pp. 432-439, 2012.
- [79] L. J. P. P. S. Rafai, "Effective viscosity of microswimmer suspensions," *Physical Review Letters*, vol. 104, p. 098102, 2010.
- [80] K. Kanek, S. Sato, H. Kotani, A. Tanaka, E. Asamizu, Y. Nakamura, N. Miyajima, M. Hirose, M. Sugiura, S. Sasamoto, T. Kimura, T. Hosouchi, A. Matsuno, A. Muraki, N. Nakazaki, K. Naruo, S. Okumura, S. Shimpo, C. Takeuchi, T. Wada, A. Watanabe, C. Yamada, M. Yasuda and S. Tabata, "Sequence Analysis of the Genome of the Unicellular Cyanobacterium *Synechocystis* sp. Strain PCC6803. II. Sequence Determination of the Entire Genome and Assignment of Potential Protein-coding Regions," *DNA RESEARCH*, vol. 3, pp. 109-136, 1996.
- [81] J. Panoff, B. Priem, H. Morvan and F. Joset, "Sulphated exopolysaccharides produced by two unicellular strains of cyanobacteria, *Synechocystis* PCC 6803 and 6714," *Archives of Microbiology*, vol. 150, p. 558–563, 1988.
- [82] R. Rippka, . J. Deruelles, . J. B. Waterbury, . M. Herdman and R. Y. Stanier, "Generic Assignments, Strain Histories and Properties of Pure Cultures of Cyanobacteria," *Journal of General Microbiology*, vol. 111, no. 1, pp. 1-66, 1979.
- [83] J. A. Sánchez Pérez, E. M. Rodríguez Porcel, J. L. Casas López, J. M. Fernández Sevilla and Y. Chisti, "Shear rate in stirred tank and bubble column bioreactors," *Chemical Engineering Journal*, vol. 124, pp. 1-5, 2006.

- [84] J. H. Rushton, E. W. Costich and H. J. Everett, "Power characteristics of mixing impellers part I," *Chemical Engineering Progress*, vol. 46, pp. 395-404, 1950.
- [85] H. Furukawa, Y. Kato, Y. Inoue, T. Kato, Y. Tada and S. Hashimoto, "Correlation of power consumption for several kinds of mixing impellers," *International Journal of Chemical Engineering*, vol. 106496, no. 106496, pp. 1-6, 2012.
- [86] Y. Kato, Y. Tada, Y. Takeda, Y. Hirai and Y. Nagatsu, "Correlation of power consumption for propeller and Pfaudler-type impellers," *Journal of Chemical Engineering of Japan*, vol. 42, pp. 6-9, 2009.
- [87] K. J. Erratt, I. F. Creed and C. G. Trick, "Comparative effects of ammonium, nitrate and urea on growth and photosynthetic efficiency of three bloom-forming cyanobacteria," *Freshwater Biology*, vol. 63, pp. 626-638, 2018.
- [88] R. R. L. Guillard, "Handbook of phycological methods, culture methods and growth measurements.," in *Division rates. In: Stein, J. R. (ed.)*, London, Cambridge University Press, 1973, pp. 289-311.
- [89] R. A. Andersen, *Algal culturing techniques*, Hong Kong: Elsevier Inc., 2005.
- [90] P. Dechatiwongse, S. Srisamai, G. Maitland and K. Hellgardt, "Effects of light and temperature on the photoautotrophic growth and photoinhibition of nitrogen-fixing cyanobacterium *Cyanothece* sp. ATCC 51142," *Algal Res*, vol. 5, pp. 103-111, 2014.
- [91] H. Fadlallah, M. Jarrahi, É. Herbert, R. Ferrari, A. Méjean and H. Peerhossaini, "Active Fluids: Effects of Hydrodynamic Stress on Growth of Self-Propelled Fluid Particles," *Journal of Applied Fluid Mechanics*, vol. 13, no. 2, pp. 561-570, 2020.
- [92] M. Isleten-Hosoglu, I. Gultepe and M. Elibol, "Optimization of carbon and nitrogen sources for biomass and lipid production by *Chlorella saccharophila* under heterotrophic conditions and development of Nile red fluorescence based method for quantification of its neutral lipid content," *Biochemical Engineering Journal*, vol. 61, pp. 11-19, 2012.
- [93] A. R. A. Cordara, C. Pagliano, P. Van Alphen, R. Pirone, G. Saracco, F. B. dos Santos, K. Hellingwerf and N. Vasile, "Analysis of the light intensity dependence of the growth of *Synechocystis* and of the light distribution in a photobioreactor energized by 635 nm light," *PeerJ*, vol. 6, p. e5256, 2018.
- [94] B. Wang, C. Q. Lan and M. Horsman, "Closed photobioreactors for production of microalgal biomasses," *Biotechnology Advances*, vol. 30, pp. 904-912, 2012.

- [95] G. Hodaifa, M. E. Martínez, R. Órpez and S. Sánchez, "Influence of hydrodynamic stress in the growth of *Scenedesmus obliquus* using a culture medium based on olive-mill wastewater," *Chemical Engineering and Processing*, vol. 49, pp. 1161-1168, 2010.
- [96] M. Mehdizadeh Allaf and C. G. Trick, "Multiple-stressor design-of-experiment (DOE) and one-factor-at-a-time (OFAT) observations defining *Heterosigma akashiwo* growth and cell permeability," *Journal of Applied Phycology*, vol. 31, p. 3515–3526, 2019.
- [97] T. Kiørboe, "Turbulence, phytoplankton cell size, and the structure of pelagic food webs," *Advances in Marine Biology*, vol. 29, pp. 1-72, 1993.
- [98] Z. V. Finkel, "Light absorption and size scaling of light-limited metabolism in marine," *Limnology and Oceanography*, vol. 46, pp. 86-94, 2001.
- [99] Z. V. Finkel, J. Beardall, K. J. Flynn, A. Quigg, T. A. V. Rees and J. A. Raven, "Phytoplankton in a changing world: cell size and elemental stoichiometry," *Journal of Plankton Research*, vol. 32, pp. 119-137, 2010.
- [100] K. L. M. G. J. G. U. R. T. R. L. Schlüter, "Adaptation of a globally important coccolithophore to ocean warming and acidification," *Nature Climate Change*, vol. 4, pp. 1024-1030., 2014.
- [101] A. Einstein, "Berichtigung zu meiner arbeit: Eine neue bestimmung der moleküldimensionen," *AnP*, vol. 339, pp. 591-592, 1911.
- [102] A. Einstein, "A new determination of molecular dimensions," *Annals of Physics*, vol. 19, pp. 289-306, 1906).
- [103] T. D. I.M. Krieger, "A mechanism for non- Newtonian flow in suspensions of rigid spheres," *T. Soc Rheol.*, vol. 3, pp. 137-152, 1959.
- [104] D. A. Fletcher and J. A. Theriot, "An introduction to cell motility for the physical scientist," *Physical Biology*, vol. 1, no. 1, 2004.
- [105] A. K. Tsirogiannia, N. M. Moutsopoulos and H. M. Moutsopoulos, "Wound healing, and the immune response," *Injury*, vol. 37, no. 1, pp. S5-S12, 2006.
- [106] S. Jahromi, Experimental analysis and simulation of bacteria chemotactic behavior in response to antibacterials [master's thesis], Hamilton, Ontario: McMaster University, 2019.
- [107] T. Contributors, "GitHub," [Online]. Available: <http://soft-matter.github.io/trackpy/v0.4.2/>. [Accessed 27 February 2021].



- [108] J. C. Crocker and E. . R. Weeks, "Department of Physics-Emory University," [Online]. Available: <http://www.physics.emory.edu/faculty/weeks//idl/tracking.html>. [Accessed 27 February 2021].
- [109] D. Berg and H. Brown, "Chemotaxis in Escherichia coli analysed by three-dimensional tracking," *Nature*, vol. 239, no. 5374, pp. 500-504, 1972.
- [110] M. Warren and J. Rottler, "Atomistic mechanism of physical ageing in glassy materials," 2009..
- [111] P. Chaudhuri, L. Berthier and W. Kob, "Universal nature of particle displacements close to glass and jamming transitions," *Physical Review Letters*, vol. 99, no. 6, pp. 2-5, 2007.
- [112] R. W. Thimijan and R. D. Heins, "Photometric, Radiometric, and Quantum Light Units of Measure: A Review of Procedures for Interconversion," *HortScience*, vol. 18, no. 6, pp. 818-822, 1982.
- [113] L. Li, "Biologydictionary.net Editors.," 14 November 2014. [Online]. Available: <https://biologydictionary.net/heterotroph/>. [Accessed 15 April 2021].
- [114] J. S. Mattick, "Type IV Pili and Twitching Motility," *Annual Review of Microbiology*, vol. 56, p. 289–314, 2002.
- [115] T. D. Palmer, W. J. Ashby, J. D. Lewis and A. Zijlstra, "Targeting tumor cell motility to prevent metastasis," *Advanced Drug Delivery Reviews*, vol. 63, no. 8, pp. 568-581, 2011.

## Appendices

### A. Appendix A

$N_p$  was determined using the following empirical correlations developed by Kato *et al.* and Furukawa *et al.* [35, 36] for propeller and pfaudler-type impellers in agitated reactors:

$$N_p = \{[1.2\pi^4\beta^2]/[8d^3/(D^2H)]\}f \quad \text{Equation 0-1}$$

$$f = C_L/Re_G + C_t\{[C_{tr}/Re_G + Re_G]^{-1} + (f\sim/C_t)^{1/m}\}^m \quad \text{Equation 0-2}$$

$$Re_G = \{[\pi \eta \ln(D/d)]/(4 d/\beta D)\}Re_d \quad \text{Equation 0-3}$$

$$C_L = 0.215 \eta n_p (d/H)[1 - (d/D)^2] \\ + 1.83 (b \sin\theta / H)(n_p / 2 \sin\theta)^{1/3} \quad \text{Equation 0-4}$$

$$C_t = [(3X^{1.5})^{-7.8} + (0.25)^{-7.8}]^{-1/7.8} \quad \text{Equation 0-5}$$

$$m = [(0.8 X^{0.373})^{-7.8} + 0.333^{-7.8}]^{-1/7.8} \quad \text{Equation 0-6}$$

$$C_{tr} = 23.8 (d/D)^{-3.24} (b \sin\theta/D)^{-1.18} X^{-0.74} \quad \text{Equation 0-7}$$

$$f\sim = 0.0151(d/D)C_t^{0.308} \quad \text{Equation 0-8}$$

$$X = \gamma n_p^{0.7} b \sin^{1.6}\theta/H \quad \text{Equation 0-9}$$

$$\beta = 2 \ln(D/d) [(D/d) - (d/D)] \quad \text{Equation 0-10}$$

$$\gamma = [\eta \ln(D/d) / (\beta D/d)^5]^{1/3} \quad \text{Equation 0-11}$$

$$\eta = 0.711 \{0.157 + [n_p \ln(D/d)]^{0.611}\}/\{n_p^{0.52} [1 - (d/D)^2]\} \quad \text{Equation 0-12}$$

Where  $n_p$  corresponds to the number of the blades which is 2 in our experiment;  $\theta$  is the pitch angle of the blade that is equal to  $\pi/2$  because a flat magnetic agitation bar has been used that is analogic to the paddle mixing impeller without a central axis.  $Re_G$  is the modified Reynolds number and  $Re_d$  is the impeller Reynolds number as defined in Equation 2-3.

## B. Appendix B



**Figure B-1. Scale and micropipette used for calculating density**

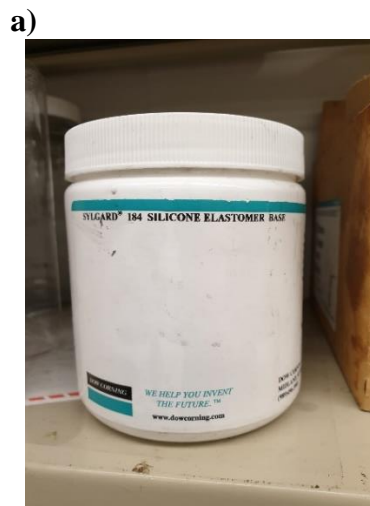


**Figure B-2. Sylgard 184 Silicone Elastomer Kit including a) Base and b) Curing agent**

a)



b)



**Figure B-3. a) Thermo Scientific™ Sorvall™ Legend™ XT/XF Centrifuge, US b) Thermo Scientific™, SPECTRONIC™ 200 Spectrophotometer, US.**

## C. Appendix C

The summary of the failed trials in viscosity measurements of suspensions of *synechocystis* sp. in chapter 2 is brought here as a learning experience for future readers.

At first, a falling-ball viscometer (Gilmont Instruments) with a glass ball and tube was used every other day to measure the viscosity of the bacterial samples during their growth period. The glass tube was filled with 10 ml samples at 20 °C and the glass ball was added carefully and allowed to drop into the tube. The instrument was restored to its normal vertical position and the time of the descent between two sets of fiduciary lines was measured. During the experiments, care was taken to ensure that no air bubbles were attached to the ball's surface. The suspension viscosity was calculated using the following equation:

$$\eta = K (\rho_f - \rho)t \quad \text{Equation C-13}$$

where  $\eta$  is the viscosity ( $c_p$ ),  $\rho_f$  is the density of glass ball which is equal to  $2.53 \text{ (gm.cm}^3\text{)}$ , and  $\rho$ ,  $t$ ,  $K$ , is the density of bacterial sample ( $\text{gm.cm}^{-3}$ ), time of descent (minutes), and viscometer constant, respectively. The viscometer constant ( $K$ ) was obtained by calibrating the instrument using DI-water and tabulated values of the viscosity of water.

However, the accuracy of the viscometer was 0.2 to 10 *cP* which was not proper for measuring the viscosity of the suspensions of *synechocystis* sp.

It was realized that the viscosity of the suspensions is close to water. So, Cannon-Fenske viscometer (Cannon Instrument Company) was used. The glass tube was filled with a 10 *ml* sample at 20 °C and placed into the holder. Suction was applied until the sample reached the center of the top bulb and the time of the descent between two sets of fiduciary lines was measured. The suspension viscosity was calculated using the following equation:

$$\eta = K\rho t \quad \text{Equation C-14}$$

where  $\eta$  is the viscosity (*cp*),  $\rho$  is the density,  $t$  is the time of descent (*s*), and  $K$  is the viscometer constant (*cST.s<sup>-1</sup>*). During the experiments, care was taken to ensure that no air bubbles were created. It has two constants at 40 °C (0.01505 (*cST.s<sup>-1</sup>*)) and 100 °C (0.01498 (*cST.s<sup>-1</sup>*)). At any other temperature, the constant can be obtained by interpolation or extrapolation. The difference between the internationally accepted value for water viscosity and measured values showed that the accuracy of the device is not enough for suspensions of *synechocystis* sp.

Before utilizing Cannon-Ubbelohde viscometer size 50 (Cannon Instrument Company), a size 75 was used. The measured values for the DI- water which was the control sample revealed that a smaller size should be used for more accurate results.

For comparing the results of dead-cell suspensions and passive spherical rigid particles, suspensions two types of seed particles for PIV including Al<sub>2</sub>O<sub>3</sub> and hollow glass spheres were used. They are about 15 microns in diameter. The suspensions were prepared at the same concentrations as the suspensions of *synechocystis* sp. The vendor of the falling ball neither published in the manual nor revealed after contacting by email the inner diameter dimensions for the glass tube of the falling ball viscometer because this was considered proprietary information. However, after carrying out the experiment and measurements it was realized that the falling ball and Cannon-Ubbelohde viscometer (size 75) were not suitable because the suspensions could not pass the tubes and clogged them.

It is worth mentioning that some preliminary measurements were performed with a type of plate rheometer but the device could not keep the sample in place and splashed out. In other words, the sample viscosity was too small for the rheometer.

Moreover, a small sample adapter laboratory viscometer (AMETEK Brookfield) with the characteristics shown in Table C-1 was utilized. However, the accuracy of the device was not in the range required for measuring the viscosity of the suspensions of *synechocystis* sp.

**Table C-1. Small sample adapter information**

Information	
<b>Model</b>	Spindle: SC4-21 Sample Chamber: SC4-13R(P) Sample Volume: 7.1 mL Shear Rate (sec <sup>-1</sup> ): 0.93 RPM

## D. Appendix D

The output power of the laser pointer used in the experiment was 0.005 W and the light source ranged up to 30 meters an output wavelength of 650 nm maximum. It emitted one light beam (single dot) and the diameter of the output beam was 1.5 mm.

For obtaining the laser light intensity, the number of photons in the light source of the laser pointer is needed. The amount of energy that a photon has can be calculated from Planck's law:

$$E = h\nu = \frac{hc}{\lambda} \quad \text{Equation A-13}$$

where h is Planck's constant which equals  $6.626 \times 10^{-34}$  Js, c is the speed of light ( $3.0 \times 10^8$  ms<sup>-1</sup>) and  $\lambda$  is the wavelength.

The light intensity (or optical intensity) is the optical power per unit area, which is transmitted through an imagined surface perpendicular to the propagation direction. The unit of the light intensity is Wm<sup>-2</sup> (where 1 Watt equals 1 joule per second).

Using aforementioned information and Equation A-13, the amount of energy in a single photon is:

$$E = \frac{hc}{\lambda} = \frac{6.626 \times 10^{-34} (Js) \times 2.998 \times 10^8 (ms^{-1})}{650 \times 10^{-9} (m)} = 3 \times 10^{-19} (J)$$

Since the power is 0.005 W the number of photons coming out of the laser pointer is:

$$\text{The number of photons per second} = \frac{0.005 (Js^{-1})}{3 \times 10^{-19} (J/photon)} = 1.67 \times 10^{16} (photon s^{-1})$$

The object is to obtain the light intensity in micromole photon per second and square meter ( $\mu mol \text{ photon } m^{-2} s^{-1}$ ). This term is based on the number of photons in a certain waveband incident per unit time (s) on a unit area ( $m^2$ ) divided by the Avogadro constant ( $6.022 \times 10^{23} \text{ mol}^{-1}$ ). It is used commonly to describe PAR in the 400-700 nm waveband [112]. So, the light intensity is:

$$\text{Light intensity} = 1.67 \times 10^{16} (photon s^{-1}) \times \frac{1}{\pi(1.5 \times 10^{-3})^2 (m^2)} \times \frac{1}{6.022 \times 10^{23} (mol^{-1})} = 39.15 \times 10^{10} (\mu mol \text{ photon } m^{-2} s^{-1}) \text{ (in a single dot)}$$

## E. Appendix E

### E.1 Animate:

```

from __future__ import division, unicode_literals, print_function # for compatibility with
Python 2 and 3
import matplotlib as mpl
import matplotlib.pyplot as plt
import matplotlib.animation as animation
from matplotlib.animation import FuncAnimation
mpl.rc('figure', figsize=(11, 9))
mpl.rc('image', cmap='gray')
import numpy as np
import pandas as pd
from pandas import DataFrame, Series # for convenience
import trackpy as tp #is a Python package for particle tracking in 2D, 3D, and higher
dimensions.

f = pd.read_csv('allframes.csv')
t = pd.read_csv('trajallframes.csv')

```

```

number_frames = 471
number_particles = 12

x_total = []
y_total = []
for particle_id in range(12):

    x_list = []
    y_list = []
    frame_id = 0
    while (frame_id < 471):

        t_filt = t[ t['particle'] == particle_id ]
        t_filt = t_filt[ t_filt['frame'] == frame_id]
        if t_filt.empty:
            frame_id += 1
            continue

        x = t_filt['x'].values[0]
        y = t_filt['y'].values[0]
        x_list.append(x)
        y_list.append(y)
        frame_id += 1

    x_total.append(x_list)
    y_total.append(y_list)

x_total = sorted(x_total, key=lambda x: len(x), reverse=True)
y_total = sorted(y_total, key=lambda x: len(x), reverse=True)

fig, ax = plt.subplots()
lines = []
for i in range(12):
    line, = ax.plot(x_total[i], y_total[i], color='k')
    lines.append(line)
    # this part is added jsut for crooping the pic and video

    # fro one single particle
    ax.set(ylim=(1250, 1450))
    ax.set(xlim=(2100, 2650))

    # for abunch of particles
    # ax.set(ylim=(700, 2500))

```



```

# ax.set(xlim=(250, 1600))

#line, = ax.plot(x_total[0], y_total[0], color='k')
#line1, = ax.plot(x_total[1], y_total[1], color='r')

for n in range(471):

    j=0
    if n < len(x_total[j]):
        lines[j].set_data(x_total[j][:n], y_total[j][:n])

    j=1
    if n < len(x_total[j]):
        lines[j].set_data(x_total[j][:n], y_total[j][:n])

    j=2
    if n < len(x_total[j]):
        lines[j].set_data(x_total[j][:n], y_total[j][:n])
    j=3
    if n < len(x_total[j]):
        lines[j].set_data(x_total[j][:n], y_total[j][:n])

    j=4
    if n < len(x_total[j]):
        lines[j].set_data(x_total[j][:n], y_total[j][:n])

    j=5
    if n < len(x_total[j]):
        lines[j].set_data(x_total[j][:n], y_total[j][:n])
    j=6
    if n < len(x_total[j]):
        lines[j].set_data(x_total[j][:n], y_total[j][:n])
    j=7
    if n < len(x_total[j]):
        lines[j].set_data(x_total[j][:n], y_total[j][:n])
    j=8
    if n < len(x_total[j]):
        lines[j].set_data(x_total[j][:n], y_total[j][:n])
    j=9
    if n < len(x_total[j]):
        lines[j].set_data(x_total[j][:n], y_total[j][:n])

    j=10

```

```

if n < len(x_total[j]):
    lines[j].set_data(x_total[j][:n], y_total[j][:n])

j=11
if n < len(x_total[j]):
    lines[j].set_data(x_total[j][:n], y_total[j][:n])

fig.canvas.draw()
fig.savefig('Frame%03d.png' %n)

```

.....

## E.2 Detecting Run and Tumble:

```

from __future__ import division, unicode_literals, print_function # for compatibility with
Python 2 and 3
import matplotlib as mpl
import matplotlib.pyplot as plt
import matplotlib.animation as animation
from matplotlib.animation import FuncAnimation
mpl.rc('figure', figsize=(11, 9))
mpl.rc('image', cmap='gray')
import numpy as np
import pandas as pd
from pandas import DataFrame, Series # for convenience
import trackpy as tp #is a Python package for particle tracking in 2D, 3D, and higher
dimensions.

t = pd.read_csv('trajallframes.csv')
number_particles = 2

x_total = []
y_total = []
for particle_id in range(number_particles):

    x_list = []
    y_list = []
    frame_id = 0
    while (frame_id < 469): #471

        t_filt = t[ t['particle'] == particle_id ]
        t_filt = t_filt[ t_filt['frame'] == frame_id]

        if t_filt.empty:
            frame_id += 1

```

```

        continue

    x = t_filt['x'].values[0]
    y = t_filt['y'].values[0]
    x_list.append(x)
    y_list.append(y)
    frame_id += 1

x_total.append(x_list)
y_total.append(y_list)

x_total = sorted(x_total, key=lambda x: len(x), reverse=True)
y_total = sorted(y_total, key=lambda x: len(x), reverse=True)

x_one_particle = x_total[0]
y_one_particle = y_total[0]
distance = []
for i in range(1, len(x_one_particle)):
    d_x = x_one_particle[i] - x_one_particle[i-1]
    d_y = y_one_particle[i] - y_one_particle[i-1]
    d = np.sqrt(d_x**2 + d_y**2)
    distance.append(d)

fig, ax = plt.subplots()
plt.plot(x_one_particle, y_one_particle)
plt.xlabel(r'x ($\mu$m)')
plt.ylabel(r'y ($\mu$m)')

# scape area diameter
tumble = 3
# radius of the red circle
radius = 5

for i in range(5, len(distance)):
    # displacement smaller than scape area diameter for 4 consecutive movement (1
    movement = 1 frame = 5 seconds) total time = 5*5 = 25 s (to convert to real time real* speed
    of the video)
    if distance[i] > tumble and distance[i-1] > tumble and distance[i-2] > tumble and
    distance[i-3] > tumble and distance[i-4] > tumble:
        circle = plt.Circle((x_one_particle[i], y_one_particle[i]), radius, color='r', fill=False) # plot
        the circle at the center of ith point
        plt.gcf().gca().add_artist(circle)

```

```
i += 2
plt.show()
```



### E.3 Interaction Frequency

```
import pandas as pd
import math
#import sys

df = pd.read_csv('1_15minRestInLightAll.csv')

frames = df['frame'].unique();
print(len(frames))

A= []
counter = 0
for i in range(len(frames)):

    if i > 8998:
        break

    print("check frame", i)
    frame = frames[i]
    df_filter = df[df['frame'] == frame]
    numb_particles = len(df_filter)

    for k in range(numb_particles):
        x_particle_key = df_filter.loc[df_filter.index[k], 'x']
        y_particle_key = df_filter.loc[df_filter.index[k], 'y']

        for j in range(k+1, numb_particles):

            x_particle = df_filter.loc[df_filter.index[j], 'x']
            y_particle = df_filter.loc[df_filter.index[j], 'y']

            if math.sqrt((x_particle - x_particle_key)**2 + (y_particle -
y_particle_key)**2) <= 35:
                counter += 1
```

```
A.append(counter)
counter = 0
```

```
# convert list to DataFrame
df1 = pd.DataFrame(A)
# saving the dataframe
df1.to_csv('CollisionFreq.csv')
```

.....

#### **E.4 Mean Square Displacement and Velocity**

```
from __future__ import division, unicode_literals, print_function # for compatibility with
Python 2 and 3
import matplotlib as mpl
import matplotlib.pyplot as plt
import matplotlib.animation as animation
from matplotlib.animation import FuncAnimation
mpl.rc('figure', figsize=(11, 9))
mpl.rc('image', cmap='gray')
import numpy as np
import pandas as pd
from pandas import DataFrame, Series # for convenience
import trackpy as tp #is a Python package for particle tracking in 2D, 3D, and higher
dimensions.
import scipy.stats as stats
from sklearn.linear_model import LinearRegression
from sklearn import metrics

t = pd.read_csv('traj1_15minRestInLight.csv')

#number_frames = 453
number_particles = 183;

#particle_id = 0
x_total = []
y_total = []
for particle_id in range(number_particles):

    x_list = []
    y_list = []
    frame_id = 0
    while (frame_id < 451):
```

```

t_filt = t[ t['particle'] == particle_id ]
t_filt = t_filt[ t_filt['frame'] == frame_id]

if t_filt.empty:
    frame_id += 1
    continue

x = t_filt['x'].values[0]
y = t_filt['y'].values[0]
x_list.append(x)
y_list.append(y)
frame_id += 1

x_total.append(x_list)
y_total.append(y_list)

x_total = sorted(x_total, key=lambda x: len(x), reverse=True)
y_total = sorted(y_total, key=lambda x: len(x), reverse=True)

numb_particles = len(x_total)
print("number of particles", numb_particles)
distances = []
delta_x = []
deltas = []
for particle_ID in range(numb_particles):
    x_one_particle = x_total[particle_ID]
    y_one_particle = y_total[particle_ID]
    distance = []
    for i in range(1,len(x_one_particle)):
        d_x = x_one_particle[i] - x_one_particle[i-1]
        d_y = y_one_particle[i] - y_one_particle[i-1]
        d = np.sqrt(d_x**2 + d_y**2)
        distance.append(d)
        delta_x.append(d_x)

    if len(distance) < 450:
        print(len(distance))
        continue
    distances.append(distance)
    deltas.append(delta_x)

distances=np.array([np.array(xi[:450]) for xi in distances])
distances_mean = np.mean(distances, axis=0)

```

```

deltas=np.array([np.array(xi[:450]) for xi in deltas])
deltas_mean = np.mean(deltas, axis=0)

##### my MSD vs dx
#density = stats.gaussian_kde(deltas_mean)
plt.figure()
n, x, _ = plt.hist(deltas_mean, bins=np.linspace(-8, 8, 15), histtype='step', density=True,
linewidth=2) # deltas_mean, bins=np.linspace(-3, 3, 20), histtype='step', density=True
#plt.plot(x, density(x))
plt.ylabel(r'PDF') # r'MSD ( $\mu m^2$ )' # PDF (MSD, dx)
plt.xlabel('x ( $\mu m$ )');
plt.legend(['Flashlight - Sample 1 - test 2'])
plt.grid(color='k', linestyle='-', linewidth=0.05) # , linewidth=2
plt.show()

###velocity vs time
# 453 frame, 90 s, 5 f/s so 1s/5f
# to convert f*1s/5f and x=vt so v=msd/ans of previous line
plt.figure()
np.seterr(divide='ignore', invalid='ignore')
time = np.arange(0, len(deltas_mean))/8
vel = np.abs(deltas_mean)/time
plt.plot(time, vel, '-', color='black', alpha=1, linewidth=0.6) # '-' # marker='o', markersize=3,
color='violet', alpha=0.6, linewidth=1.5
#plt.axhline(0.05, color='red', linestyle='-')
plt.ylabel('Velocity ( $\mu m/s$ )')
plt.xlabel('Time (s)');
plt.legend(['Normal light condition']) #Laser pointer - Sample 2 - test 1 # Normal light
condition
#plt.xlim(20, 95);
#plt.ylim(-0.01, 0.03);
plt.show()

```

# Curriculum Vitae

**Name:** Zahra Habibi

**Post-secondary Education and Degrees:** Shiraz University  
Shiraz, Fars, Iran  
2007- 2012 B.A.

Isfahan University of Technology  
Isfahan, Isfahan, Iran  
2012- 2015 M.A.

The University of Western Ontario  
London, Ontario, Canada  
2018-2021 M.A.

**Related Work Experience** Teaching Assistant  
The University of Western Ontario  
2019-2021

## Publications:

Mehdizadeh Allaf, Malihe. **Habibi, Zahra.** de Bruyn, John R. DeGroot, Christopher T. Peerhossaini, Hassan. (2022). Rheological and biophysical properties of living fluids under shear: active suspensions of *synechocystis* sp. cpcc 534. Journal of Fluids Engineering, 144(2): 021208 (13 pages).

Mehdizadeh Allaf, Malihe. **Habibi, Zahra.** Samadi, Zahra. DeGroot, Christopher T. Rehmman Lars. de Bruyn, John R. Peerhossaini, Hassan. (2020). Physical and rheological properties of active fluids under shear stress- suspensions of *synechocystis*. ASME 2020 Fluids Engineering Division Conference (FEDSM), Orlando, Florida, USA, July 12-16.

**Habibi, Zahra.** Karami, Mohammad. Jarrahi, Mojtaba. Shirani, Ebrahim. Peerhossaini, Hassan. (2018). Some observations on the spatiotemporal orbits structure and heat transfer enhancement in pulsating flow. International Journal of Thermal Science, 125, 428–439.

**Habibi, Zahra.** Karami, Mohammad. Shirani, Ebrahim. Jarrahi, Mojtaba. Peerhossaini, Hassan. (2016). Heat transfer study of pulsating flow in a twisted duct. Eurotherm Seminar 106, Oct., Paris, France.

Karami, Mohammad. Jarrahi, Mojtaba. **Habibi, Zahra.** Shirani, Ebrahim. Peerhossaini, Hassan. (2014). Chaotic heat transfer in a laminar pulsating flow with constant wall temperature. ASME 2014 Fluids Engineering Division Conference (FEDSM & ICNMM), Illinois, USA.